

1. REPORT NUMBER  CA15-2421	2. GOVERNMENT ASSOCIATION NUMBER	3. RECIPIENT'S CATALOG NUMBER
4. TITLE AND SUBTITLE BENCHMARKING RECENTLY DEVELOPED PROCEDURES FOR DESIGNING PILE FOUNDATIONS IN LATERALLY SPREADING GROUND	5. REPORT DATE July 18, 2014	
	6. PERFORMING ORGANIZATION CODE	
7. AUTHOR  Kengo Kato, H. Benjamin Mason, PhD., Scott A. Ashford, PhD, PE	8. PERFORMING ORGANIZATION REPORT NO.	
9. PERFORMING ORGANIZATION NAME AND ADDRESS School of Civil and Construction Engineering Oregon State University 101 Kearney Hall Corvallis, Oregon 97331	10. WORK UNIT NUMBER	
	11. CONTRACT OR GRANT NUMBER  65A0453	
12. SPONSORING AGENCY AND ADDRESS California Department of Transportation Division of Engineering Services 1801 30th Street, MS #9-2/5i Sacramento, CA 95816	13. TYPE OF REPORT AND PERIOD COVERED Final Report	
	14. SPONSORING AGENCY CODE	

15. SUPPLEMENTARY NOTES

16. ABSTRACT  
 Recent earthquakes in Chile, New Zealand, and Japan provide an opportunity to benchmark recently developed Caltrans design procedures for bridge piles that will withstand liquefaction and lateral spreading. Specifically, case history data from the 2010 Chile earthquake, the 2010-2011 earthquake swarm around Christchurch, New Zealand, and the 2011 Tohoku earthquake in Japan were collected. The data collected included soil information, structural details, and post-earthquake damage observations. From the collected case history data, one bridge with the most complete data set from each country was chosen for complete analysis. The Mataquito Bridge in Chile, the South Brighton Bridge in New Zealand, and the Mihama Bridge in Japan were selected. Within this report, pile foundations are analyzed for the three identified bridges with the proposed Caltrans design procedures using the collected and screened case history data. The computed results are compared with actual bridge pile performance. The comparisons are used to suggest potential refinements to the Caltrans design procedures. The comparisons show that, in general, for the three case histories considered, the Caltrans design procedure worked well. While there were some variations in agreement between the calculated and observed performance, all of the bridges were "predicted" to perform reasonably well, and all were observed to be in service soon after the earthquakes. Recently, much more case history data has become available from the three earthquake events, some with observed poor performance. This broader set of case history data should be analyzed to better refine and improve the Caltrans method further, including bridges with good and poor performance.

17. KEY WORDS bridge piles, liquefaction, lateral spreading, earthquake, pile foundations, Mataquito Bridge in Chile, South Brighton Bridge in New Zealand, Mihama Bridge in Japan, Caltrans design procedures, bridge pile performance	18. DISTRIBUTION STATEMENT No restriction. This document is available to the public through the National Technical Information Service, Springfield, Virginia 22161	
19. SECURITY CLASSIFICATION (of this report)  Unclassified	20. NUMBER OF PAGES  166	21. COST OF REPORT CHARGED

## **DISCLAIMER STATEMENT**

This document is disseminated in the interest of information exchange. The contents of this report reflect the views of the authors who are responsible for the facts and accuracy of the data presented herein. The contents do not necessarily reflect the official views or policies of the State of California or the Federal Highway Administration. This publication does not constitute a standard, specification or regulation. This report does not constitute an endorsement by the Department of any product described herein.

For individuals with sensory disabilities, this document is available in alternate formats. For information, call (916) 654-8899, TTY 711, or write to California Department of Transportation, Division of Research, Innovation and System Information, MS-83, P.O. Box 942873, Sacramento, CA 94273-0001.

Oregon State University  
School of Civil and Construction Engineering

**BENCHMARKING RECENTLY DEVELOPED PROCEDURES FOR  
DESIGNING PILE FOUNDATIONS IN LATERALLY SPREADING  
GROUND**

By

**Kengo Kato**

*Graduate Student Researcher*

and

**H. Benjamin Mason, PhD**

*Assistant Professor*

and

**Scott A. Ashford, PhD, PE**

*Dean, College of Engineering*

Final Report on a Research Project Funded by  
Caltrans under Facilities Contract No. 65A0453

School of Civil and Construction Engineering

Oregon State University

101 Kearney Hall

Corvallis, Oregon 97331

18 July 2014

## **ACKNOWLEDGMENTS**

This study was made possible by funding from the California Department of Transportation under contract No. 65A0453. The authors would like to thank Tom Shantz (Caltrans) for advice and guidance as well as Pedro Arduino for discussions about pile modeling.

## ABSTRACT

Recent earthquakes in Chile, New Zealand, and Japan provide an opportunity to benchmark recently developed Caltrans design procedures for bridge piles that will withstand liquefaction and lateral spreading. Specifically, case history data from the 2010 Chile earthquake, the 2010-2011 earthquake swarm around Christchurch, New Zealand, and the 2011 Tohoku earthquake in Japan were collected. The data collected included soil information, structural details, and post-earthquake damage observations. From the collected case history data, one bridge with the most complete data set from each country was chosen for complete analysis. The Mataquito Bridge in Chile, the South Brighton Bridge in New Zealand, and the Mihama Bridge in Japan were selected. Within this report, pile foundations are analyzed for the three identified bridges with the proposed Caltrans design procedures using the collected and screened case history data. The computed results are compared with actual bridge pile performance. The comparisons are used to suggest potential refinements to the Caltrans design procedures. The comparisons show that, in general, for the three case histories considered, the Caltrans design procedure worked well. While there were some variations in agreement between the calculated and observed performance, all of the bridges were “predicted” to perform reasonably well, and all were observed to be in service soon after the earthquakes. Recently, much more case history data has become available from the three earthquake events, some with observed poor performance. This broader set of case history data should be analyzed to better refine and improve the Caltrans method further, including bridges with good and poor performance.

# Table of Contents

DISCLAIMER.....	i
ACKNOWLEDGMENTS .....	ii
ABSTRACT .....	iii
Table of Contents .....	iv
List of Figures .....	vi
List of Tables .....	x
Chapter 1. INTRODUCTION .....	1
1.1. Background and Objective.....	1
1.2. Organization.....	2
Chapter 2. CASE HISTORY DATA COLLECTION .....	3
2.1. Introduction.....	3
2.2. Case history data of 2010 $M_w$ 8.8 Chile earthquake .....	7
2.2.1. Overview of 2010 Chile earthquake .....	7
2.2.2. Case history data of liquefaction-induced damage .....	9
2.3. Case history data of 2010, 2011 Earthquake sequences in Darfield and Christchurch in New Zealand .....	12
2.3.1. Overview of 2010, 2011 Earthquake sequences in Darfield and Christchurch in New Zealand .....	12
2.3.3. Case history data of liquefaction induced damages .....	16
2.4. Case history data of 2011 Tohoku Earthquake, Japan, $M_w$ 9.0.....	21
2.4.1. Overview of 2011 Tohoku Earthquake.....	21
2.4.2. Case history data of liquefaction induced damages .....	24
2.5. Summary.....	39
Chapter 3. CASE HISTORY DATA ANALYSIS .....	40
3.1 Introduction.....	40
3.2 Case study: the Mataquito Bridge in Chile .....	41
4.2.1. Observed damages of the Mataquito Bridge.....	41
3.2.2. Liquefaction potential evaluation.....	42
3.2.3. Description of south abutment foundation of Mataquito Bridge .....	43
3.2.4. Analysis of the Mataquito Bridge with the equivalent single pile method .....	44

3.3	Case study: South Brighton Bridge in New Zealand .....	64
3.3.1.	Observed damages of South Brighton.....	64
3.3.2.	Liquefaction potential evaluation.....	65
3.3.3.	Description of South Brighton Bridge .....	67
3.3.4.	Analysis of the South Brighton Bridge with equivalent single pile method.....	68
3.4	Case study: the Mihama Bridge in Japan.....	90
3.4.1.	Observed damages of the Mihama Bridge .....	90
3.4.2.	Liquefaction potential evaluation.....	91
3.4.3.	Description of the Mihama Bridge.....	92
3.4.4.	Analysis of the Mihama Bridge with equivalent single pile method .....	93
3.5	Summary .....	112
Chapter 4.	DISCUSSION .....	115
4.1.	Introduction.....	115
4.2.	Pile modeling .....	115
4.3.	P-y curve .....	116
4.4.	Pushover analysis.....	117
4.5.	Other consideration.....	118
Chapter 5.	CONCLUSIONS.....	119
REFERENCES	.....	120
APPENDIX A	.....	125
APPENDIX B	.....	136
APPENDIX C	.....	147
APPENDIX D	.....	151

## List of Figures

Figure 2.1 Elevation and plan views of typical abutment for Puente Mataquito (courtesy Ministerio de Obras P'ublicas, Chile) (McGann et al. 2012).....	10
Figure 2.2 Locations of subsurface explorations (sondaje) relative to the Puente Mataquito abutments (after Ministerio de Obras P'ublicas, Chile) (McGann et al. 2012).....	10
Figure 2.3 SPT resistance profiles near NE and SW abutments of Puente Mataquito after Petrus (2006). 11	
Figure 2.4 Mataquito bridge: (a) Lateral spreading on the south end of the bridge, S35.050712° W72.162258°; (b) approach fill settlement at the north abutment of the bridge (70 cm offset at the bridge deck), S35.050712° W72.162258°; (c) sand boils at the north end, S35.051961° W72.163217° (Ledezma et al. 2012) .....	11
Figure 2.5 Observed fault-normal horizontal acceleration time histories at various locations in the Christchurch region from the 22 February earthquake with reference to the inferred surface projection of the causative fault which dips to the south-east (Cubrinovski et al. 2011).....	14
Figure 2.6 Areas of induced liquefaction by the 4 September 2010 (red bordered areas) and 22 February 2011 (white shaded areas) earthquakes and associated fault ruptures (red – fault rupture with surface trace; blue – fault rupture with no surface trace) (NZ-GEER 2011).....	15
Figure 2.7 Satellite image of South Brighton Bridge post-earthquake (NZ-GEER 2011).....	17
Figure 2.8 Aerial view of South Brighton bridges, displacements of the river banks (in centimeters) for the Christchurch and Darfield earthquakes (Cubrinovski et al. 2013).....	18
Figure 2.9 South Brighton bridge; a) horizontal movement of abutments compared to bridge deck; b) vertical position of abutment compared to bridge deck (NZ-GEER 2011) .....	18
Figure 2.10 Plastic hinging in abutment piles of Bridge Street Bridge (Palermo et al. 2011).....	19
Figure 2.11 Comparison of the displacement of slope in front of western abutment following, a) Darfield event, b) Christchurch event (NZ-GEER 2011).....	19
Figure 2.12 Soil profile, SPT and CPT data of South Brighton Bridge (Cubrinovski et al. 2013).....	20
Figure 2.13 The map that liquefaction observed in Kanto area (JGS 2011).....	23
Figure 2.14 General drawing of Mihama Bridge (PWRI 2011) .....	26
Figure 2.15 Ground difference in level near A2 abutment (approximately 20cm) (PWRI 2011) .....	26
Figure 2.16 No gaps between the deck and A2 abutment (Chiba city 2011).....	27
Figure 2.17 Ruptured bolts of A2 abutment (Chiba city 2011) .....	27
Figure 2.18 Ground settlement at the side of A1 abutment (Chiba city 2011) .....	27
Figure 2.19 Ground settlement at the side of A1 abutment (H=260mm) (Chiba city 2011) .....	27

Figure 2.20 Ground settlement at the face of A1 abutment H=(Chiba city 2011).....	28
Figure 2.21 Ground displacement (L=180mm) and settlement (H=330mm) near A1 abutment (Chiba city 2011).....	28
Figure 2.22 Ground settlement at the face of A1 abutment H=630mm (Chiba city 2011).....	28
Figure 2.23 Gap at the face of A1 abutment (Chiba city 2011).....	28
Figure 2.24 Cracks on the sea bank in front of the A1 abutment W=100mm (Chiba city 2011).....	28
Figure 2.25 Cracks on the sea bank in front of the A1 abutment (Chiba city 2011).....	28
Figure 2.26 Cracks on the sea bank W=100mm (Chiba city 2011).....	29
Figure 2.27 Cracks on the A1 abutment approaching road W=50mm (Chiba city 2011).....	29
Figure 2.28 Gap between retaining wall and A1 abutment (Downstream side) (PWRI 2011).....	29
Figure 2.29 Gap between retaining wall and A1 abutment (about 7cm) (PWRI 2011).....	29
Figure 2.30 Displacement of the bearing of A1 abutment (Chiba city 2011).....	29
Figure 2.31 Loosed bridge fall prevention device (PWRI 2011).....	30
Figure 2.32 No gaps between A1 abutment and upstream side retaining wall (PWRI 2011).....	30
Figure 2.33 Observed cracks near the A1 abutment (Chiba city 2011).....	31
Figure 2.34 Boring data at the liquefied site near the A1 abutment (Investigated during 23-26 April in 2011) (Chiba city 2011).....	32
Figure 2.35 Boring data at the liquefied site near the A1 abutment (No.1 site) (Investigated at 23-26 April in 2011) (Chiba city 2011).....	34
Figure 2.36 Boring data at the liquefied site near the A1 abutment (No.2 site) (Investigated at 23-26 April in 2011) (Chiba city 2011).....	35
Figure 2.37 The A1 abutment drawings.....	36
Figure 2.38 Pile dimension properties of A1 abutment.....	37
Figure 2.39 Pile dimension properties of A2 abutment.....	38
Figure 3.1 Results of the liquefaction potential evaluation, the Mataquito Bridge.....	42
Figure 3.2 Sketch of south abutment foundation of the Mataquito Bridge.....	43
Figure 3.3 Sketch of the approach embankment of the Mataquito Bridge.....	44
Figure 3.4 Modeling of an equivalent single pile, the Mataquito Bridge.....	44
Figure 3.5 Bending moment – bending curvature of the group pile section, the Mataquito Bridge.....	45
Figure 3.6 Bending moment – bending curvature of the abutment section, the Mataquito Bridge.....	46
Figure 3.7 p-y curve for the Mataquito Bridge’s abutment.....	49
Figure 3.8 Modification factor near liquefiable layers, the Mataquito Bridge.....	52
Figure 3.9 Slope stability analysis model to determine coefficient of horizontal acceleration, the Mataquito Bridge.....	54

Figure 3.10 Estimated ground displacement with PGA =0.461g, the Mataquito Bridge .....	55
Figure 3.11 Estimated ground displacement with PGA =0.390g, the Mataquito Bridge .....	56
Figure 3.12 Results of the pushover analysis of the Mataquito Bridge .....	58
Figure 3.13 Pushover analysis vs slope stability analysis, the Mataquito Bridge (PGA = 0.461g).....	59
Figure 3.14 Pushover analysis vs slope stability analysis, the Mataquito Bridge (PGA = 0.390g).....	60
Figure 3.15 Deflection, estimated bending moment, shear force and subgrade reaction with API sand (O’Neill) model, the Mataquito Bridge.....	61
Figure 3.16 Deflection, estimated bending moment, shear force and subgrade reaction with residual shear strength model, the Mataquito Bridge.....	62
Figure 3.17 Results of the liquefaction potential evaluation based on SPT, the South Brighton Bridge...	65
Figure 3.18 Results of the liquefaction potential evaluation based on CPT, the South Brighton Bridge ...	66
Figure 3.19 Sketch of the South Brighton Bridge.....	67
Figure 3.20 Sketch of the approach embankment of the South Brighton Bridge .....	67
Figure 3.21 Modeling of an equivalent single pile, the South Brighton Bridge .....	68
Figure 3.22 Bending moment – bending curvature of the equivalent single pile for group pile section, the South Brighton Bridge .....	69
Figure 3.23 Bending moment – bending curvature of the equivalent single pile for abutment section, the South Brighton Bridge .....	70
Figure 3.24 p-y curve of the abutment section, the South Brighton Bridge .....	75
Figure 3.25 Modification factor near liquefiable layers, the South Brighton Bridge .....	78
Figure 3.26 Slope stability analysis model to determine the coefficient of horizontal acceleration, the South Brighton Bridge .....	80
Figure 3.27 Estimated ground displacement, the South Brighton Bridge.....	81
Figure 3.28 Results of the pushover analysis with 2×5 group piles, the South Brighton Bridge .....	83
Figure 3.29 Results of the pushover analysis with battered pile (+14 degree), the South Brighton Bridge	84
Figure 3.30 Results of the pushover analysis with battered pile (+14 degree), the South Brighton Bridge	84
Figure 3.31 Pushover analysis vs slope stability analysis with 2×5 group piles, the South Brighton Bridge .....	85
Figure 3.32 Pushover analysis vs slope stability analysis with battered pile (+14 degree), the South Brighton Bridge .....	86
Figure 3.33 Pushover analysis vs slope stability analysis with battered pile (-14 degree), the South Brighton Bridge .....	86
Figure 3.34 Estimated deflection, bending moment, shear force and subgrade reaction of the abutment foundation, the South Brighton Bridge .....	88

Figure 3.35 Results of the liquefaction potential evaluation, Mihama Bridge .....	91
Figure 3.36 Sketch of the Mihama Bridge .....	92
Figure 3.37 Sketch of the embankment of the Mihama Bridge .....	93
Figure 3.38 Modeling of an equivalent single pile, the Mihama Bridge .....	93
Figure 3.39 Bending moment – bending curvature of group pile section, the Mihama Bridge.....	94
Figure 3.40 Bending moment – bending curvature of abutment section, the Mihama Bridge .....	95
Figure 3.41 p-y curve of crust layer of the Mihama Bridge’s abutment.....	98
Figure 3.42 Modification factor near liquefiable layers, the Mihama Bridge.....	101
Figure 3.43 Slope stability analysis model to determine coefficient of horizontal acceleration, the Mihama Bridge.....	102
Figure 3.44 The results of slope stability analysis, the Mihama Bridge .....	104
Figure 3.45 Pushover analysis of the Mihama Bridge .....	106
Figure 3.46 Shear force – Displacement diagram, the Mihama Bridge.....	107
Figure 3.47 Estimated deflection, bending moment, shear force and subgrade reaction using API sand model ( $n \times m_p = 6.3$ ), Mihama Bridge.....	109
Figure 3.48 Estimated deflection, bending moment, shear force and subgrade reaction using the residual shear strength, Mihama Bridge .....	109
Figure 3.49 Estimated deflection, bending moment, shear force and subgrade reaction with observed ground displacement, Mihama Bridge.....	110
Figure 4.1 Recommended model of p-y curve for pile cap or abutment .....	117

## List of Tables

Table 2.1. Specific site's structural names of 2011 Chile earthquake .....	4
Table 2.2 Specific site's structural names of 2010, 2011 Earthquake sequences in Darfield and Christchurch in New Zealand .....	5
Table 2.3 Specific site's structural names of 2011 Tohoku earthquake in Japan .....	6
Table 2.4 Peak Ground Acceleration for each site (Boroschek et al. 2010) .....	8
Table 2.5 Observed ground motions at strong motion stations (Cubrinovski et al. 2011).....	13
Table 2.6 Acceleration records at the bridge sites (KiK-net).....	22
Table 3.1 Observed damages of the ground and bridge structure, the Mataquito Bridge.....	41
Table 3.2 Pile section properties of the Mataquito Bridge for original single pile .....	45
Table 3.3 Dimension parameters of the Mataquito Bridge .....	46
Table 3.4 Reduction factor for vicinity of liquefied layer for the Mataquito Bridge.....	51
Table 3.5 Reduction factor for each depth, the Mataquito Bridge.....	51
Table 3.6 Slope stability results. Displacements are determined using Bray and Travasarou (2007), the Mataquito Bridge (PGA = 0.461g) .....	55
Table 3.7 Slope stability results. Displacements are determined using Bray and Travasarou (2007), the Mataquito Bridge (PGA = 0.390g) .....	56
Table 3.8 Soil models and input parameters for the Mataquito Bridge .....	57
Table 3.9 Soil models and input parameters for liquefiable layer, the Mataquito Bridge .....	58
Table 3.10 Estimated ground displacement, the Mataquito Bridge (PGA = 0.461g) .....	59
Table 3.11 Estimated ground displacement, the Mataquito Bridge (PGA = 0.390g) .....	60
Table 3.12 Comparison of the estimated bending moment to yield and allowable bending moment, the Mataquito Bridge .....	62
Table 3.13 Comparison the estimated pile head displacement to the observed abutment displacement, the Mataquito Bridge .....	63
Table 3.14 Observed damages of the ground and bridge structure, South Brighton Bridge.....	64
Table 3.15 Pile section properties of the South Brighton Bridge for original single pile .....	69
Table 3.16 Dimension parameters of the South Brighton Bridge.....	70
Table 3.17 Reduction factor for vicinity of liquefied layer for the South Brighton Bridge.....	77
Table 3.18 Reduction factor for each depth, the South Brighton Bridge.....	77
Table 3.19 Slope stability results using Bishop method, South Brighton Bridge.....	81
Table 3.20 Soil properties of the South Brighton Bridge for LPile .....	82

Table 3.21 Soil models and input parameters for liquefiable layer, the South Brighton Bridge .....	83
Table 3.22 Estimated ground displacement, the South Brighton Bridge.....	87
Table 3.23 Comparison of the estimated bending moment to yield and allowable bending moment, the South Brighton Bridge .....	88
Table 3.24 Comparison the estimated pile head displacement to the observed abutment displacement, the South Brighton Bridge .....	89
Table 3.25 Observed damages of the ground and bridge structure, the Mihama Bridge.....	90
Table 3.26 Pile section properties of the Mihama Bridge for original single pile .....	94
Table 3.27 Dimension parameters of the Mihama Bridge .....	95
Table 3.28 Reduction factor for vicinity of liquefied layer for the Mihama Bridge.....	100
Table 3.29 Reduction factor for each depth, the Mihama Bridge .....	100
Table 3.30 Slope stability analysis results using Bishop method, displacements are determined using Bray and Travasarou (2007), the Mihama Bridge .....	103
Table 3.31 Input parameters for pushover analysis of the Mihama Bridge .....	105
Table 3.32 Input parameters for liquefiable layer of the Mihama Bridge.....	106
Table 3.33 Estimated ground displacement, the Mihama Bridge .....	108
Table 3.34 Comparison of the estimated bending moment to yield and allowable bending moment, Mihama Bridge .....	110
Table 3.35 Comparison of the estimated pile head displacements to the observed ground displacements .....	111
Table 3.36 Comparison of estimated displacement with observed displacement of each bridge.....	113
Table 3.37 Comparison of estimated the yield and allowable bending moment of each bridge.....	114
Table 4.1 Comparison of initial slope of p-y curve for each abutment.....	116

# **Chapter 1. INTRODUCTION**

## **1.1. Background and Objective**

Pile foundations have suffered extensive damage from liquefaction induced ground lateral spreading. The pile foundation deflections and the ground displacements can in turn cause significant damage to bridge superstructures. Recent research (e.g., Ashford et al. 2011) has culminated in general guidelines for designing pile foundations located in laterally spreading ground. In the guidelines, pile modeling, pile foundation-superstructure interaction, soil-pile interaction, and ground displacement due to liquefaction are considered. These factors strongly affect the pile foundation performance, so appropriate parameters are required for engineering design.

Recent earthquakes in Chile, New Zealand, and Japan provide an opportunity to benchmark Caltrans design procedures for deep foundations in liquefaction and lateral spreading. Case history data for three earthquake events are publically reported by earthquake engineering reconnaissance organizations. These earthquake events provide different characteristics of liquefaction induced ground failures surrounding pile foundations. Therefore, case history data from the 2010 Chile earthquake, the 2010-2011 earthquake swarm around Christchurch, New Zealand, and the 2011 Tohoku earthquake in Japan can be utilized to understand actual soil-pile foundations interactions.

The objective of this current study is to benchmark recently developed procedures (Ashford et al. 2011; Shantz 2013) for designing pile foundations in liquefaction induced lateral spreading. Case history data, including all required information to analyze the pile foundation performance against lateral spreading, were collected and screened. Data from three case histories include different soil characteristics and bridge configurations. Pile foundation performances selected from the collected and screened case history data are analyzed using the Caltrans design procedures. Then, the computed results are compared to actual bridge pile performances to check applicability of the guideline. Initial comparisons between computed performance and observed performance highlight potential refinements to the Caltrans design

procedures. The initial comparisons show that the current Caltrans method performs reasonably well, but this statement must be tempered by the fact that only three case histories were available at the time for benchmarking, and all were from bridges that performed well. Further case history data from the three earthquake events have recently become available. More benchmarking efforts should be carried out to further investigate the strength of the current Caltrans method.

## **1.2. Organization**

**Chapter 1: Introduction.** Introduce the objectives and background of this research.

**Chapter 2: Case history data collection.** Provide case history data from the 2010 Chile earthquake, the 2010- 2011 earthquake sequences in Darfield and Christchurch in New Zealand, and the 2011 Tohoku earthquake in Japan.

**Chapter 3: Case history data analysis using Caltrans design procedure.** Three cases are selected from case history data. Pile foundations are designed by Caltrans recommended design procedure using screened case history data. The computed results are compared with observed pile foundation performances.

**Chapter 4: Discussion.** Based on the results in Chapter 4, the strengths and weaknesses of the current Caltrans recommended design procedure are discussed.

**Chapter 5: Conclusion.** Conclusions of this research study are presented.

**Appendices.**

## Chapter 2. CASE HISTORY DATA COLLECTION

### 2.1. Introduction

Chile, New Zealand, and Japan experienced large earthquakes from 2010 to 2011, which caused significant damage to the structures, foundations, and soil.

Chile experienced a  $M_w$  8.8 earthquake in February 2010. New Zealand experienced sequences of  $M_w$  7.1 and  $M_w$  6.2 earthquakes in 2010 and 2011 (the “Darfield” and “February 2011 Christchurch” events, respectively, though the Christchurch area continued to experience significant aftershocks throughout 2011). Japan experienced a  $M_w$  9.0 earthquake in March 2011.

Liquefaction induced ground failures were observed in these earthquake events. In particular, transportation systems in liquefied areas were damaged due to the mainshocks and aftershocks. For example, bridges located along waterfronts suffered from excessive settlements and lateral spreading. As a result of liquefaction, bridge roads were out of service after the earthquake. Large ground deformations were observed around bridge sites, and deep foundations supporting bridge structures were damaged due to liquefaction.

In this chapter, earthquake case history data collected from the aforementioned three earthquakes are reported to provide qualified information for analysis of pile foundation performances in liquefaction and laterally spreading ground. These data are collected from well-organized documents (e.g., earthquake event reports by Geotechnical Extreme Events Reconnaissance). Bridge damages, ground failures, soil properties, and ground motions for each bridge site are described where possible.

Table 2.1 through Table 2.3 provide site-specific bridge data each earthquake.

**Table 2.1. Specific site's structural names of 2011 Chile earthquake**

Bridge	Location	Latitude	Longitude	Soil property	Bridge Description	Damages	References
Independencia Bridge	Santiago	-33.3864	-70.7601	No	No	Cracking	FHWA (2011)
Quilicura Railway	Santiago	-33.3675	-70.7024	No	No	Cracking	FHWA (2011)
Avenida Romero Acceso Sur overpass	Paine	-33.8614	-70.7184	No	No	Shear failure	FHWA (2011)
Avenida Chada Acceso Sur Overpas	Paine	-33.8699	-70.7262	No	No	Shear failure	FHWA (2011)
Pichibudis Bridge	Iloca	-34.8801	-72.1556	No	No	Tsunami	FHWA (2011)
Mataquito Bridge	Iloca	-35.0518	-72.1632	Yes	Yes	Lateral spreading Minor crash	FHWA (2011) GEER (2010) McGann et al. (2012) MAE (2011) Ledezma et al. (2012)
Tubul bridge	Tubul	-37.2307	-73.4576	No	No	Collapse	FHWA (2011) McGann et al. (2012)
Ramadillas Bridges	Arauco	-37.3069	-73.2651	No	No	Lateral spreading	FHWA (2011)
Juan Pablo II Bridge Over Biobío River	Concepción	-36.8231	-73.0914	Yes	No	Shear failure Ground settlement Lateral spreading	FHWA (2011) GEER (2010) Kawashima (2010) Ledezma et al. (2012) McGann et al. (2012)
Chepe Railroad Bridge Over Biobío River	Concepción	-36.8199	-73.0655	No	No	Ground settlement Lateral spreading	FHWA (2011)
Mochita Bridge	Concepción	-36.8468	-73.0554	Yes	Yes	Ground settlement Lateral spreading	FHWA (2011) GEER (2010) Ledezma(2012)
Old Biobío River Bridge	Concepción	-36.8398	-73.0692	No	No	Deck unseating Lateral spreading	FHWA (2011) GEER (2010) Kawashima (2010)
Llacolén Bridge Over Biobío River	Concepción	-36.8403	-73.0684	No	No	Deck unseating Lateral spreading	FHWA (2011) GEER (2010) Kawashima (2010) McGann et al. (2012)
Talca pedestrian bridge	Talca	-35.4203	-71.684	No	No	Deck unseating Shear failure	GEER (2010)
Raqui 1 bridge	Raqui	-37.2543	-73.4368	No	No	Lateral spreading	FHWA (2011) McGann et al. (2012)
Raqui 2 and Tubul Bridges	Raqui	-37.2518	-73.443	No	No	Lateral spreading	FHWA(2011) GEER(2010) McGann et al. (2012)

**Table 2.2 Specific site's structural names of 2010, 2011 Earthquake sequences in Darfield and Christchurch in New Zealand**

Bridge	Location	Latitude	Longitude	Soil property	Bridge Description	Damages	References
Avondale Road Bridge	Christchurch	-43.5005	172.6878	Yes	No	Lateral spreading	Christchurch City Council (2011)
Pages Road Bridge	Christchurch	-43.5092	172.7213	No	No	Lateral spreading	GEER (2011) Palermo (2011)
Swanns Road Bridge	Christchurch	-43.5222	172.6601	No	No	Settlement Lateral spreading	GEER (2011) Christchurch City Council (2011)
Colombo Street Bridge	Christchurch	-43.5272	172.6366	No	No	Lateral spreading	GEER (2011) Palermo (2011)
Armagh Street Bridge	Christchurch	-43.5287	172.6347	No	No	Longitudinal cracking	Christchurch City Council (2011)
Hereford Street Bridge	Christchurch	-43.532	172.6335	No	No	Longitudinal cracking	Christchurch City Council (2011)
Helmores Lane Bridge	Christchurch	-43.5216	172.6728	No	No	Separation between beams and props	Christchurch City Council (2011)
South Brighton Bridge	Christchurch	-43.5252	172.7241	Yes	Yes	Lateral spreading	GEER (2011) Palermo (2011) Cubrinovski et al. (2013)
Gayhurst Road Bridge	Christchurch	-43.5215	172.6727	Yes	Yes	Lateral spreading	GEER (2011) Palermo (2011) Cubrinovski et al. (2013)
Fitzgerald Avenue Bridge	Christchurch	-43.5263	172.6506	No	No	Lateral spreading	GEER (2011) Palermo (2011) Cubrinovski et al. (2013)
SH74 Anzac Drive Bridge	Christchurch	-43.5009	172.7012	Yes	Yes	Liquefaction Lateral spreading	GEER (2011) Palermo (2011) Cubrinovski et al. (2013)
Chaney's Overpass Bridge	Christchurch	-43.4298	172.6463	No	No	Less movement cracking	GEER (2011)
Horotane Valley Overpass	Christchurch	-43.5725	172.6947	No	No	Transverse crack	GEER (2011) Palermo (2011)
Port Hills Overpass	Christchurch	-43.5711	172.6934	No	No	Cracking	Palermo (2011)
Ferrymead Bridge	Christchurch	-43.5584	172.7086	No	No	Lateral spreading	GEER (2011) Palermo (2011)

**Table 2.3 Specific site's structural names of 2011 Tohoku earthquake in Japan**

Bridge	Location	Latitude	Longitude	Soil property	Bridge Description	Damages	References
Kunida Bridge	Ibaragi Prefecture Mito city	36.4183	140.4335	No	Yes	Shear failure Cracking	PWRI(2011)*
Shizukosen Bridge	Ibaragi Prefecture Naka city	36.5033	140.5162	No	No	Settlement Shear failure	PWRI(2011)*
Omiya Rikkyo	Ibaragi Prefecture Omiya city	36.5516	140.408	No	Yes	Shear failure Cracking	PWRI(2011)*
Kameda Bridge	Fukushima Prefecture Koriyama city	37.4121	140.3467	No	Yes	Cracking	PWRI(2011)*
Tenno Bridge	Miyagi Prefecture Isimaki city	38.4574	141.2908	No	Yes	Buckling	PWRI(2011)* NILIM(2011)*
Umedo Bridge	Ibaragi Prefecture Mito city	36.3801	140.4018	No	No	Ground Settlement	PWRI(2011)*
Koyagi Bridge	Iwate Prefecture Oshu city	39.1364	141.1752	No	Yes	Cracking Settlement	PWRI(2011)*
Koizumi Bridge	Miyagi Prefecture Kesenuma city	38.7693	141.5078	No	Yes	Tsunami	PWRI(2011)*
Utatsu Bridge	Miyagi Prefecture Minamisanriku city	38.7159	141.5213	No	Yes	Tsunami	PWRI(2011)* TRDB(2011)* Kawashima (2011)
Nijuichihama Bridge	Miyagi Prefecture Kesenuma city	38.7589	141.5195	No	Yes	Tsunami	PWRI(2011)* TRDB(2011)*
Ohamawatari Bridge	Miyagi Prefecture Kesenuma city	39.3291	141.8909	No	Yes	Tsunami Settlement	PWRI(2011)*
Mihama Bridge	Chiba Prefecture Chiba city	35.6322	140.0444	Yes	Yes	Lateral spreading Cracks	PWRI(2011)* Chiba City's bridge register (1983)*
Ego Bridge	Miyagi Prefecture Osaki city	38.5904	140.9731	Yes	Yes	Lateral spreading Ground settlement	PWRI(2011)* Miyagi Prefecture's bridge register (2006)* Oka et al. (2011)*

\* Written in Japanese

## **2.2. Case history data of 2010 $M_w$ 8.8 Chile earthquake**

### **2.2.1. Overview of 2010 Chile earthquake**

A moment magnitude  $M_w$  8.8 earthquake occurred on February 27, 2010 in Chile. A large area from the capital city of Santiago region to the Concepcion region, which is approximately 440 km away from Santiago, experienced strong ground motions and significant liquefaction. FHWA (2011) illustrates the conceptual diagram of a subduction zone earthquake to explain the cause of large 2010 Chile earthquake. For example, the ground motion duration recorded at Hospital de Curicó showed that ground shook for approximately 50 seconds). The long duration ground motion induced various damages on bridge structures and the surrounding soils. Additionally, liquefaction induced ground damages were widely observed following the earthquakes. In particular, bridges in the city of Concepción, onshore from the earthquake's epicenter, experienced significant liquefaction. Many bridges crossing the Biobío River suffered tolerable damages (e.g., deck settlements, deck unseating, pile deflections).

Table 2.4 shows transverse, longitudinal, and vertical peak ground accelerations for different seismic stations located throughout Chile (Boroschek et al. 2010).

**Table 2.4 Peak Ground Acceleration for each site (Boroschek et al. 2010)**

Location	Azimuth		Peak Ground Acceleration (g)				
Copiapó	0	Long.	0.016	Trans.	0.030	Vertical	0.008
Vallenar	0	Long.	0.019	Trans.	0.020	Vertical	0.010
Papudo	60	Long.	0.295	Trans.	0.421	Vertical	0.155
Viña del Mar, Marga-marga	0	Long.	0.351	Trans.	0.338	Vertical	0.261
Viña del Mar, Centro (3)	0	Long.	0.219	Trans.	0.334	Vertical	0.186
Valparaíso, UTFSM (3)	180	Long.	0.137	Trans.	0.304	Vertical	0.079
Valparaíso, Almendral (3)	310	Long.	0.224	Trans.	0.265	Vertical	0.146
Llolleo	340	Long.	0.319	Trans.	0.564	Vertical	0.702
Santiago, FCFM RM	0	Long.	0.165	Trans.	0.163	Vertical	0.138
Santiago, centro RM	270	Long.	0.218	Trans.	0.309	Vertical	0.182
Santiago Maipú RM	0	Long.	0.478	Trans.	0.561	Vertical	0.240
Santiago, Peñalolen PM	0	Long.	0.293	Trans.	0.295	Vertical	0.280
Santiago, Puente Alto RM	0	Long.	0.265	Trans.	0.263	Vertical	0.130
Santiago, La Florida RM	0	Long.	0.236	Trans.	0.165	Vertical	0.130
Matanzas	0	Long.	0.342	Trans.	0.308	Vertical	0.234
Hualañe	0	Long.	0.389	Trans.	0.461	Vertical	0.390
Curico	150	Long.	0.470	Trans.	0.409	Vertical	0.198
Talca	0	Long.	0.477	Trans.	0.424	Vertical	0.244
Constitución	0	Long.	0.552	Trans.	0.64	Vertical	0.352
Concepción	60	Long.	0.402	Trans.	0.284	Vertical	0.398
Angol	0	Long.	0.928	Trans.	0.681	Vertical	0.281
Valdivia	0	Long.	0.092	Trans.	0.138	Vertical	0.051

### 2.2.2. Case history data of liquefaction-induced damage

#### The Mataquito Bridge

The Mataquito Bridge is located at Iloca, which is 124 km away from the earthquake's epicenter. Significant liquefaction was observed around both bridge abutments. Prestressed concrete piers and I-girders support the eight span bridge. Two seat-type abutments with wingwalls on either end of the bridge support the bridge spans. Both north and south abutments are founded on  $4 \times 2$  pile groups composed of 1.5 m diameter reinforced concrete drilled shafts. The seven interior piers consist of  $3 \times 1$  groups of the same drilled shafts, which are capped at the connection to the bridge girders (in Figure 2.1) (McGann et al. 2012).

At the south abutment, approximately 4.0m of liquefiable sand layers are embedded. Non-liquefiable layers below liquefiable layers, with SPT-blow count values over 20 blows/foot, are embedded at both the abutments. Liquefiable sand layers, 4.5 m in thickness, are embedded beneath the north abutment. SPT blow count values range from 5 to 20 blows/foot within the liquefiable sand layers beneath the north abutment (i.e., some of the sand is very loose and liquefiable, and other deposits are denser). Below the liquefiable sand layer, a 9 m layer of fine, dense sand is embedded (see the Ledezma et al. (2012) reference for more soils information). Figure 2.2 and Figure 2.3 show the SPT data at the Mataquito Bridge site. The ground displacement due to liquefaction is approximately 54 cm from the edge of the abutment wall to the first row of piers. Also, a ground displacement of approximately 180 cm (over a distance of about 65 m) from the edge of the abutment wall to the river's edge was observed. The approach embankment height is 7.8 m. The approach fills settled about 70 cm relative to the abutment. The approach embankment also experienced a transverse displacement of about 60 cm from the centerline, which caused cracking of the asphalt over a distance of about 200 m. The grounds at the toe of the embankment heaved by abutment displacement as a result of liquefaction (Ledezma et al. 2012). The grounds near the north bridge site spread approximately 1.5 to 2.5 m towards the river and settled approximately 0.5 to 1.0 m (in Figure 2.4). No significant damage to the north bridge by the lateral spreading and strong shaking was confirmed. The north abutment moved toward river less than 0.02 m (FHWA 2011).

According to RENADIC (2010), peak ground accelerations (PGA) recorded at Hualañe, which is just east of Iloca, were 0.389 g (longitudinal direction), 0.390 g (vertical direction), and 0.461 g (transverse direction).

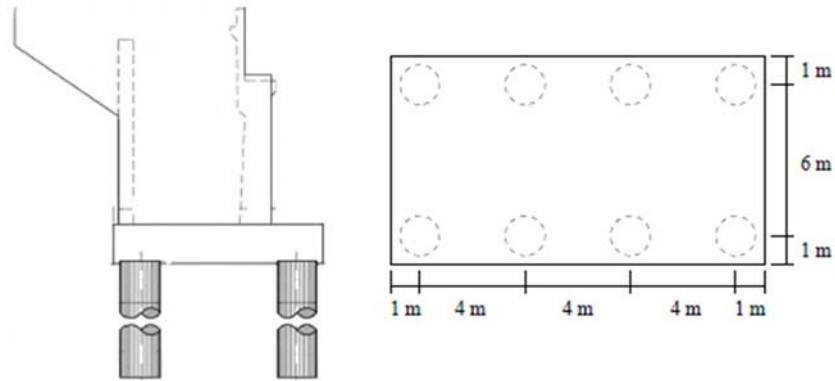


**Figure 2.1 Elevation and plan views of typical abutment for Puente Mataquito (courtesy Ministerio de Obras P'ublicas, Chile) (McGann et al. 2012)**

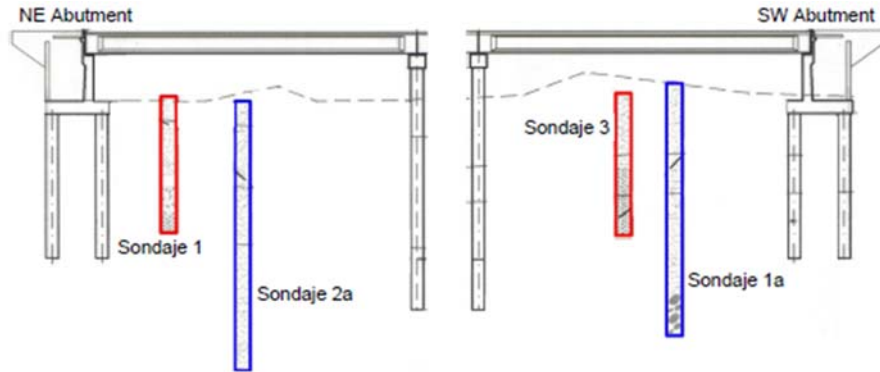


**Figure 2.2 Locations of subsurface explorations (sondaje) relative to the Puente Mataquito abutments (after Ministerio de Obras P'ublicas, Chile) (McGann et al. 2012)**

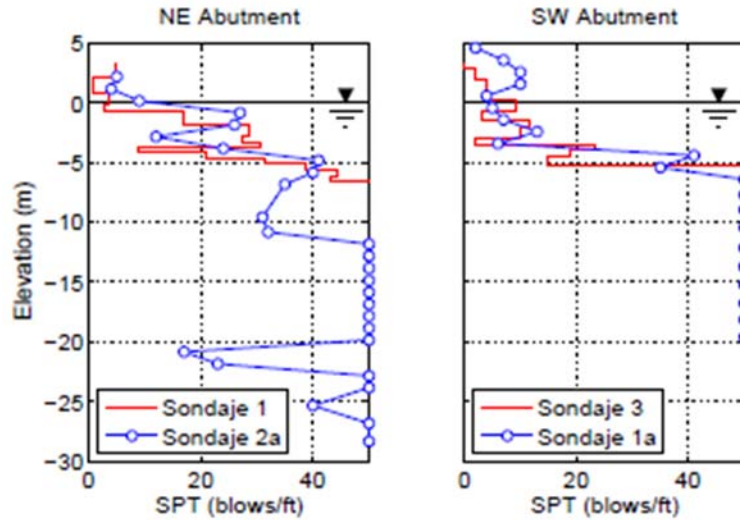


**Figure 2.3 SPT resistance profiles near NE and SW abutments of Puente Mataquito after Petrus (2006)**



**Figure 2.4 Mataquito bridge: (a) Lateral spreading on the south end of the bridge, S35.050712° W72.162258°; (b) approach fill settlement at the north abutment of the bridge (70 cm offset at the bridge deck), S35.050712° W72.162258°; (c) sand boils at the north end, S35.051961° W72.163217° (Ledezma et al. 2012)**

## **2.3. Case history data of 2010, 2011 Earthquake sequences in Darfield and Christchurch in New Zealand**

### **2.3.1. Overview of 2010, 2011 Earthquake sequences in Darfield and Christchurch in New Zealand**

On September 4, 2010, a large ( $M_w$  7.1) earthquake occurred in Darfield and on February 22, 2011 in Christchurch aftershock struck. Weak soil depositing over Christchurch city was liquefied due to the earthquakes. Especially, the bridges along the Avon River were damaged due to significant settlements and lateral spreading.

Figure 2.5 and Table 2.5 show the peak ground acceleration (PGA) of the sites recorded in strong motion in the 2011 Christchurch earthquake event (Cubrinovski et al. 2011). The range of PGA in the central business district (CBD) from 0.37g to 0.52g were recorded. The depth of hypocenter is approximately 5km below ground. The aftershock, magnitude ( $M_w=6.2$ ) occurred in 2011 Christchurch. Large PGAs were recorded at many sites (maximum PGA was 1.88g) (USGS).

Figure 2.6 shows the area of liquefaction and the sites of fault in 2010 Darfield and 2011 Christchurch earthquakes. It is confirmed that liquefaction was observed in whole area in Christchurch. Many bridges across the Avon River suffered from liquefaction induced ground failures. Significant lateral spreading and settlement of ground occurred around bridge sites and many roads was not in service after the earthquake occurred.

**Table 2.5 Observed ground motions at strong motion stations (Cubrinovski et al. 2011)**

Station Name	Code	R <sub>rup</sub> (km)	PGA <sub>h</sub> (g)	PGA <sub>v</sub> (g)	Station Name	Code	R <sub>rup</sub> (km)	PGA <sub>h</sub> (g)	PGA <sub>v</sub> (g)
Canterbury Aeroclub	CACS	12.8	0.21	0.19	Lyttelton Port Naval Point	LPOC	6.6	0.34	0.39
Christchurch Botanic Gardens	CBGS	4.7	0.50	0.35	North New Brighton School	NNBS	3.8	0.67	0.80
Christchurch Cathedral College	CCCC	2.8	0.43	0.79	Papanui High School	PPHS	8.6	0.21	0.21
Christchurch Hospital	CHHC	3.8	0.37	0.62	Pages Rd Pumping Station	PRPC	2.5	0.63	1.88
Cashmere High School	CMHS	1.4	0.37	0.85	Christchurch Resthaven	REHS	4.7	0.52	0.51
Hulverstone Dr Pumping Station	HPSC	3.9	0.22	1.03	Riccarton High School	RHSC	6.5	0.28	0.19
Heathcote Valley School	HVSC	4.0	1.41	2.21	Rolleston School	ROLC	19.6	0.18	0.08
Kaipoi North School	KPOC	17.4	0.20	0.06	Shirley Library	SHLC	5.1	0.33	0.49
Lincon School	LINC	13.6	0.12	0.09	Styx Mill Transfer Station	SMTC	10.8	0.16	0.17
Lyttelton Port	LPCC	7.1	0.92	0.51	Templeton School	TPLC	12.5	0.11	0.16

\*\* PGA<sub>h</sub> : Horizontal peak ground acceleration

\*\* PGA<sub>v</sub> : Vertical peak ground acceleration

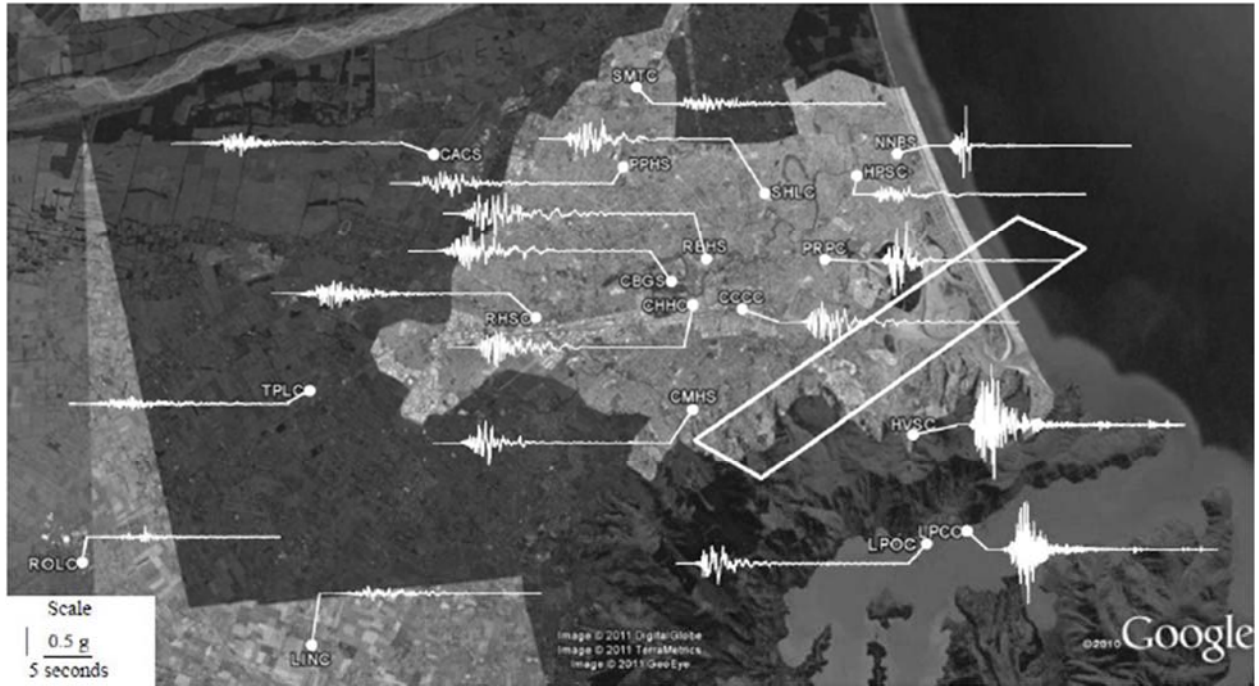


**Figure 2.5 Observed fault-normal horizontal acceleration time histories at various locations in the Christchurch region from the 22 February earthquake with reference to the inferred surface projection of the causative fault which dips to the south-east (Cubrinovski et al. 2011)**

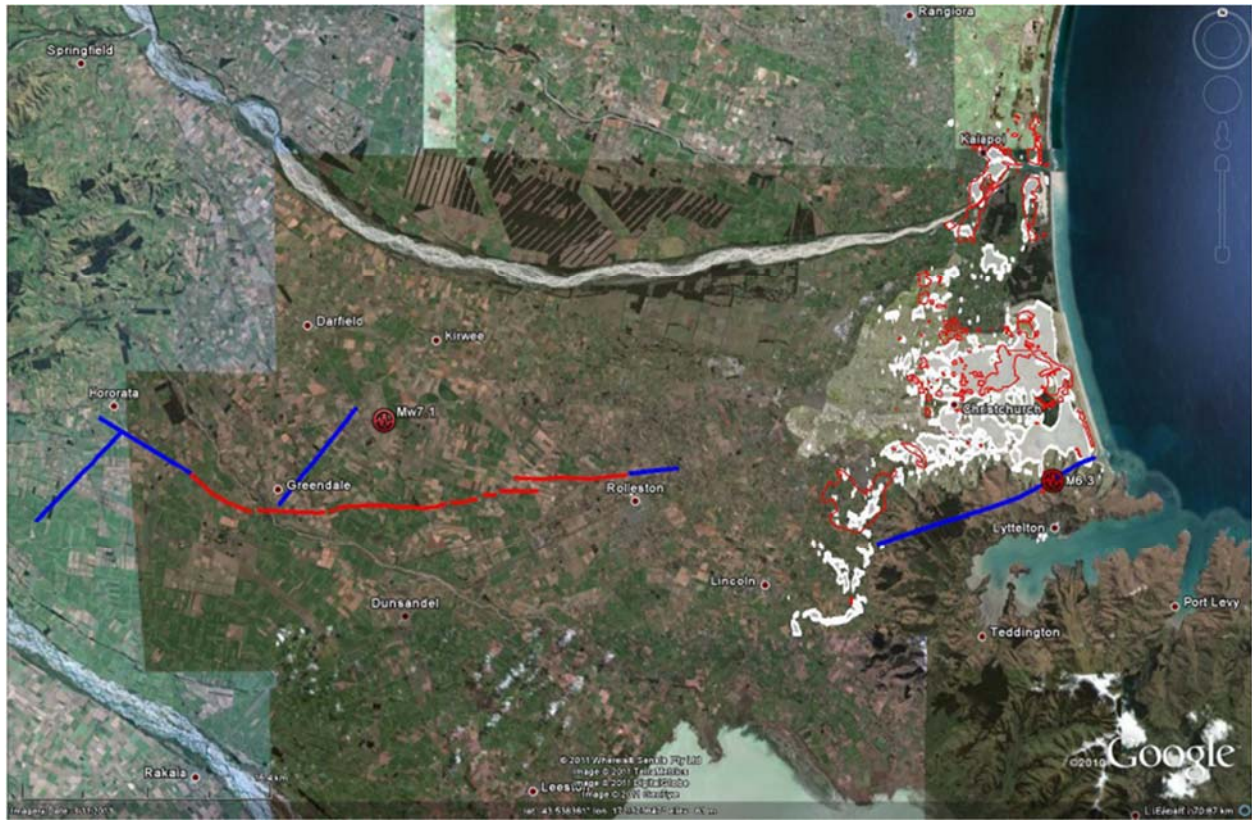


**Figure 2.6 Areas of induced liquefaction by the 4 September 2010 (red bordered areas) and 22 February 2011 (white shaded areas) earthquakes and associated fault ruptures (red – fault rupture with surface trace; blue – fault rupture with no surface trace) (NZ-GEER 2011)**

### **2.3.3. Case history data of liquefaction induced damages**

#### **The South Brighton Bridge**

South Brighton Bridge crosses the Avon River and was constructed in 1980 (in Figure 2.7). This bridge was constructed with a cast-in-place concrete three span deck (65m long) supported by precast post-tensioned I-beams. Two octagonal reinforced concrete piers with hammerhead pier caps support both the piers and the seat type abutments. The superstructure is fixed to the piers by steel shear keys (Palermo et al. 2011).

The octagonal precast concrete piles of the abutments and the pile caps of the piers are 450 mm wide, either vertical or raked (4 on 1). The length of the abutment piles is 18.7 m and the pier piles is 13.3 m long (Cubrinovski et al. 2013). The abutment longitudinal length is 1.9m, width is 16.7 m, and height is 3.57 m. The thickness of deck is 1.6 m. Ground investigations indicate that the depth of the ground water table is 1-2m below the bottom of the abutment (Haskell et al. 2013). The deck width is 15.2m (Priestley and Stockwell 1978).

The bridge embankments at both approaches were constructed with loose fill to a height of approximately 4.0 m. The upper 2.0 m of soil consist of sandy silt, fill, and lenses of peat (in Figure 2.12). Below this depth, uniform fine and medium loose sands extend up to 5 to 6 m in depth and medium dense sands extend to greater depths up to 25 m. Preliminary analyses of SPT and CPT data show that the soil up to 8 m in depth below the water table liquefied in the 2011 Christchurch earthquake (in Figure 2.7). Significant shear strains (cyclic softening) developed at the larger depths. Permanent lateral ground displacements of 2.9 m were observed approximately 23 m to the south from the west abutment of the bridge after the Christchurch earthquake (Cubrinovski et al. 2013).

Large ground distortion and slumping at the both approaches were observed. Large settlement of the approaches and vertical offset between the pile-supported bridge deck and embankment approaches on soft native soils were caused by the slumping. The slumping also caused displacement of both approaches toward river and the slope of the embankments (parallel to the river) (in Figure 2.8). The embankment approaches deformed and moved toward the river, but were restricted by the bridge structure (Cubrinovski et al. 2013).

Both abutments moved relative to the bridge deck. The east abutment moved about 0.22m, settled 0.030 m at north side, and lifted 0.045 m at south side, respectively. The west abutment moved 0.2 m, and settled 0.085 m at north side and 0.095 m at south side (in Figure 2.9). These displacements were measured after the Christchurch earthquake. The east abutment rotated about 7 degrees and the underlying soils spread laterally, which exposed the battered octagonal precast, prestressed concrete piles. Plastic hinges in the front and rear piles of the abutments were observed (in Figure 2.10). The west abutment rotated approximately 8 degrees following the Christchurch earthquake. Significant settlements of the soil beneath the west abutment occurred, which exposed the supporting piles. Note that there is fine sand underneath the abutment at this site. Figure 2.11 shows a comparison to the post-Darfield conditions. Significant settlement and ground spreading were observed (NZ-GEER 2011).



**Figure 2.7 Satellite image of South Brighton Bridge post-earthquake (NZ-GEER 2011)**

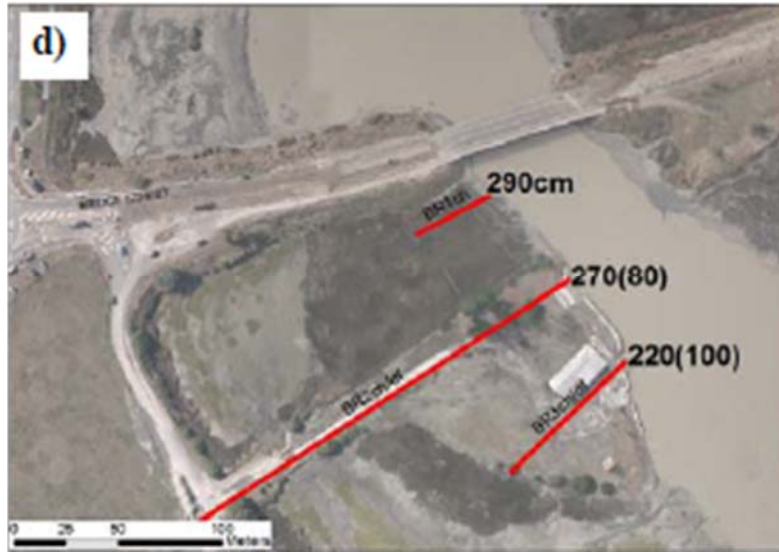


**Figure 2.8 Aerial view of South Brighton bridges, displacements of the river banks (in centimeters) for the Christchurch and Darfield earthquakes (Cubrinovski et al. 2013)**



**Figure 2.9 South Brighton bridge; a) horizontal movement of abutments compared to bridge deck; b) vertical position of abutment compared to bridge deck (NZ-GEER 2011)**



**Figure 2.10 Plastic hinging in abutment piles of Bridge Street Bridge (Palermo et al. 2011)**



**Figure 2.11 Comparison of the displacement of slope in front of western abutment following, a) Darfield event, b) Christchurch event (NZ-GEER 2011)**

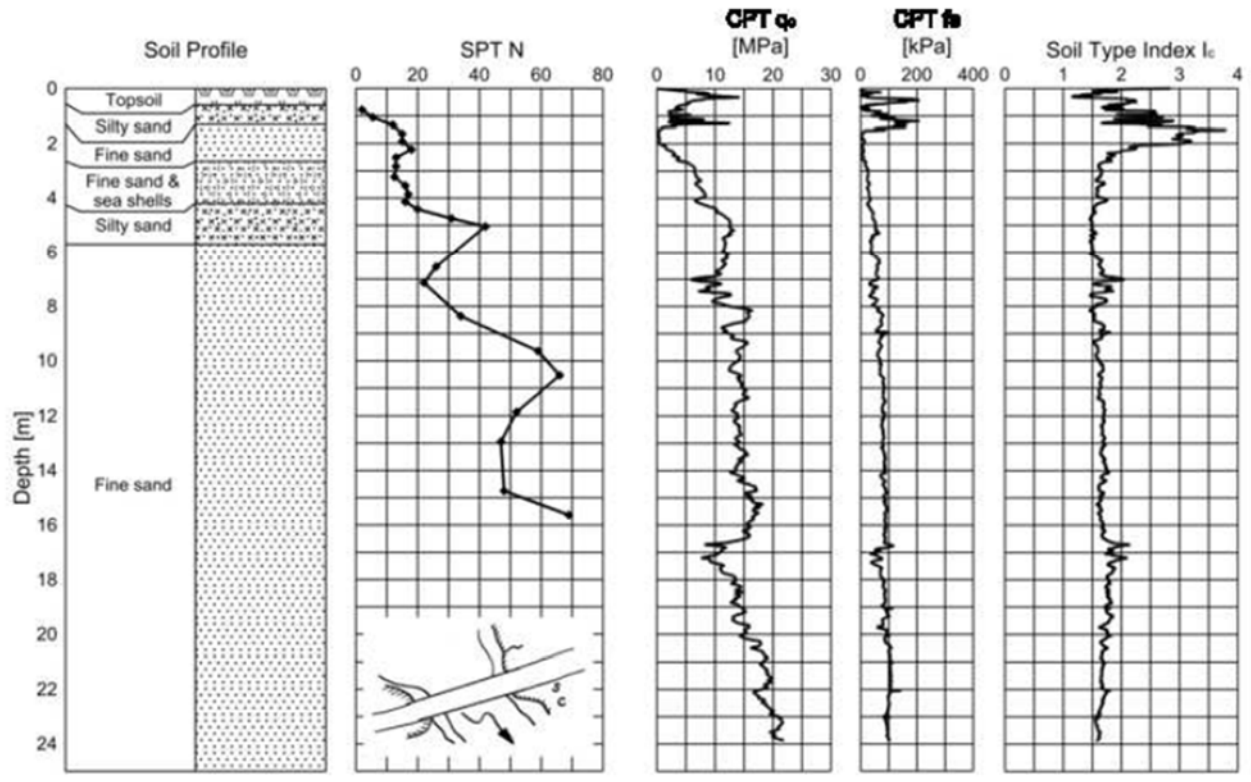


Figure 2.12 Soil profile, SPT and CPT data of South Brighton Bridge (Cubrinovski et al. 2013)

## 2.4. Case history data of 2011 Tohoku Earthquake, Japan, $M_w 9.0$

### 2.4.1. Overview of 2011 Tohoku Earthquake

On March 11, 2011, a very large ( $M_w 9.0$ ) earthquake and subsequent tsunami struck Japan. The earthquake was caused by a rupture on the subduction zone off the east coast of Japan. Because the earthquake was very large, widespread liquefaction was observed along the east coast of Japan, including the Tokyo Bay region.

Figure 2.6 shows acceleration records at the reported bridge sites (KiK-net). Large peak ground accelerations were recorded at many sites that are far from the epicenter. For example, a peak ground acceleration of 0.430 g was recorded at Ishimaki city ( $R_{rup} = 143\text{km}$ ) and a peak ground acceleration of 1.311 g was recorded at Omiya city ( $R_{rup} = 277\text{km}$ ). The variation in the seismic recordings indicates that ground accelerations are significantly affected by characteristics of soil properties and geometry.

Figure 2.13 shows liquefied sites within the Kanto area in Japan. The Tokyo and Chiba Bay areas were significantly damaged by liquefaction. The distance from the epicenter to these two bay areas is approximately 370 km and the recorded peak ground acceleration, for example in Chiba city, was 0.189 g. This acceleration is not large. However, the duration of the strong shaking is about 60 seconds at this site. The long duration shaking caused increasing excess pore water pressure, which in turn resulted in liquefaction. This observation has important implications for the northern California coast, which is prone to long-duration, high-intensity earthquake motions from the offshore subduction zone.

**Table 2.6 Acceleration records at the bridge sites (KiK-net)**

Station Name	Code	$R_{rup}$ (km)	$PGA$ (g)
Mito	IBR006	287	0.851
Omiya	IBR004	277	1.311
Koriyama	FKS018	234	1.11
Ishimaki	MYG010	143	0.487
Mizusawa	IWT011	188	0.359
Kesenuma	MYG001	143	0.430
Chiba	CHB009	370	0.189
Hurukawa	MYG006	174	0.585

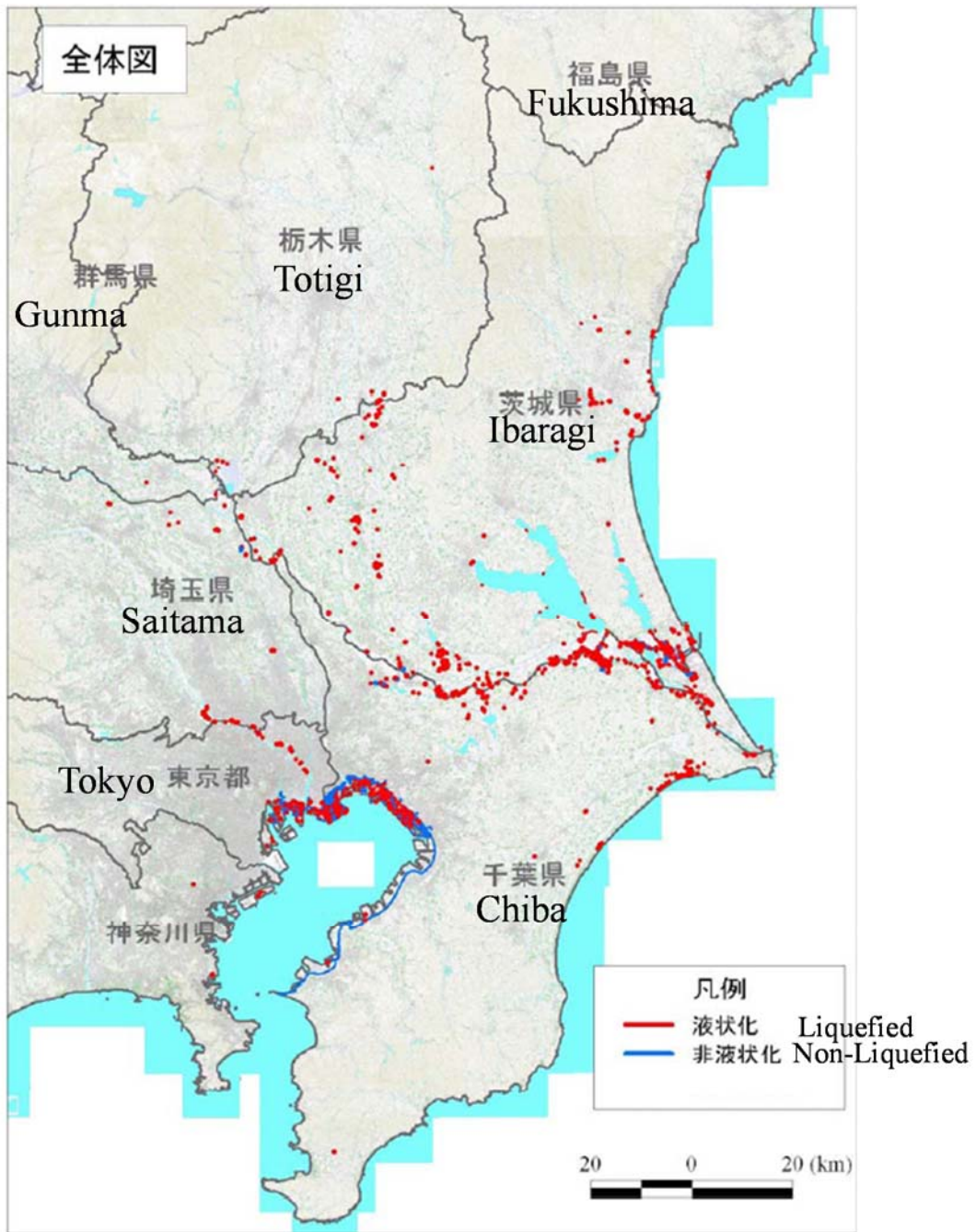


Figure 2.13 The map that liquefaction observed in Kanto area (JGS 2011)

## 2.4.2. Case history data of liquefaction induced damages

### The Mihama Bridge

Mihama Bridge crosses the Hanami River and was constructed in Chiba City in 1985. The reinforced concrete piers, supported by steel pile foundations, support the three span 177 m long and 39.0 m wide decks.

Figure 2.15- Figure 2.17 show the ground damage at the sea embankment that is at the vicinity of the east A2 abutment. Liquefaction caused many cracks on the sea embankment and on the ground near A2 abutment. Moreover, sand boils were observed. A ground settlement of about 20 cm at the side of the A2 abutment was measured (in Figure 2.15), which was caused by liquefaction judging from the relative ground settlement to the A2 abutment. This observation indicates that the A2 abutment did not settle (i.e., no discernible abutment settlement was measured). In addition, no gap between the A2 abutment and the deck was observed (in Figure 2.16). Two bearings were installed on the A2 abutment, however, the forward bolts that fixed the deck plates with the bearings were ruptured during the earthquake (in Figure 2.17). The backward bolts were loosened during the earthquake, and no gaps between the deck and bearings of A2 abutment were observed. Although some cracks on the box culvert were observed, there is possibility that these were not caused by the earthquake because the observed cracks appeared to be older (PWRI 2011).

Figure 2.18-Figure 2.23 show the ground displacement and settlement around the A1 abutment. The approximately 7 cm horizontal displacement perpendicular to the river of the A1 abutment was confirmed by measuring the gap between the retaining wall and A1 abutment (in Figure 2.28 and Figure 2.29). No ground settlement between the retaining wall and the A1 abutment was observed. Further, the approach road and the bearings did not experience significant damage. These observations indicate that A1 abutment and the retaining wall did not settle due to liquefaction. The differences in ground elevation between the box culvert and adjacent walkway were measured as approximately 33 cm (in Figure 2.21). Since the A1 abutment did not settle as mentioned above, it can be inferred the sea embankment and the walkway only settled approximately 33 cm. Figure 2.20 shows a settlement approximately 70 cm

at the face of the A1 abutment. Moreover, the horizontal ground displacement at the face of A1 abutment was also caused by liquefaction (in Figure 2.23). Spalling of concrete on the deck was observed, and the thickness of the spalling was about 1cm (PWRI 2011).

Figure 2.30 shows the bearing displacement of the A1 abutment, and a small gap between the deck and the parapet. Figure 2.31 shows that the bridge fall prevention device was loosened during the earthquake. Figure 2.32 shows that there were no gaps between upstream side retaining wall and the A1 abutment. No cracks were observed on the wall of A1 abutment (PWRI 2011).

Figure 2.33 shows the locations and cracks on the approach roadway. The ground damages (displacement and settlement) were also investigated. Four cracks were observed around the A1 abutment and the largest crack was about 0.18m. Standard penetrations testing (SPT) was conducted at the liquefied site around the A1 abutment April 23 – 26 in 2011 after the earthquake. Figure 2.34 - Figure 2.36 show the results of the SPT. Original SPT data, from when the bridge was constructed, are attached on the general drawing.

Judging from Standard penetration test (SPT) data (in Figure 2.34), loose sand fill soil from 2.0m to 12.0m, the loose sand layer and the loose sandy silt layer are embedded from 2.0m to -6.0m, the soft clayer silt from -6.0m to -7.5m, the dense sand layer from -7.5m to -9.5m, the soft clay layer from -9.5m to -13.5m, medium dense sand layer from -13.5m to -18.5m, dense sand layer from -18.0m to -23.5m, silt layer from -23.5m to -31.0m are embedded, respectively. The elevation of water table is 2.0m. (Chiba city 2011).

Figure 2.37 - Figure 2.39 show the piles and both A1 and A2 box culvert type abutment drawings. The A1 abutment is supported by 42 (3×12) steel pipe piles (i.e. not filled with concrete). The A1 steel pipe pile is 33m long that is composed of three 11m long portions. The diameter of each portion is 1,016mm. The thickness of the first portion (just beneath of the A1 abutment) is 14mm, and the second and third portions are 12mm thick. The 42 (3×12) steel pipe pile supporting A2 abutment is 44m long and composed of four 11m portions. The A2 steel pipe pile diameter is 1,016mm. The thickness of the first portion (beneath of the A2 abutment) is 14mm and the other portions are 12mm thickness.





Figure 2.16 No gaps between the deck and A2 abutment (Chiba city 2011)



Figure 2.17 Ruptured bolts of A2 abutment (Chiba city 2011)



Figure 2.18 Ground settlement at the side of A1 abutment (Chiba city 2011)



Figure 2.19 Ground settlement at the side of A1 abutment (H=260mm) (Chiba city 2011)



Figure 2.20 Ground settlement at the face of A1 abutment H=(Chiba city 2011)



Figure 2.21 Ground displacement (L=180mm) and settlement (H=330mm) near A1 abutment (Chiba city 2011)



Figure 2.22 Ground settlement at the face of A1 abutment H=630mm (Chiba city 2011)



Figure 2.23 Gap at the face of A1 abutment (Chiba city 2011)

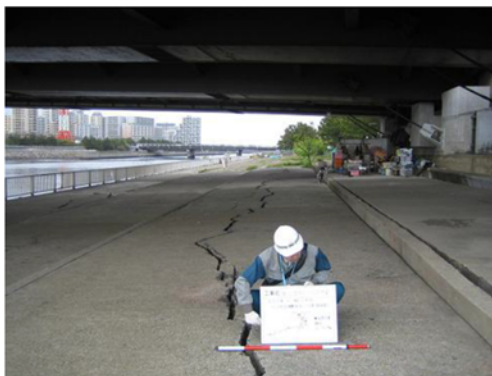


Figure 2.24 Cracks on the sea bank in front of the A1 abutment W=100mm (Chiba city 2011)



Figure 2.25 Cracks on the sea bank in front of the A1 abutment (Chiba city 2011)



Figure 2.26 Cracks on the sea bank  
W=100mm (Chiba city 2011)



Figure 2.27 Cracks on the A1 abutment  
approaching road W=50mm (Chiba city  
2011)



Figure 2.28 Gap between retaining wall and  
A1 abutment (Downstream side) (PWRI  
2011)



Figure 2.29 Gap between retaining wall and  
A1 abutment (about 7cm) (PWRI 2011)



Figure 2.30 Displacement of the bearing of A1 abutment (Chiba city 2011)



**Figure 2.31 Loosed bridge fall prevention device (PWRI 2011)**



**Figure 2.32 No gaps between A1 abutment and upstream side retaining wall (PWRI 2011)**

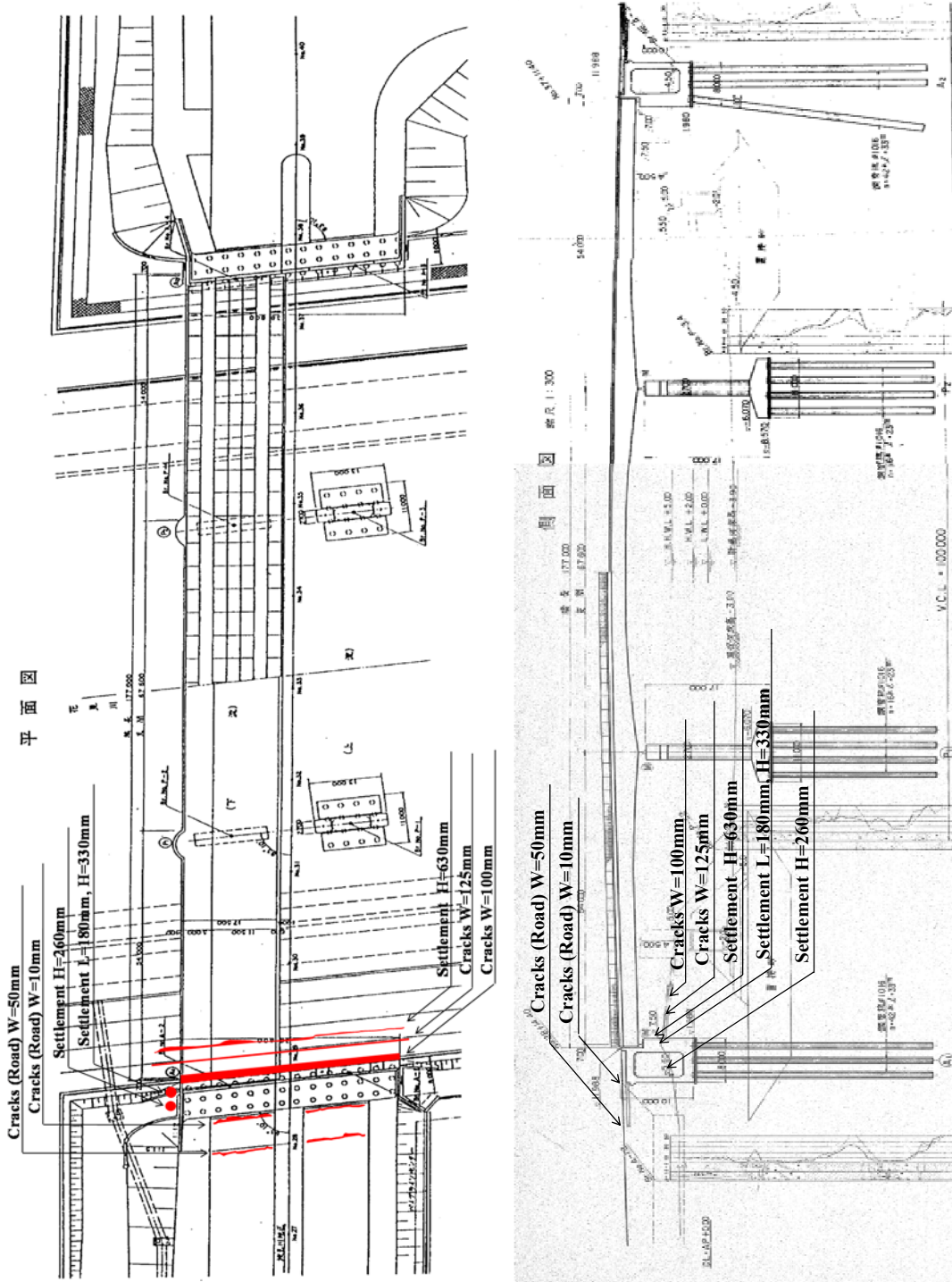


Figure 2.33 Observed cracks near the A1 abutment (Chiba city 2011)

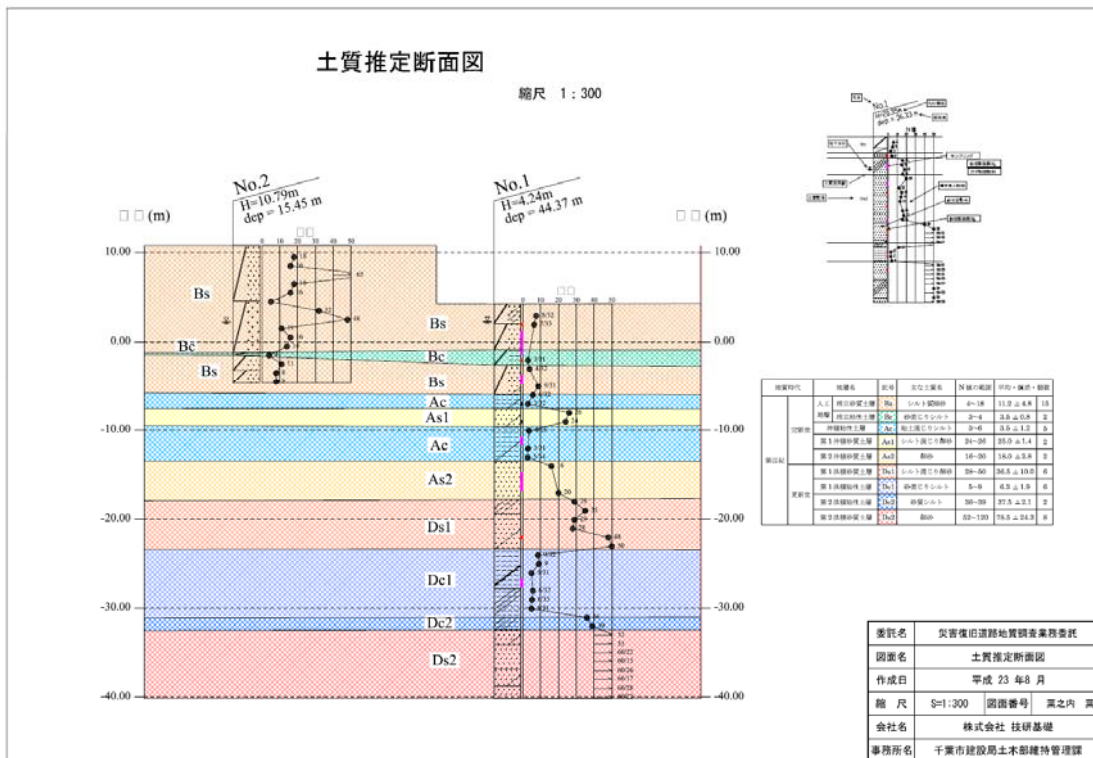
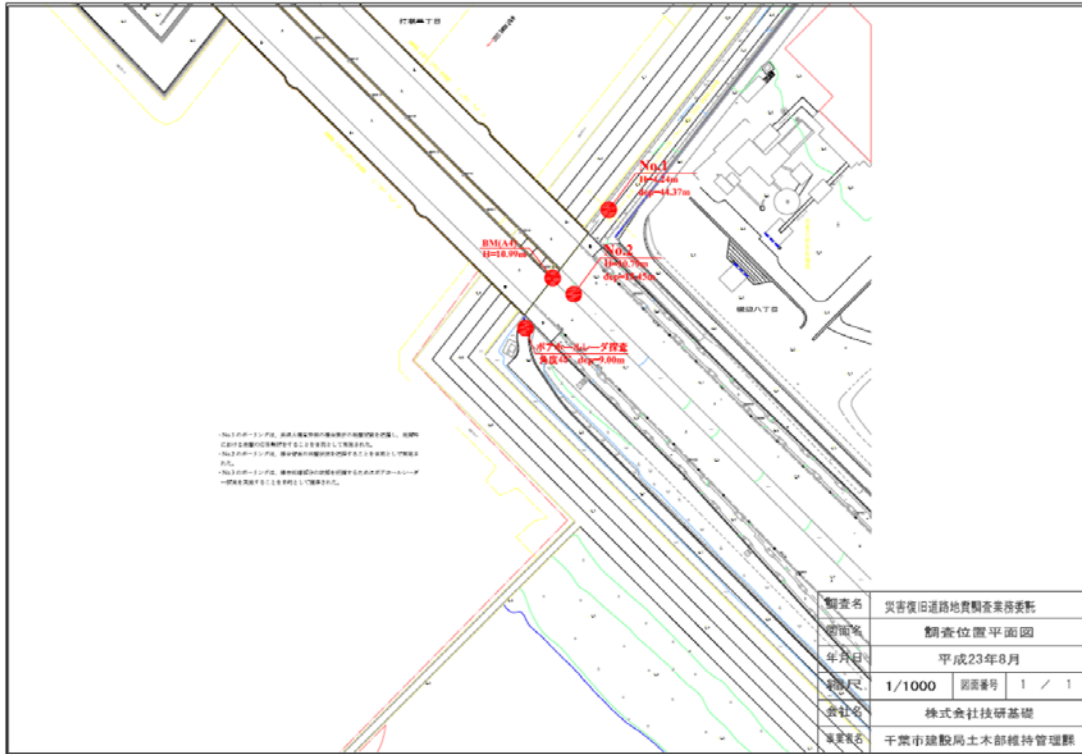


Figure 2.34 Boring data at the liquefied site near the A1 abutment (Investigated during 23-26 April in 2011) (Chiba city 2011)

# ボーリング柱状図

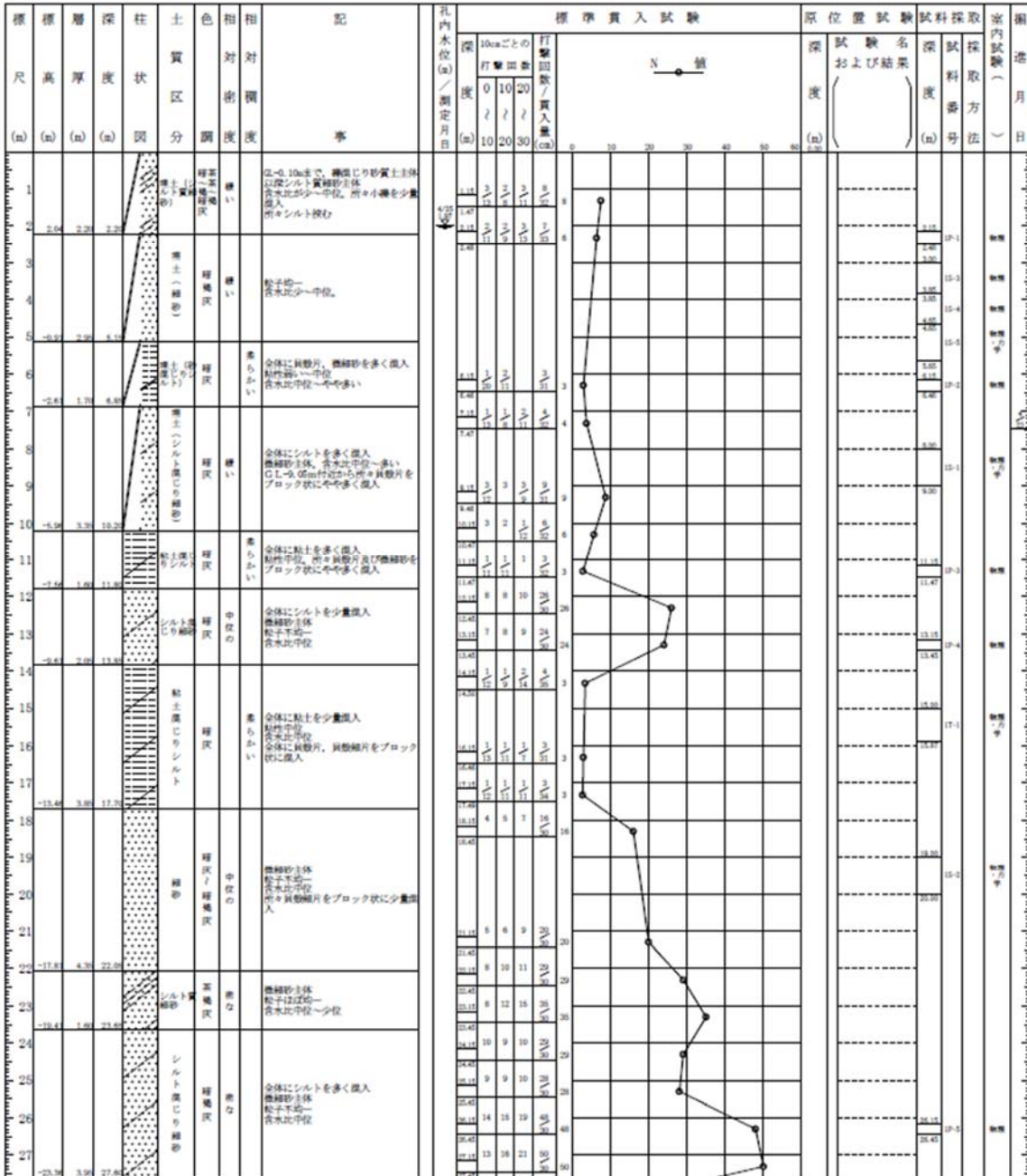
調査名 災害復旧道路地質調査業務委託

ボーリング№									
--------	--	--	--	--	--	--	--	--	--

事業・工事名

シート№

ボーリング名	No. 1	調査位置	千葉県美浜区磯辺八丁目			北緯	35° 37' 42.60"								
発注機関	千葉県建設局土木部維持管理課			調査期間	平成 23年 4月 23日 ~ 23年 4月 26日			東経	140° 2' 55.07"						
調査業者名	電設		主任技師	現場代理人	コ	ア	ボーリング責任者								
孔口標高	日= 4.26m	角	180°	方	北0°	東90°	西270°	南180°	地盤勾配	水平0°	使用機種	試験機	エンジン	ハンマー落下用具	ポンプ
総掘進長	44.37m	度	90°	度	度	度	度	度	度	度	度	度	度	度	度
												KAN0-KR100H	ヤンマー-NFD12-EK	平日動落下式	KAN0-V5







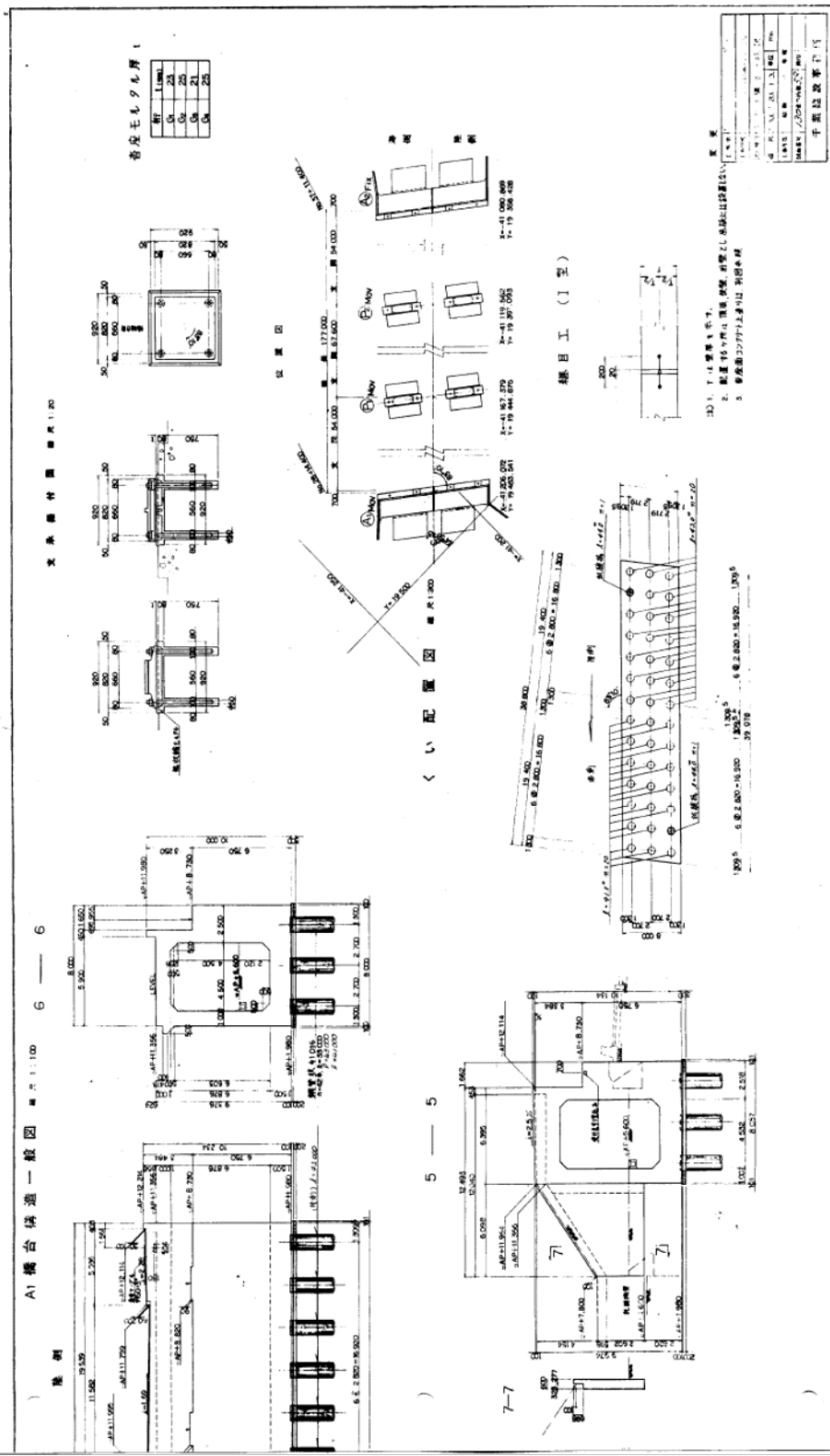


Figure 2.37 The A1 abutment drawings





## **2.5. Summary**

In Chapter 2, case history data for 2010 Chile earthquake, 2010-2011 Christchurch, New Zealand earthquake sequence, and 2011 Tohoku earthquake in Japan were described. In 2010 Chile and 2011 Tohoku earthquake, shaking-induced damage, tsunami-induced damage, and liquefaction-induced damage was observed. In 2010, 2011 sequences earthquake in New Zealand, the significant liquefaction and liquefaction-induced ground failures were observed. The focus of this report, and this chapter, is on liquefaction-induced ground failure. Ground settlement and lateral spreading occurred in the vicinity of the abutments and embankments of bridges in all three countries. As a result of the ground displacements, the foundations of abutments and piers were displaced. Approach roads to bridges settled and many bridges were closed after the earthquakes occurred. The most complete case history data, in terms of earthquake data, soils information, bridge details, and damage details, were selected from three particular bridges – the Mataquito Bridge in Chile, the South Brighton Bridge in New Zealand, and the Mihama Bridge in Japan. These three bridge case histories are the focus of the analysis section of this report.

## **Chapter 3. CASE HISTORY DATA ANALYSIS**

### **3.1 Introduction**

High quality data, including soil profiles (SPT or CPT), bridge descriptions, and ground and bridge damages, were selected from the collected data for estimating the pile foundation performance. The selected data also includes the accurate ground deformations or structure displacements due to liquefaction. Because the recommended procedures require an estimate of ground displacement, a comparison of the estimated displacement to observed deformations or displacement can show the accuracy of the procedures.

The Mataquito Bridge in Chile, South Brighton Bridge in New Zealand, and Mihama Bridge in Japan were selected. These bridges suffered from minor to large liquefaction and lateral spreading. Also, these bridges are composed of different spans, abutment sizes, pile foundations, and materials. The analysis and designing for these bridge's pile foundations can estimate the important factors for applicability of the procedures.

All symbols and equations utilized in this section are from Shantz (2013).

### 3.2 Case study: the Mataquito Bridge in Chile

#### 4.2.1 Observed damages of the Mataquito Bridge

Bridge performances and ground failures of the Mataquito Bridge as discussed in Chapter 2 are mentioned again here to compare the results of the analysis and the observed damages. Table 3.1 shows the observed damages on the Mataquito Bridge. The backfill soil of the north abutment settled approximately from 0.05m to 0.1m. Ground displacement due to liquefaction was approximately 54cm from the edge of the north abutment wall to the first row of piers. The approach embankment also experienced transverse displacement about 60cm from the centerline. North abutment displaced less than 0.02m, however no cracks on the abutment, and no settlement or rotation of the abutment was observed.

According to RENADIC (2010), peak ground accelerations (PGAs) recorded at Hualañe, which is located at east of Iloca, were 0.389g in the longitudinal direction, 0.390g in the vertical direction, and 0.461g in the transverse direction.

**Table 3.1 Observed damages of the ground and bridge structure, the Mataquito Bridge**

Observed damages	
Ground failures	<ul style="list-style-type: none"> <li>- Backfill soil of the north abutment settled from 0.5m to 1.0m</li> <li>- Ground displacement due to liquefaction about 54cm from the edge of the north abutment wall to the first row of piers was observed</li> <li>- The approach embankment also experienced transvers displacement about 60cm from the centerline</li> </ul>
Bridge damages	<ul style="list-style-type: none"> <li>- North abutment displaced less than 0.02m, however no cracks on the abutment was observed.</li> <li>- No settlement and rotation of the abutment was observed.</li> </ul>

### 3.2.2. Liquefaction potential evaluation

Liquefaction potential evaluation for the north Mataquito Bridge abutment is performed to identify the potential occurrence of liquefaction and the thickness of liquefiable layers. The evaluation procedures followed Idriss and Boulanger (2008). Details of the procedures are described in Appendix A.

Figure 3.1 shows that the result of liquefaction potential evaluation. Cyclic resistance ratio (CRR) is estimated based on SPT N-value reported by Ledezma et al. (2011). Factor of safety shows that most susceptible liquefiable layer is embedded from 0m to -4.5m. Although the factor of safety at the depth 11m are less than one, the factor of safety is close to one and this layer is thin. Displacement effects against piles are relatively small. Also, the factor of safety at the depth from 21m to 22m is less than one, however, this layer is not expected to liquefy because of high vertical effective stress. Therefore, liquefaction is not expected at this depth. Ledezma et al. (2011) reported that liquefiable fine sand layer, 5m thickness, at north abutment is embedded. Judging from liquefaction potential evaluation and Ledezma et al. (2011), the liquefiable layer at the Mataquito Bridge is embedded from 0m to -4.5m.

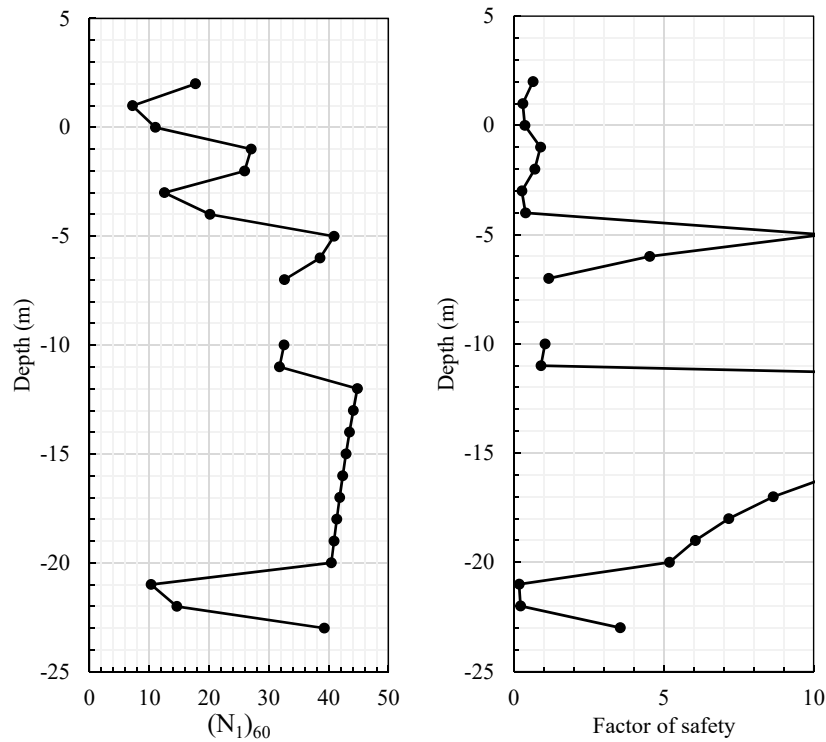


Figure 3.1 Results of the liquefaction potential evaluation, the Mataquito Bridge

### 3.2.3. Description of north abutment foundation of Mataquito Bridge

The width of the north abutment of Mataquito Bridge is 14.0m, the height 10.0m, and the length 8.0m, respectively. Eight reinforced concrete piles (Diameter B = 1.5m, 6m spacing and 17m long) support the north abutment (McGann et al. 2012). The embankment height 7.8m and the 25° degree of slope are assumed. No SPT N-values of the backfill are reported. Then, the friction angle of the backfill is estimated using the SPT N-value from 0m – 2.5m of the in front of the abutment. For liquefiable layer, Ledezma et al. (2012) reported that SPT N-value of liquefiable layer is from 5 to 20 blows/foot that is obtained before the earthquake. Judging from the SPT N-value provided by Ledezma et al. (2012), average N-value for the liquefiable layer is approximately 10. Internal friction angle is determined using equation (4.1), which is developed by Hatanaka and Uchida (1996).

$$\phi = \sqrt{20N_1} + 20 \quad (33)$$

Soil unit weight is estimated from Kulhawy and Mayne (1990). Figure 3.2 shows the sketch of the soil layers and the approach embankment of Mataquito Bridge. Figure 3.3 shows the sketch of the embankment.

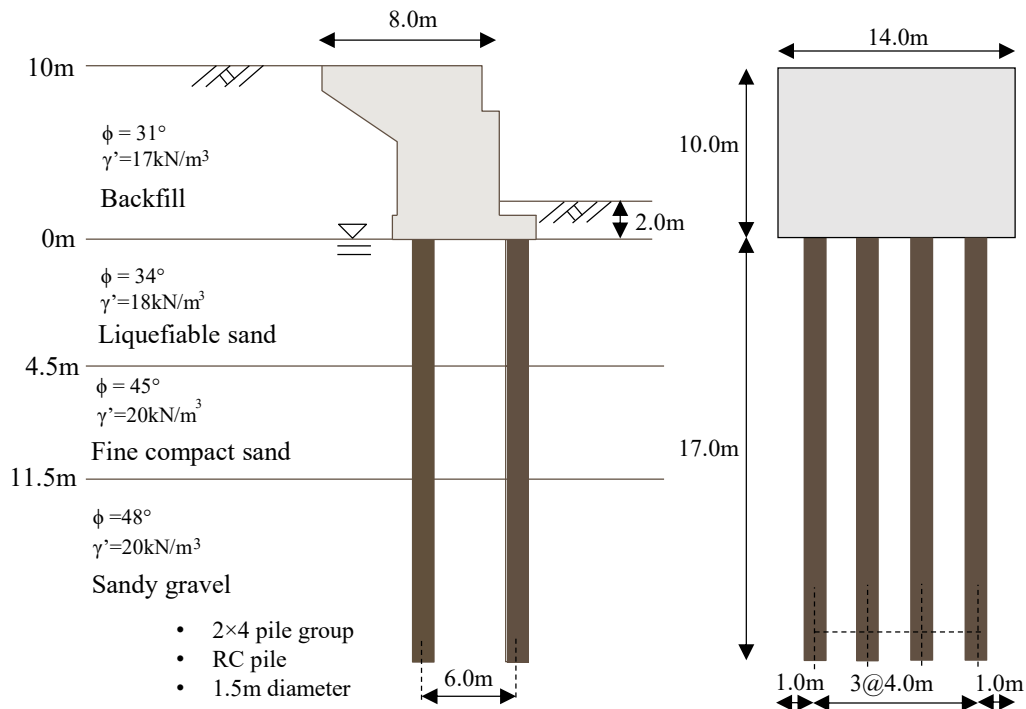
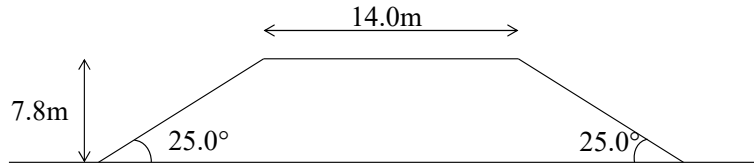


Figure 3.2 Sketch of north abutment foundation of the Mataquito Bridge



**Figure 3.3 Sketch of the approach embankment of the Mataquito Bridge**

### 3.2.4. Analysis of the Mataquito Bridge with the equivalent single pile method

#### 1. Modeling a group pile as an equivalent single pile

An equivalent non-linear single pile is modeled simply by multiplying bending stiffness by the number of piles. The abutment section is described as very stiff pile, and the bending stiffness is multiplied by a number of piles and one hundred. Figure 3.4 shows the modeling of group pile with an equivalent single pile.

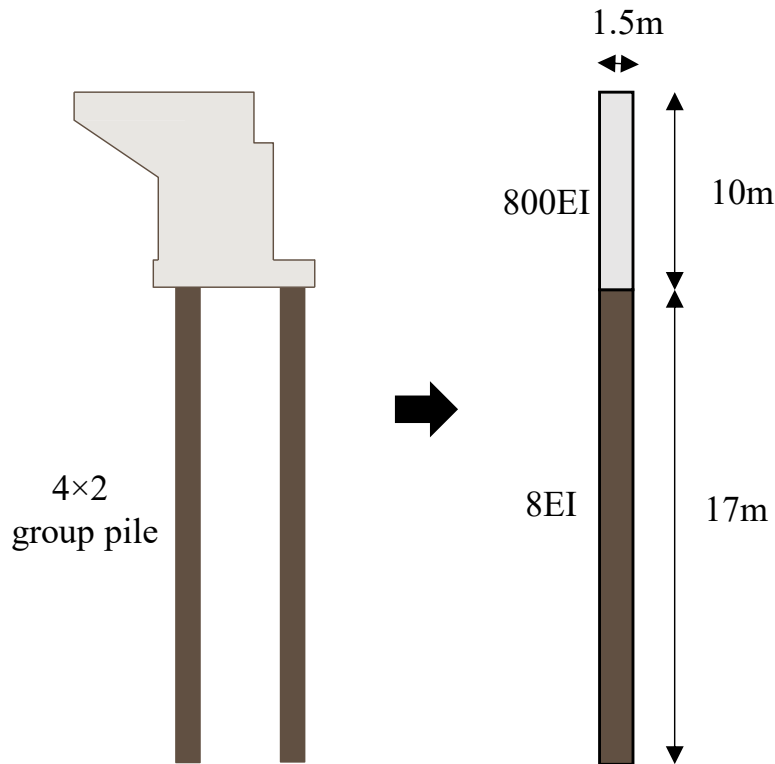


**Figure 3.4 Modeling of an equivalent single pile, the Mataquito Bridge**

**File section properties**

The following properties shown in Table 3.2 are utilized to model the equivalent non-linear single pile. The bar size and number of bars are referred from McGann et al. (2012). Figure 3.5 and Figure 3.6 show the bending moment and bending curvature diagram of the group pile section and the abutment section. Parameters used for LPILE 2012 to model the equivalent non-linear single pile of the Mataquito Bridge are shown in Appendix B.

**Table 3.2 Pile section properties of the Mataquito Bridge for original single pile**

Concrete compressive strength (MPa)	Yield stress of reinforcing bar (MPa)	Elastic modulus of reinforcing bar (GPa)	Bar size (mm)	Number of bars	Concrete Cover to Edge of Bar (mm)
25	412	200	36	30	70

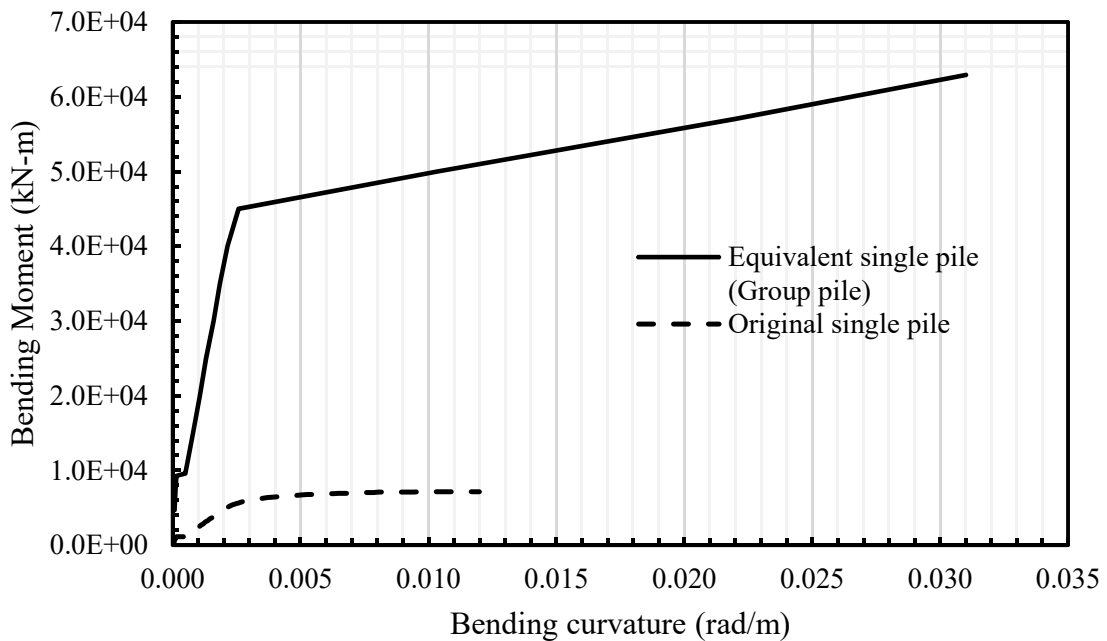


**Figure 3.5 Bending moment – bending curvature of the group pile section, the Mataquito Bridge**

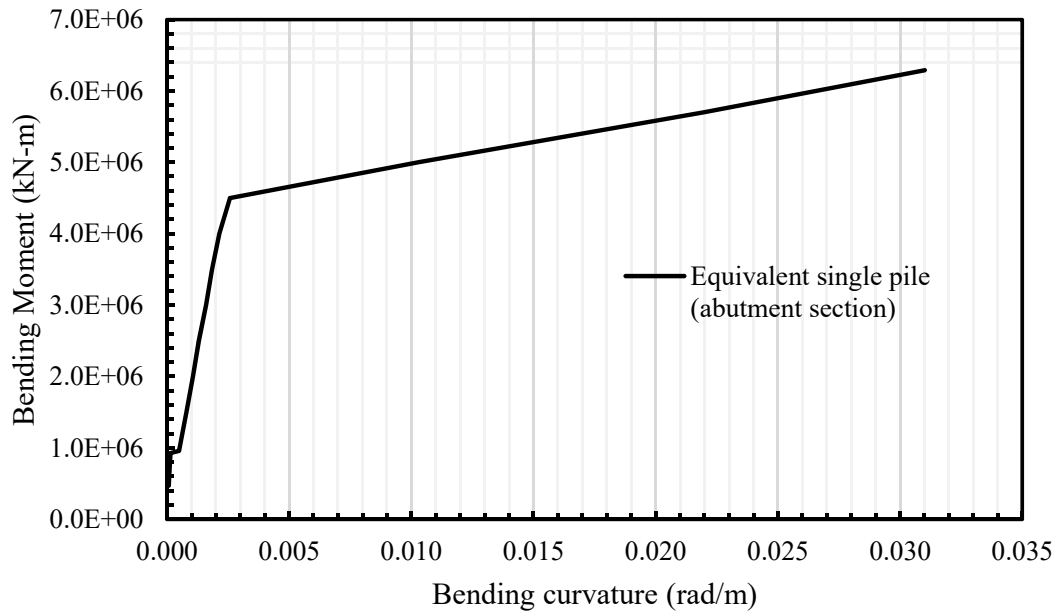


**Figure 3.6 Bending moment – bending curvature of the abutment section, the Mataquito Bridge**

## 2. Calculation of Foundation Loads Due to the Soil Crust

### 2.1. Dimension parameters of the pile cap

To estimate the lateral load of the crust layer against the piles, the length and width dimensions  $W_T$  and  $W_L$ , the pile cap thickness  $T$ , the embedment depth to top the cap  $D$ , and the crust thickness,  $Z_c$ , are required. These parameters are shown in Table 3.3.

**Table 3.3 Dimension parameters of the Mataquito Bridge**

$W_T$ (m)	$W_L$ (m)	$T$ (m)	$D$ (m)	$Z_c$ (m)
14.0	8.0	10.0	0.0	10.0

### 2.2. Determination of p-y curve for crust layer

The elevation of the abutment bottom is the same as that of the ground water table. Case A, which considers the bottom of the abutment acts in the crust layer, is not appropriate for the Mataquito Bridge case. Therefore, Case B is utilized to calculate passive loads and to develop p-y response.

The ultimate force  $F_{ULT-B}$  is expressed as

$$F_{ULT-B} = F_{PASSIVE-B} + F_{SIDES-B}$$

#### $F_{PASSIVE-B}$

$F_{PASSIVE-B}$  is expressed as

$$F_{PASSIVE-B} = \left( \bar{\sigma}_v \cdot K_p + 2 \cdot c' \cdot \sqrt{K_p} \right) \cdot (T) \cdot (W_T) \cdot (k_w)$$

Coefficient of passive pressure  $K_p$  is calculated using Rankine theory.

$$\begin{aligned} K_p &= \tan^2 \left( 45 + \frac{\phi}{2} \right) \\ &= \tan^2 \left( 45 + \frac{40}{2} \right) = 4.60 \end{aligned}$$

$k_w$  is developed by Ovesen (1964) and is expressed as the following equation.

$$\begin{aligned} k_w &= 1 + (K_p - K_a)^{\frac{2}{3}} \cdot \left[ 1.1 \cdot \left( 1 - \frac{T}{D+T} \right)^4 + 1.6 / \left( 1 + \frac{5W_T}{T} \right) + 0.4 \cdot (K_p - K_a) \cdot \left( 1 - \frac{T}{D+T} \right)^3 / \left( 1 + \frac{0.05W_T}{T} \right) \right] \\ &= 1 + (4.60 - 0.217)^{\frac{2}{3}} \cdot \left[ 1.1 \cdot \left( 1 - \frac{10}{0+10} \right)^4 + 1.6 / \left( 1 + \frac{5 \cdot 14}{10} \right) + 0.4 \cdot (4.60 - 0.217) \cdot \left( 1 - \frac{10}{0+10} \right)^3 / \left( 1 + \frac{0.05 \cdot 14}{10} \right) \right] \\ &= 1.53 \end{aligned}$$

Therefore,

$$F_{PASSIVE-B} = \left( 85 \cdot 4.60 + 2 \cdot 0 \cdot \sqrt{4.60} \right) \cdot (10) \cdot (14) \cdot (1.53) = 83,752 (kN)$$

#### $F_{SIDES-B}$

$F_{SIDES-B}$  is calculated using the following equation.

$$\begin{aligned} F_{SIDES-B} &= 2 \cdot \left( \bar{\sigma}_v \cdot \tan(\delta) + \alpha c' \right) \cdot W_L \cdot T \\ &= 2 \cdot \left( 85 \cdot \tan(40/3) + 0.5 \cdot 0 \right) \cdot 8.0 \cdot 10 = 3,223 (kN) \end{aligned}$$

## FULT-B

The total ultimate crust load of case B becomes the following value.

$$F_{ULT-B} = 83,752 + 3,223 = 86,975(kN)$$

### 2.3. Determination of $\Delta_{MAX}$

The maximum displacement  $\Delta_{MAX}$  of crust layer for p-y curve at the maximum force is calculated by following equation.

$$\Delta_{MAX} = (T) \cdot (0.05 + 0.45 \cdot f_{depth} \cdot f_{width})$$

The modification factors  $f_{depth}$  and  $f_{width}$  are expressed with the following equations.

$$\begin{aligned} f_{depth} &= EXP\left[-3 \cdot \left(\frac{Z_c - D}{T} - 1\right)\right] \\ &= EXP\left[-3 \cdot \left(\frac{10-0}{10} - 1\right)\right] = 1 \end{aligned}$$

$$\begin{aligned} f_{width} &= \left\{ \left[ 10 / \left( \frac{W_T}{T} + 4 \right) \right]^4 + 1 \right\}^{-1} \\ &= \left\{ \left[ 10 / \left( \frac{14}{10} + 4 \right) \right]^4 + 1 \right\}^{-1} = 0.078 \end{aligned}$$

Then, the maximum displacement  $\Delta_{MAX}$  becomes the following equation.

$$\begin{aligned} \Delta_{MAX} &= (T) \cdot (0.05 + 0.45 \cdot f_{depth} \cdot f_{width}) \\ &= (10) \cdot (0.05 + 0.45 \cdot 1 \cdot 0.078) = 0.85(m) \end{aligned}$$

### p-y curve for the abutment section

$F_{ULT}$  is the total lateral force of crust layer along with the abutment. To obtain the p-y curve of the abutment section,  $F_{ULT}$  is divided by the pile cap (abutment) height.  $p_{ult}$  is calculated by the following equation.

$$p_{ULT} = F_{ULT}/T = 86,975/10 = 8,697(kN/m)$$

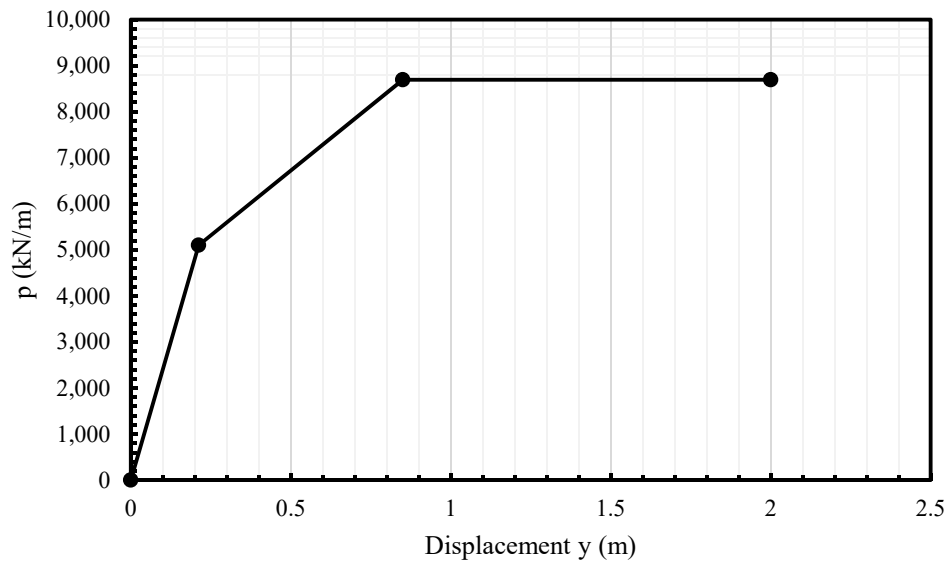


**Figure 3.7 p-y curve for the Mataquito Bridge's abutment**

### **3. Calculation of p - y Curves for Piles**

The subgrade reactions for the equivalent single pile is described as the following equation.

$$P_{SUPER} = n \cdot m_p \cdot P_{SINGLE}$$

#### **3.1. Evaluating the group reduction factor**

Non-liquefiable soil layer

The modification factor  $m_p$  for non-liquefiable soil layers for group piles can be evaluated using Mokwa et al. (2000). With this method, the reduction factor is described simply as a function of pile space. For the group piles of the Mataquito Bridge, the average  $m_p$  should be used.

$$m_p = \frac{\text{First\_row} + \text{Second\_row}}{2} = \frac{0.87 + 0.77}{2} = 0.82$$

### Liquefiable soil layer

The reduction factor for liquefiable soil layers is calculated a function of correlated SPT N-values.  $(N_1)_{60,CS}$  values should be averaged through the liquefiable layer. According to Ledezma et al, (2012) the SPT values are from 5 to 20 blow counts. In this analysis,  $(N_1)_{60,CS}$  is assumed as equal to  $N_1$  because no information about rod properties or fines content was provided.  $(N_1)_{60,CS} = 10$  is used for  $m_p$ .

$$\begin{aligned} m_p &= 0.0031(N_1)_{60,CS} + 0.00034(N_1)_{60,CS}^2 \\ &= 0.0031 \cdot 10 + 0.00034 \cdot 10^2 = 0.065 \end{aligned}$$

For the Mataquito Bridge analysis,  $m_p = 0.15$  for the liquefiable layer is also applied.

### **3.2.Modification of the group reduction factor near liquefied soil layer boundary**

The effective distance of the vicinity of liquefied layer for p-y curve is estimated by pile diameter and modification factor  $S_b$ . The  $S_b$  and the effective distance are obtained from the following equations.

$$S_b = 2 - (B - 1) / 2 = 2 - (1.5 - 1) / 2 = 1.75$$

$$S_b \cdot B = 1.75 \cdot 1.5(m) = 2.62(m)$$

The subgrade reaction of a group pile for Winkler type soils is described as a function of the relative displacement of piles, the stiffness factor  $k$ , and the reduction factor  $m_p$ . In this analysis,  $m_p$  is also modified to account for the effect of liquefaction for p-y curve at the vicinity of liquefied layer. Table 3.4 shows the reduction factor  $m_p$  at the vicinity of liquefied layer and Table 3.5 shows reduction factors for each depth.

**Table 3.4 Reduction factor for vicinity of liquefied layer for the Mataquito Bridge**

Distance from the liquefied layer (m)	Adjustment factor	$m_p$
0.9	$\frac{1}{3} + \frac{2}{3} \cdot \frac{P_L}{P_H} = 0.37$	$0.37 \cdot 0.82 = 0.31$
1.7	$\frac{2}{3} + \frac{1}{3} \cdot \frac{P_L}{P_H} = 0.69$	$0.69 \cdot 0.82 = 0.56$
2.62	1	0.82

**Table 3.5 Reduction factor for each depth, the Mataquito Bridge**

Depth (m)	$m_p$	$n \times m_p$
0-10	1	1
10-14.5	0.065	0.52
14.5-15.4	0.31	2.5
15.4-16.2	0.56	4.5
16.2-27	0.82	6.5

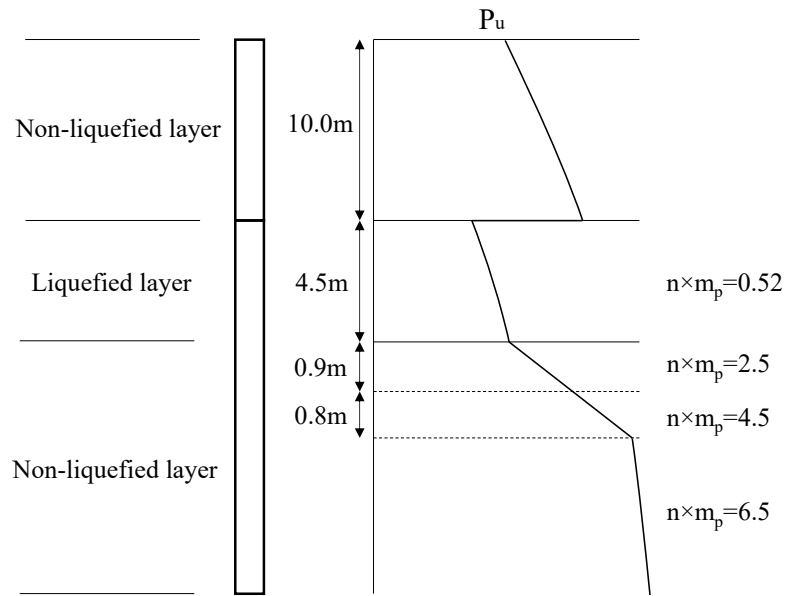


**Figure 3.8 Modification factor near liquefiable layers, the Mataquito Bridge**

#### 4. Estimation of ground displacement

##### Slope stability analysis

The restricted crust displacement is evaluated using the formula developed by Bray and Travasarou (2007). The horizontal acceleration is estimated using GeoStudio 2012 software. For Mataquito Bridge case, the abutment was not plunged into wing walls and no damages were observed on the abutment. A lateral force from the bridge deck against the backfill soil is not expected. Therefore,  $F_{DECK}$  is not considered for the Mataquito Bridge.

The residual shear strength calculated using Kramer (2008) is applied for the liquefied layer. The average effective stress at the center of liquefiable layer is given by following equation. The average  $(N_1)_{60}$ -value of the liquefiable layer is 10.

- 1) For the liquefiable layer under backfill soil and the abutment

$$\begin{aligned}\bar{\sigma}'_v &= 17(kN / m^3) \cdot 10(m) + 18(kN / m^3) \cdot 2.25(m) - 9.8(kN / m^3) \cdot 2(m) \\ &= 188(kPa) = 3,926(psf)\end{aligned}$$

$$\begin{aligned}S_r &= 2,116 \cdot \exp \left[ -8.444 + 0.109 \cdot \overline{(N_1)_{60}} + 5.379 \cdot \left( \bar{\sigma}'_v / 2,116 \right)^{0.1} \right] \\ &= 2,116 \cdot \exp \left[ -8.444 + 0.109 \cdot 10 + 5.379 \cdot (3,926 / 2,116)^{0.1} \right] = 413(psf) = 19(kPa)\end{aligned}$$

- 2) For the liquefiable layer under the front of the abutment

$$\begin{aligned}\bar{\sigma}'_v &= 17(kN / m^3) \cdot 2(m) + 18(kN / m^3) \cdot 2.25(m) - 9.8(kN / m^3) \cdot 2.25(m) \\ &= 52(kPa) = 1,086(psf)\end{aligned}$$

$$\begin{aligned}S_r &= 2,116 \cdot \exp \left[ -8.444 + 0.109 \cdot \overline{(N_1)_{60}} + 5.379 \cdot \left( \bar{\sigma}'_v / 2,116 \right)^{0.1} \right] \\ &= 2,116 \cdot \exp \left[ -8.444 + 0.109 \cdot 10 + 5.379 \cdot (1,086 / 2,116)^{0.1} \right] = 207(psf) = 9.9(kPa)\end{aligned}$$

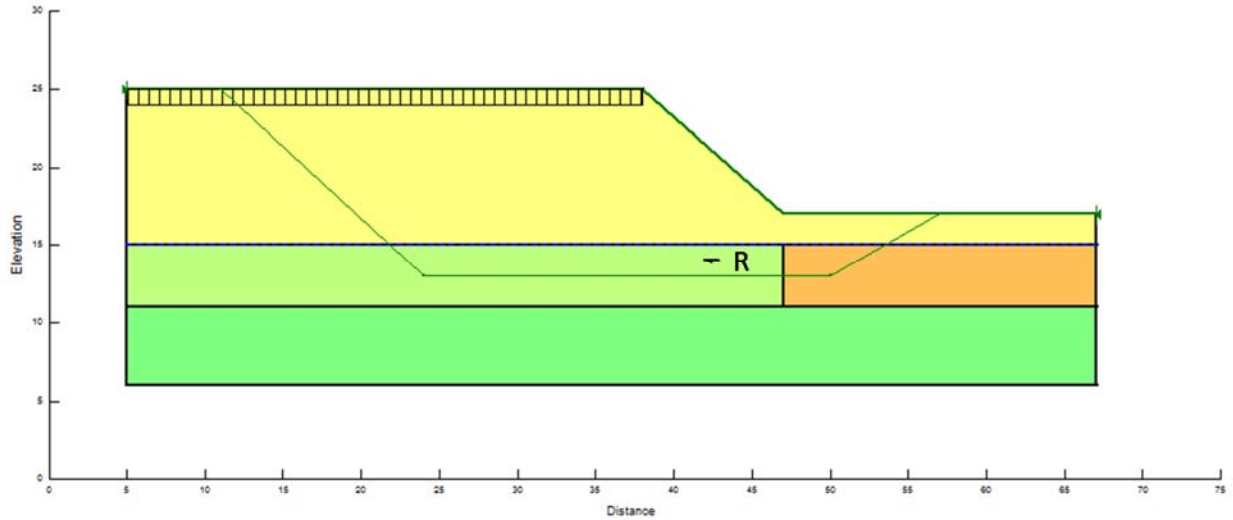


**Figure 3.9 Slope stability analysis model to determine coefficient of horizontal acceleration, the Mataquito Bridge**

The effective width is calculated using the following equation.

$$W_{\text{Effective}} = W_T + m/2 \cdot H$$

$$= 14.0 + 2.14/2 \cdot 7.8 = 22.3(m)$$

For slope stability analysis, Bishop, Janbu, and Spencer analysis methods are utilized to estimate possible displacements. Table 3.6 and Table 3.7 show results of slope stability analysis using the Bishop method. PGA was recorded in the transverse and longitudinal direction, respectively. The displacements are estimated using both transverse and longitudinal PGA values. The results using Spencer and Janbu methods are shown in Appendix C. Figure 3.10 and Figure 3.11 show the displacement – shear force diagram using the Bishop, Janbu, and Spencer methods. The following shows a sample calculation of the displacement using Bray and Travararou (2007).

$$D(cm) = \exp \left\{ -0.22 - 2.83 \cdot \ln(0.087) - 0.333 \cdot [\ln(0.087)]^2 + 0.566 \cdot \ln(0.087) \cdot \ln(0.461) \right. \\ \left. + 3.04 \cdot \ln(0.461) - 0.244 \cdot [\ln(0.461)]^2 + 0.278 \cdot (8.8 - 7) \right\}$$

$$= 43.6(cm)$$

**Table 3.6 Slope stability results. Displacements are determined using Bray and Travasarou (2007), the Mataquito Bridge (PGA = 0.461g)**

Bishop			
$k_y$	R (kN/m)	$R \cdot W_{T\text{-effective}}$ (kN)	D (cm)
0.087	0	0	43.6
0.11	90	2,007	29.1
0.14	200	4,460	18.5
0.17	310	6,913	12.5
0.2	420	9,366	8.8
0.23	530	11,819	6.4
0.26	640	14,272	4.8
0.29	750	16,725	3.7
0.32	880	19,624	2.9

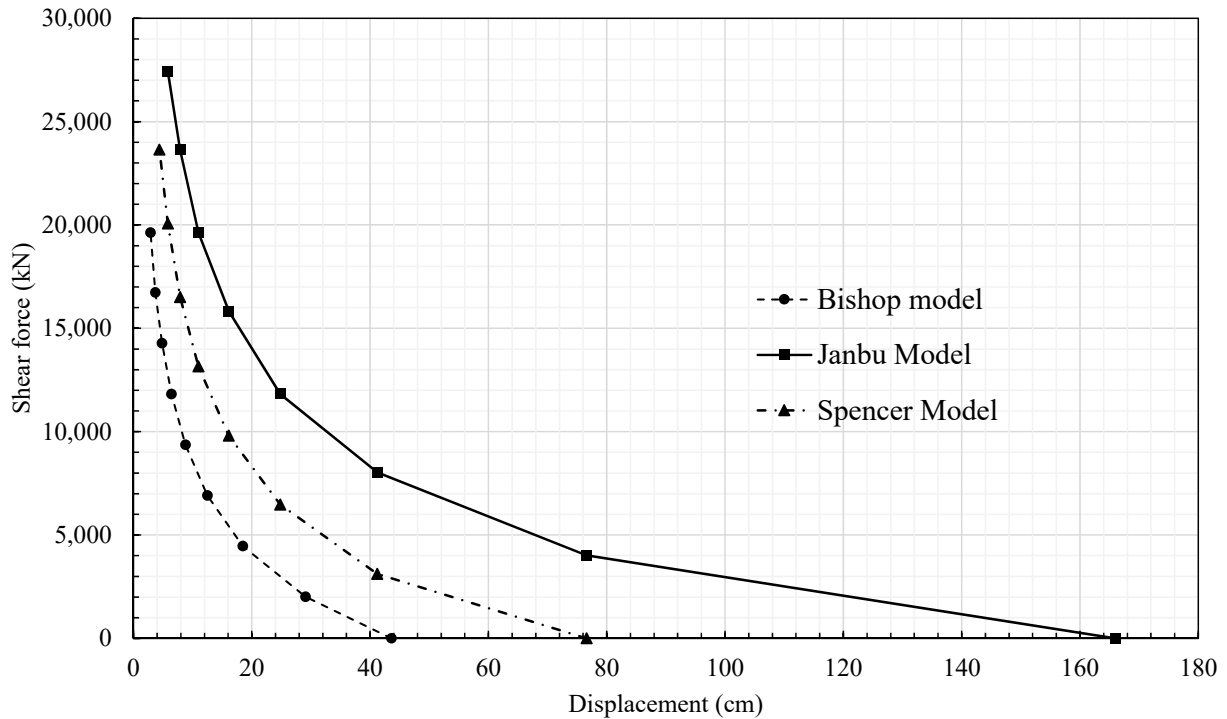


**Figure 3.10 Estimated ground displacement with PGA =0.461g, the Mataquito Bridge**

**Table 3.7 Slope stability results. Displacements are determined using Bray and Travasarou (2007), the Mataquito Bridge (PGA = 0.390g)**

Bishop			
$k_y$	R (kN/m)	$R \cdot W_{T\text{-effective}}$ (kN)	D (cm)
0.087	0	0	30.8
0.11	90	2,007	20.1
0.14	200	4,460	12.5
0.17	310	6,913	8.2
0.2	420	9,366	5.7
0.23	530	11,819	4.1
0.26	640	14,272	3
0.29	750	16,725	2.3
0.32	880	19,624	1.8

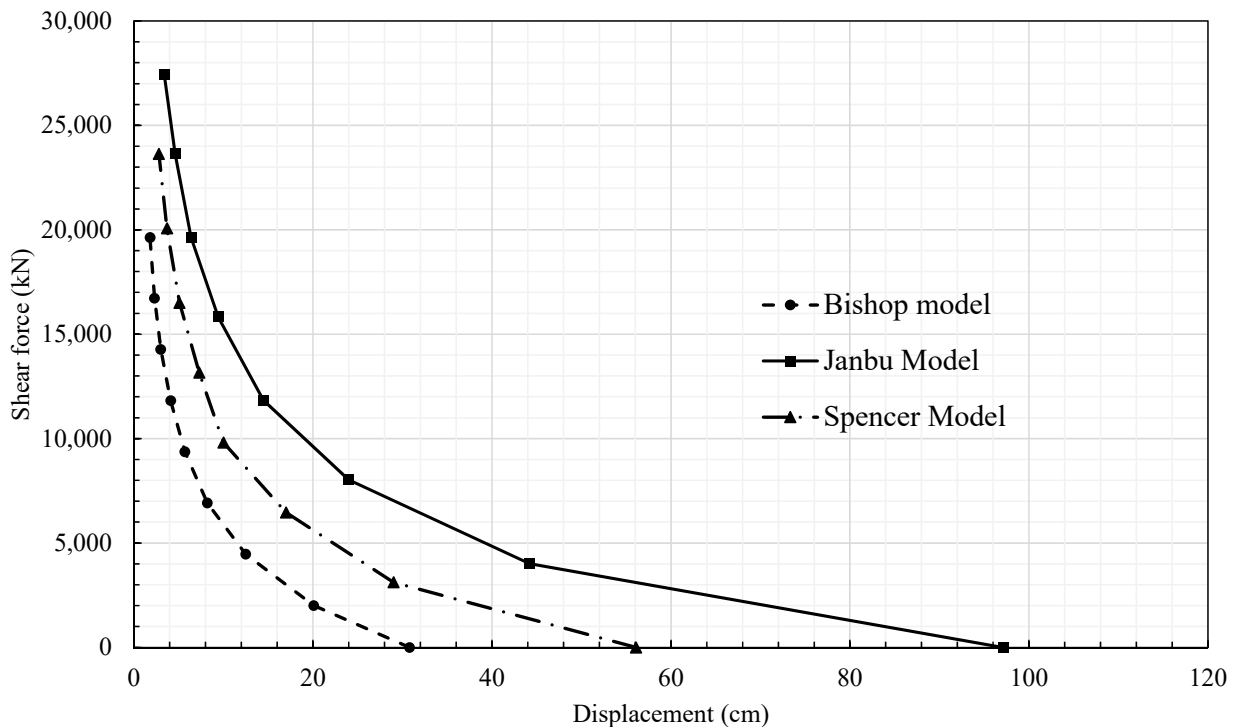


**Figure 3.11 Estimated ground displacement with PGA =0.390g, the Mataquito Bridge**

## **Pushover analysis**

### *Input parameters*

The internal friction angle  $\phi$  of the back fill soil is determined using Hatanaka and Uchida (1996). Soil unit weight is referred from Kulhawy and Mayne (1990). The modulus of subgrade reactions are referred from Brandenberg et al. (2013). Table 3.8 shows the input parameters for each soil layers.

p-y curve model	Elevation of top of soil layer (m)	Elevation of bottom of soil layer (m)	Effective soil unit (kN/m <sup>3</sup> )	Friction angle (degree)	Undrain shear strength (KPa)	Modulus of subgrade reaction (kN/m <sup>3</sup> )	Strain Factor $\epsilon_{50}$
User input p-y curve	0	10	17	-	-	-	-
Several models used	10	14.5	-	-	-	-	-
Sand (Reese)	14.5	11.5	20	46	-	150,000	-
Sand (Reese)	14.5	27	20	48	-	170,000	-

**Table 3.8 Soil models and input parameters for the Mataquito Bridge**

Several soil models are applied for the liquefiable layer (from 10m to 14.5m) to calibrate soil displacement. Shantz (2013) recommended two ways for estimating the average shear force of the pile throughout the liquefiable layer: modifying the p-y response using modification factor  $m_p$  and applying residual shear strength with no modification factor ( $m_p = 1$ ) and Matlock soft clay model. Two sand models are used: Sand (Reese) and API sand (O'Neill). A liquefied sand (Rollins) model is also used. Table 3.9 shows the utilized soil models and input parameters for the liquefiable layer. Figure 3.12 shows the results of the pushover analysis.

**Table 3.9 Soil models and input parameters for liquefiable layer, the Mataquito Bridge**

p-y curve model	Elevation of top of soil layer (m)	Elevation of bottom of soil layer (m)	Effective soil unit (kN/m <sup>3</sup> )	Friction angle (degree)	Undrain shear strength (KPa)	Modulus of subgrade reaction (kN/m <sup>3</sup> )	Strain Factor $\epsilon_{50}$
Sand (Reese)	10	14.5	18	34	-	37,000	-
API Sand (O'Neill)	10	14.5	18	34	-	37,000	-
Liquefied sand (Rollins)	10	14.5	18	-	-	-	-
Soft clay (Matlock)	10	14.5	18	-	19 <sup>1)</sup>	-	0.05

1) Estimated using Kramer (2008)

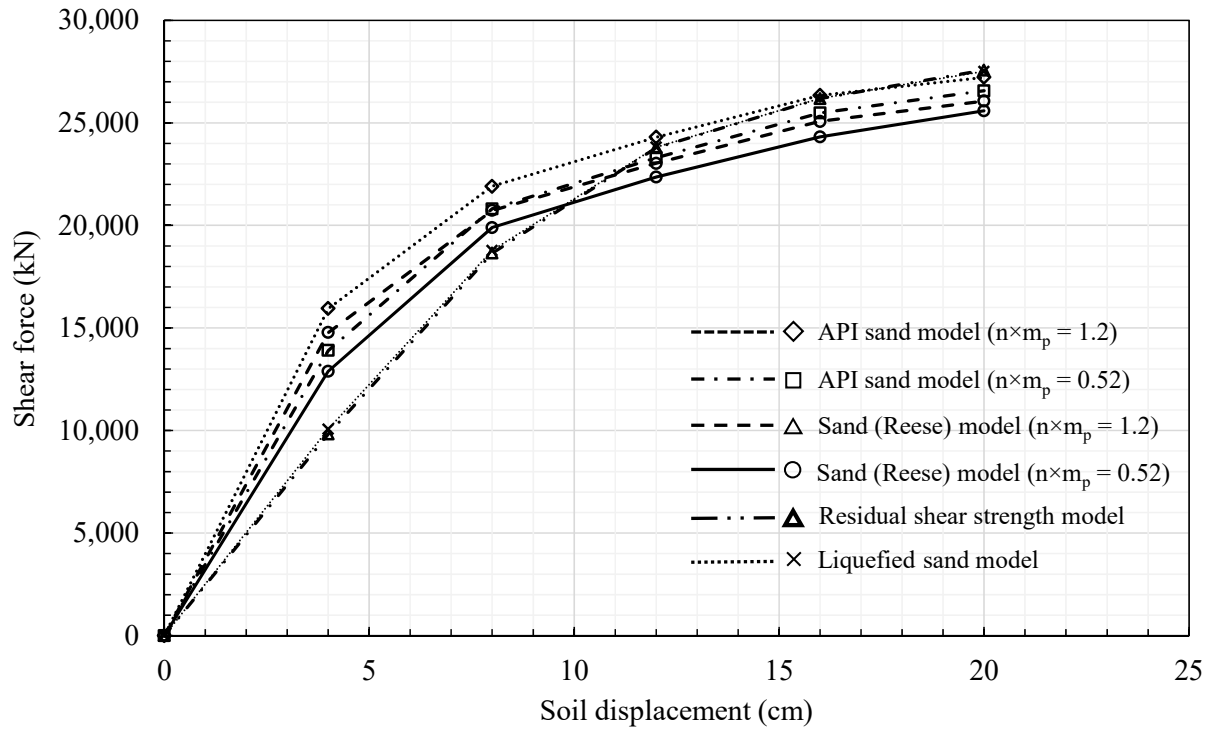


**Figure 3.12 Results of the pushover analysis of the Mataquito Bridge**

## Ground displacement

In order to determine the displacement, the intersection points of the pushover analysis and the slope stability analysis are determined. Figure 3.13 and Figure 3.14 show the intersection points of both  $PGA = 0.461g$  and  $0.390g$ . The estimated ground displacements with  $PGA = 0.461$  are from 4cm to 10cm and with  $PGA = 0.390g$  are from 3.5cm to 8cm.

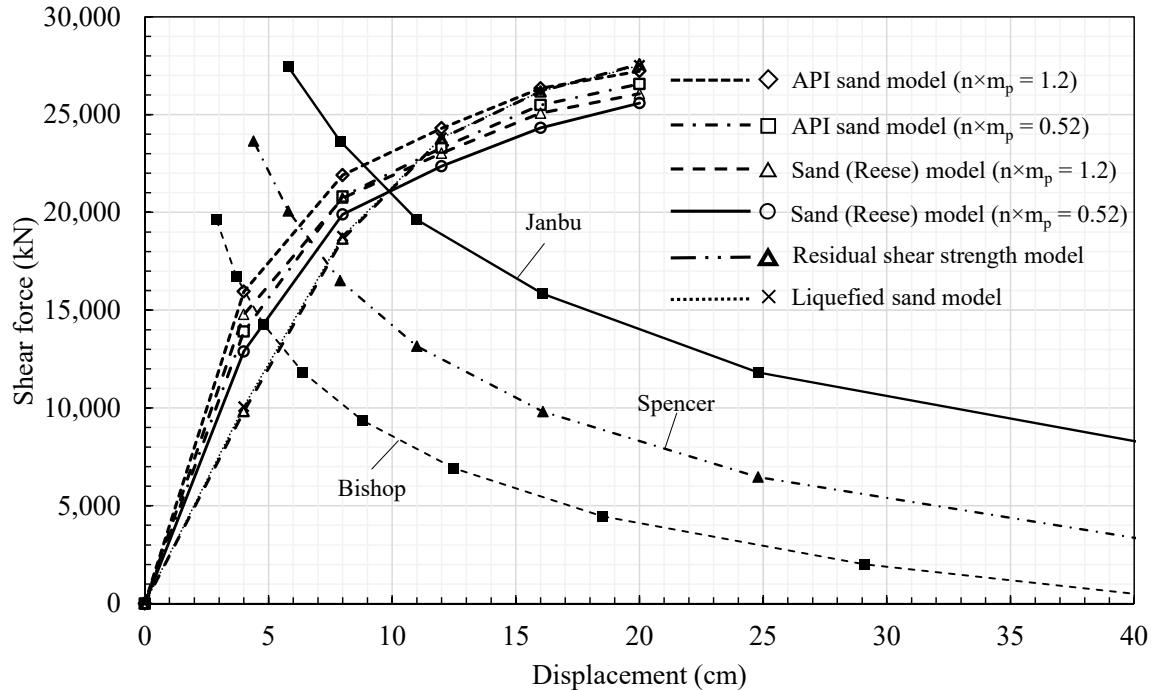


**Figure 3.13 Pushover analysis vs slope stability analysis, the Mataquito Bridge ( $PGA = 0.461g$ )**

**Table 3.10 Estimated ground displacement, the Mataquito Bridge ( $PGA = 0.461g$ )**

	Displacement (cm)		
	Bishop	Spencer	Janbu
API sand model ( $n \times m_p = 2.8$ )	4.0	6.0	9.0
API sand model ( $n \times m_p = 0.52$ )	4.5	6.5	9.5
Sand (Reese) model ( $n \times m_p = 2.8$ )	4.5	6.5	9.5
Sand (Reese) model ( $n \times m_p = 0.52$ )	5.0	7.0	10.0
Residual shear strength model	5.5	7.5	10.0
Liquefied sand model	5.5	7.5	10.0

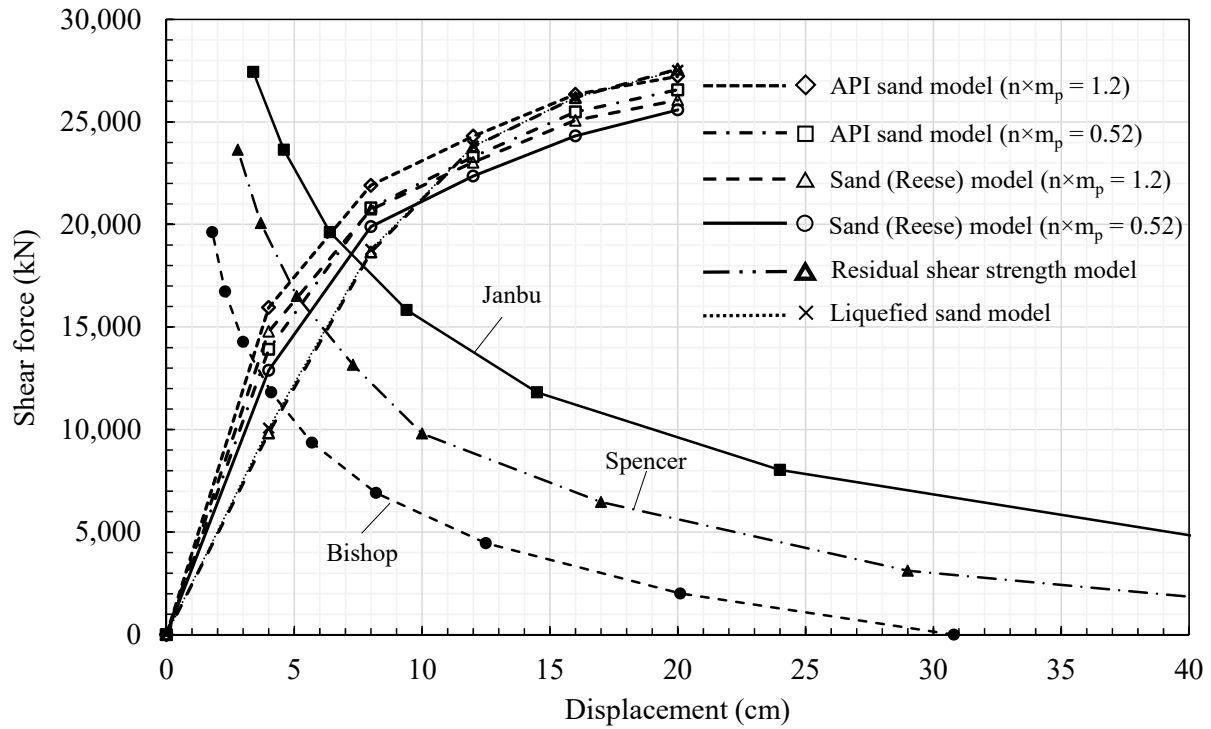


**Figure 3.14 Pushover analysis vs slope stability analysis, the Mataquito Bridge (PGA = 0.390g)**

**Table 3.11 Estimated ground displacement, the Mataquito Bridge (PGA = 0.390g)**

	Displacement (cm)		
	Bishop	Spencer	Janbu
API sand model ( $n \times m_p = 2.8$ )	3.5	5.0	6.5
API sand model ( $n \times m_p = 0.52$ )	3.5	5.0	7.0
Sand (Reese) model ( $n \times m_p = 2.8$ )	4.0	5.5	7.0
Sand (Reese) model ( $n \times m_p = 0.52$ )	4.0	5.5	7.5
Residual shear strength model	4.5	6.0	8.0
Liquefied sand model	4.5	6.0	8.0

## 5. Results: Analysis of the Mataquito Bridge

Figure 3.15 and Figure 3.16 show the analysis of the Mataquito Bridge with API sand (O'Neill) model ( $n \times m_p = 2.8$ ) and residual shear strength model. The API sand (O'Neill) and the residual shear strength model provide the maximum and minimum displacement. Table 3.12 shows the comparison of estimated bending moment with yield and allowable bending moment. The estimated bending moment does not exceed the allowable bending moment. From the observations of the Mataquito Bridge, reported in Section 2.2, although the back fill soil of abutment settled approximately 0.5-1.0m, no settlement and no cracks on the abutment were observed, which indicate that actual abutment's piles are not damaged significantly by liquefaction induced lateral spreading. The estimated bending moment with Bishop method and the residual shear strength method do not exceed the allowable bending moment. Therefore, the ground displacement estimated using Bishop method and residual shear strength model provide reasonable results compared to the observations.

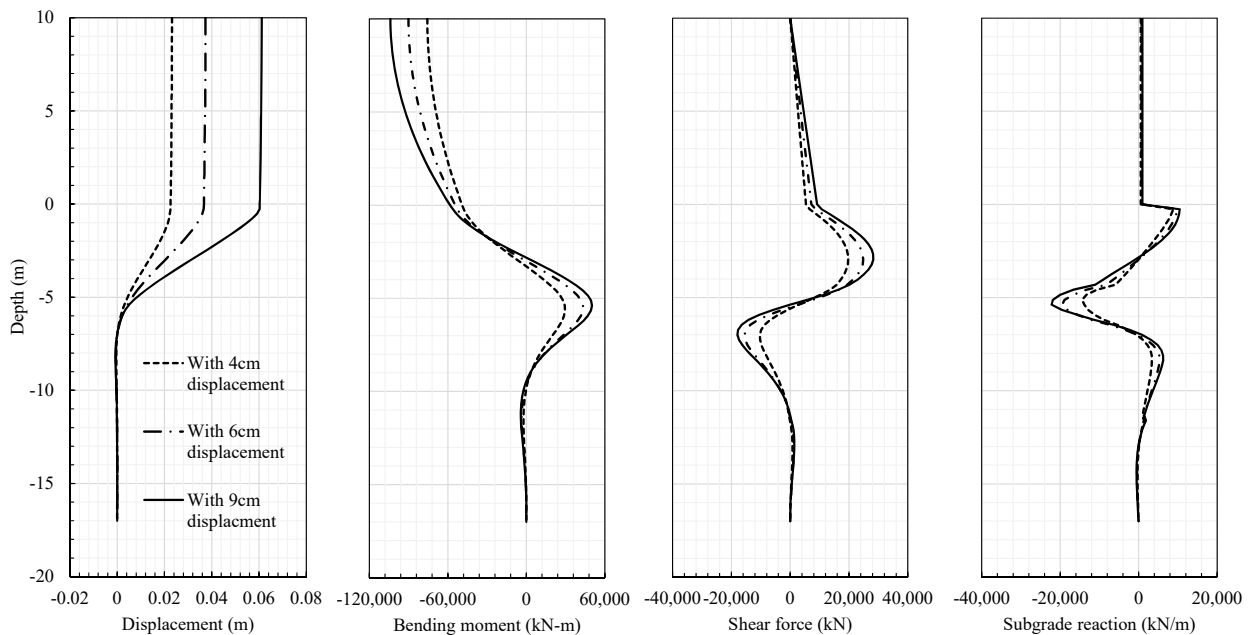


**Figure 3.15 Deflection, estimated bending moment, shear force and subgrade reaction with API sand (O'Neill) model, the Mataquito Bridge**

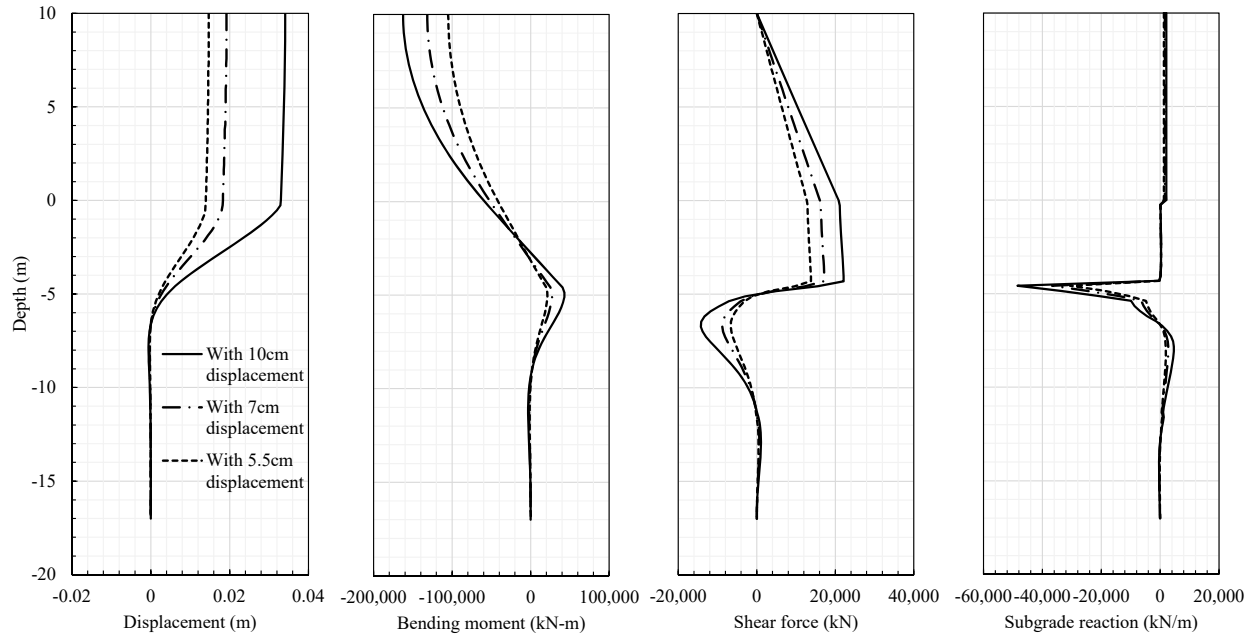


**Figure 3.16 Deflection, estimated bending moment, shear force and subgrade reaction with residual shear strength model, the Mataquito Bridge**

**Table 3.12 Comparison of the estimated bending moment to yield and allowable bending moment, the Mataquito Bridge**

Soil model	Soil displacement (cm)	Estimated maximum bending moment (kN-m)	Yield bending moment (kN-m)	Allowable bending Moment (kN-m)
API sand	4.0	47,622		
(O'Neill) model	6.0	52,428		
Residual shear strength model	5.5	38,099	45,000	62,920
	7.0	47,372		
	10.0	53,068		

Table 3.13 shows the comparison the estimated pile head displacement to the observed abutment displacement. The estimated pile head displacements with API sand (O'Neill) model exceed the observed one, however the estimated one using the residual shear strength model with 5.5cm (estimated by Bishop method) and 7.0cm (estimated by Spencer method) of displacement match up with the observations. Considering the estimated bending moment, the Bishop method with the residual shear strength model provides reasonable results.

**Table 3.13 Comparison the estimated pile head displacement to the observed abutment displacement, the Mataquito Bridge**

Soil model	Ground displacement (cm)	Pile head displacement (cm)	Observed abutment displacement (cm)
API sand	4.0	2.3	Less than 2.0cm
(O'Neill)	6.0	3.7	
model	9.0	6.1	
Residual	5.5	1.5	
shear strength	7.0	1.9	
model	10.0	3.4	

**3.3 Case study: South Brighton Bridge in New Zealand**

**3.3.1. Observed damages of South Brighton**

Bridge performance and ground failures of South Brighton Bridge discussed in Chapter 2 are repeated here to compare the results of the analysis and the observed damages. Table 3.14 shows that observed ground failures and bridge damages. Large ground distortion and slumping at the both approaches were observed. Large settlement of the approaches and vertical offset between the pile-supported bridge deck and embankment approaches on soft native soils were caused by the slumping. Lateral displacement at the vicinity of the west abutment is approximately 0.29m. The east abutment moved about 22 cm to the north and settled about 3 to 4.5 cm. The west abutment moved less than 20 cm to the south and settled 8.5 to 9.5 cm. The west abutment also rotated approximately 8 degrees. The east abutment rotated about 7 degrees.

There is no peak ground acceleration record at the South Brighton Bridge. Therefore, in this case study, the averaged peak ground acceleration recorded at the CBD in Christchurch (0.377g) is used.

**Table 3.14 Observed damages of the ground and bridge structure, South Brighton Bridge**

Observed damages	
Ground failures	- Large ground distortion and slumping at the both approaches were observed
	- Large settlement of the approaches and vertical offset between the pile-supported bridge deck and embankment approaches on soft native soils were caused by the slumping
	- Lateral displacement at the vicinity of the west abutment is approximately 290mm
Bridge damages	- The east abutment moved about 22 cm to the north and settled about 3 to 4.5 cm.
	- The west abutment moved less than 20 cm to the south and settled 8.5 to 9.5 cm
	- The west abutment also rotated approximately 8 degrees
	- The east abutment rotated about 7 degrees

### 3.3.2. Liquefaction potential evaluation

Liquefaction potential evaluation for the South Brighton Bridge is performed using Idriss and Boulanger (2008). Details of the procedures are described in Appendix A.

Liquefaction potential evaluation analysis based on SPT N-values (in Figure 3.17) shows all soil layers should not liquefy from the earthquake. Since correlated N-value below ground water table is over 20, the fine sand layer can be classified as dense sand layer. Judging from the comparison to the observed ground failures, the SPT based liquefaction potential evaluation is unrealistic.

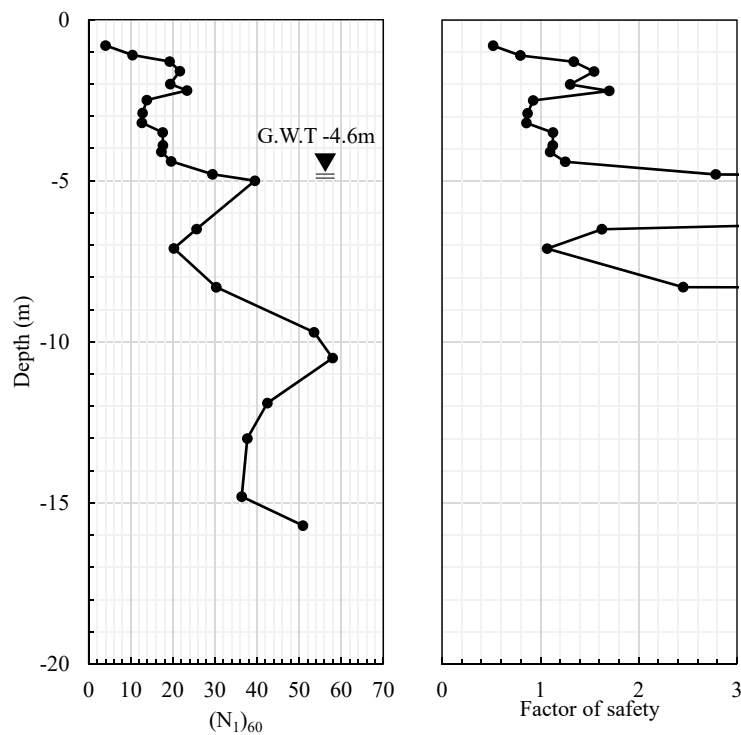


**Figure 3.17 Results of the liquefaction potential evaluation based on SPT, the South Brighton Bridge**

However, Figure 3.18 shows the factor of safety evaluated based on CPT data. The fine sand layer up to -8m below ground water table is identified as a liquefiable layer. Also, the soil layers below -10m is expected to liquefy. Cubrinovski et al. (2013) reported that the fine sand layer up to 8m deposit below the ground water table is susceptible in liquefaction, which is analyzed using CPT data. Observations show that liquefaction induced lateral spreading was confirmed around the bridge. Judging from observations and the report by Cubrinovski et al. (2013), CPT based liquefaction potential evaluation is reasonable. Therefore, liquefaction for the layer up to 8m below ground water table is expected.

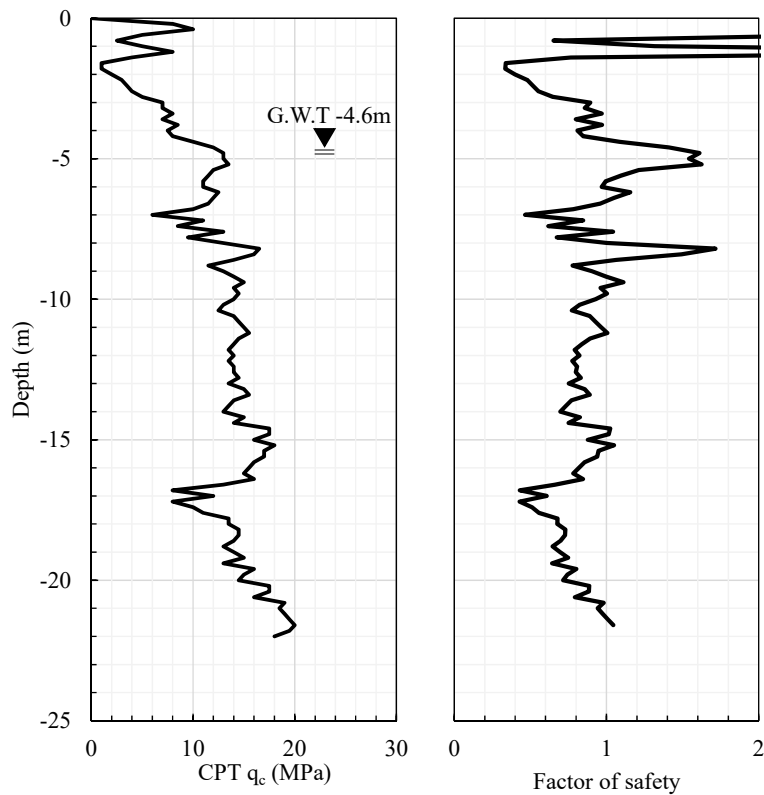


**Figure 3.18 Results of the liquefaction potential evaluation based on CPT, the South Brighton Bridge**

### 3.3.3. Description of South Brighton Bridge

The width of the west abutment of the South Brighton Bridge is 16.7m, the height is 3.6m, and the length is 1.9m (Haskell et al. 2013). Ten prestressed octagonal piles (section width  $B = 0.45\text{m}$ , 3.75m spacing and 18.7m length) support the abutment (Cubrinovski et al. 2013). The west embankment height is 4.0m and the degree of slope is about  $20.0^\circ$ . The internal friction angle of all layers is determined using empirical estimation by Hatanaka and Uchida (1996). Soil unit weight is referred from Kulhawy and Mayne (1990). Figure 3.19 and Figure 3.20 show the sketch of the soil layers and the approach embankment of South Brighton Bridge.

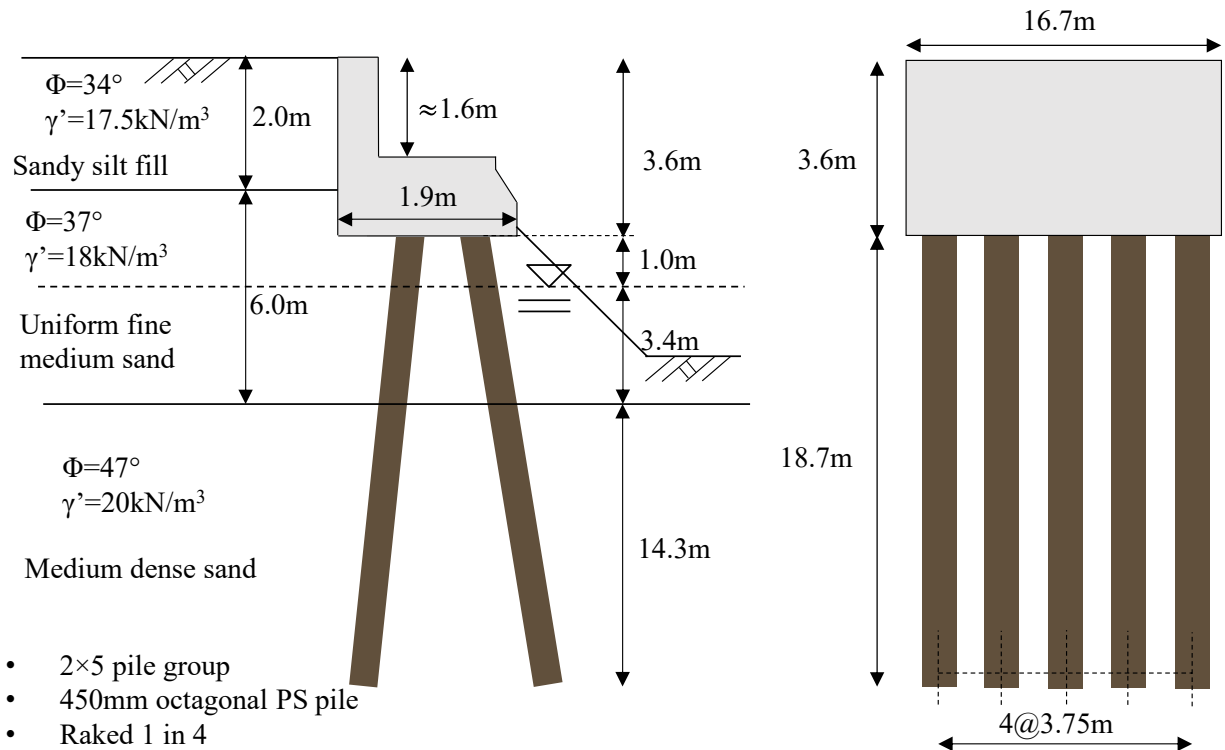


Figure 3.19 Sketch of the South Brighton Bridge

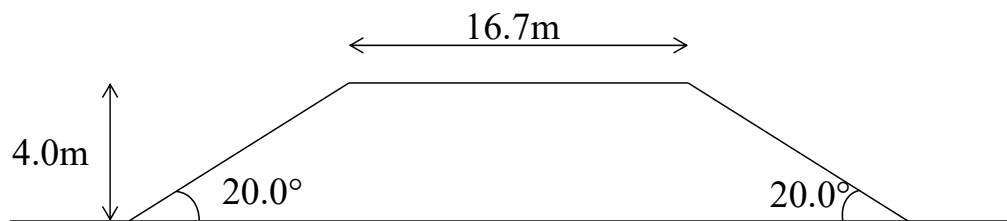


Figure 3.20 Sketch of the approach embankment of the South Brighton Bridge

### 3.3.4. Analysis of the South Brighton Bridge with equivalent single pile method

#### 1. Modeling a group pile as an equivalent single pile

The South Brighton Bridge west abutment is supported by 4:1 raked, battered piles. To take into account the effect of batter on an equivalent non-linear single pile, three cases are considered. 1) 2×5 group piles are modeled as an equivalent single pile. The bending stiffness is multiplied by 10. The pile inclination is zero. 2) The first row piles are modeled as an equivalent non-linear single pile. The bending stiffness is multiplied by 5, and 14 degree inclination is applied for the equivalent non-linear single pile. 3) The second row piles are modeled as an equivalent non-linear single pile. The bending stiffness is multiplied by 5, and -14 degree inclination is applied for the equivalent non-linear single pile.

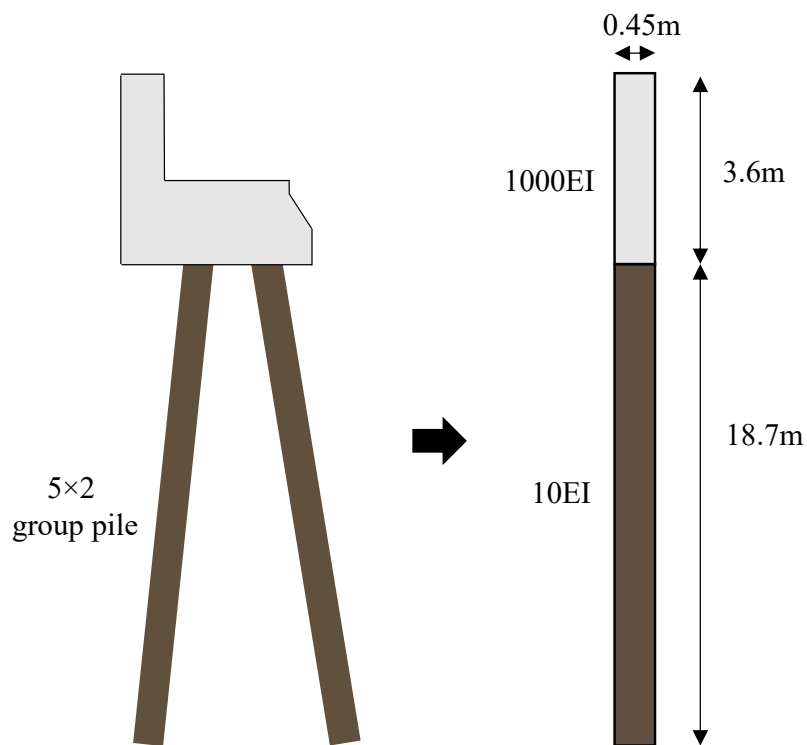


Figure 3.21 Modeling of an equivalent single pile, the South Brighton Bridge

**Pile section parameters**

In this analysis, the prestressed concrete pile properties are referred from the AASHTO/PCI standard prestressed concrete pile sections (AASHTO 2006). The pile section properties are shown in Table 3.15. More details of pile section properties are tabulated in Appendix B. Figure 3.22 and Figure 3.23 show the bending moment and bending curvature diagram for both the group pile section and the abutment section. The details of modeling an equivalent single pile are also described in Appendix B.

**Table 3.15 Pile section properties of the South Brighton Bridge for original single pile**

Concrete compressive strength (MPa)	Prestressing Strand Type	Strand/Bar Size	Number of Strands / PS Bars	Prestress Force Before Losses (kN)	Fraction of Loss of Prestress	Cover Over Strands (mm)
24	Grade 270 ksi Lo-Lax	1 / 2'' 7-wire A=0.153sq. in.	10	1370	0.1	20

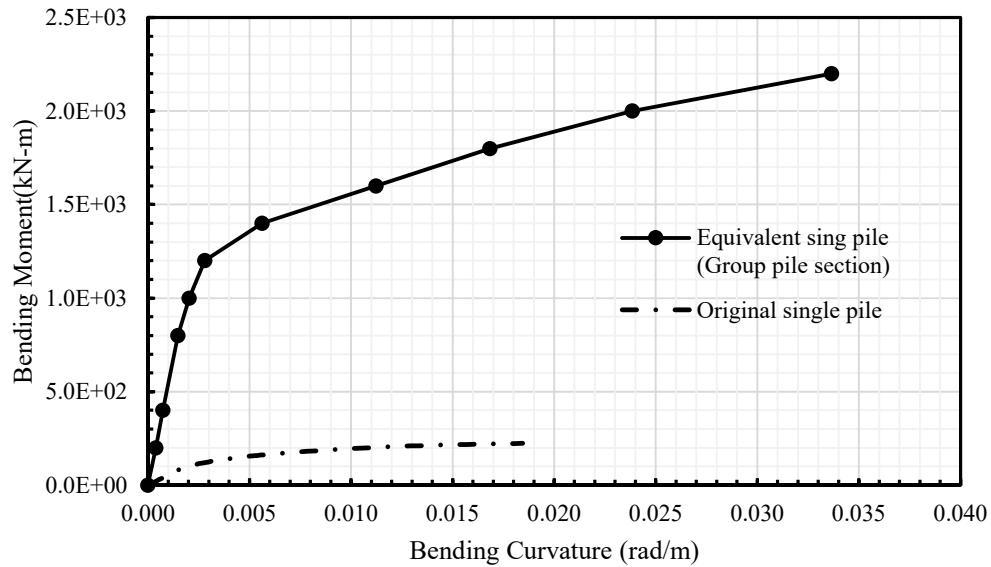


**Figure 3.22 Bending moment – bending curvature of the equivalent single pile for group pile section, the South Brighton Bridge**

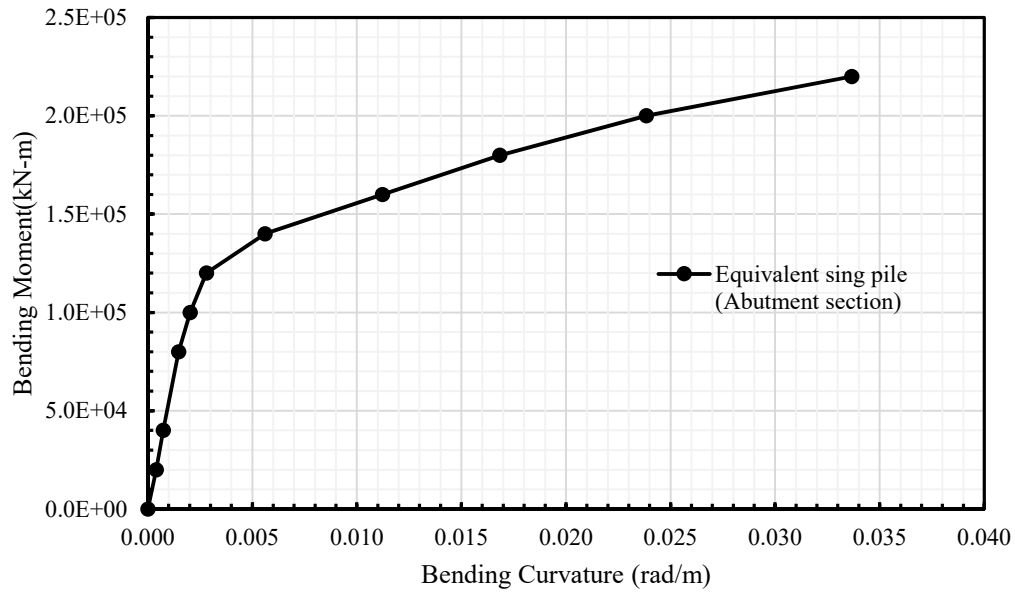


**Figure 3.23 Bending moment – bending curvature of the equivalent single pile for abutment section, the South Brighton Bridge**

## 2. Calculation of Foundation Loads Due to the Soil Crust

### 2.1. Dimension parameters of the pile cap

To estimate the lateral load of crust layer against piles, longitudinal width dimensions  $W_T$  and  $W_L$ , pile cap thickness  $T$ , depth to top of cap  $D$ , and crust thickness  $Z_c$  are required. These parameters are shown in Table 3.16.

**Table 3.16 Dimension parameters of the South Brighton Bridge**

$W_T$ (m)	$W_L$ (m)	$T$ (m)	$D$ (m)	$Z_c$ (m)
16.4	1.9	3.6	0.0	4.6

## 2.2. Determination of p-y curve for curst layer

### Case A

$F_{ULT-A}$  is expressed as

$$F_{ULT-A} = F_{PASSIVE-A} + F_{PILES-A} + F_{SIDES-A}$$

### $F_{PASSIVE-A}$

$F_{PASSIVE-A}$  is calculated using the following equation.

$$F_{PASSIVE} = \left( \bar{\sigma}'_v \cdot K_p + 2 \cdot c' \cdot \sqrt{K_p} \right) \cdot (T) \cdot (W_T) \cdot (k_w)$$

$$\bar{\sigma}'_v = 1.8(m) \cdot 17.5(kN / m^3) = 31.5(kN / m^2)$$

Coefficient of passive pressure  $K_p$  is calculated using the following equation. Note that  $\delta$  is  $\phi/3$ .

$$\begin{aligned} K_p &= \tan^2 \left( 45 + \frac{\phi}{2} \right) \cdot \left[ 1 + \left( 0.8152 - 0.0545 \cdot \phi + 0.001771 \cdot \phi^2 \right) \cdot \frac{\delta}{\phi} - 0.15 \cdot \left( \frac{\delta}{\phi} \right)^2 \right] \\ &= \tan^2 \left( 45 + \frac{34}{2} \right) \cdot \left[ 1 + \left( 0.8152 - 0.0545 \cdot 34 + 0.001771 \cdot 34^2 \right) \cdot \frac{34/3}{34} - 0.15 \cdot \left( \frac{34/3}{34} \right)^2 \right] \\ &= 4.40 \end{aligned}$$

$k_w$  is developed by Ovesen (1964) and is expressed as the following equation.

$$\begin{aligned} k_w &= 1 + (K_p - K_a)^{\frac{2}{3}} \cdot \left[ 1.1 \cdot \left( 1 - \frac{T}{D+T} \right)^4 + 1.6 / \left( 1 + \frac{5W_T}{T} \right) + 0.4 \cdot (K_p - K_a) \cdot \left( 1 - \frac{T}{D+T} \right)^3 / \left( 1 + \frac{0.05W_T}{T} \right) \right] \\ k_w &= 1 + (4.40 - 0.28)^{\frac{2}{3}} \cdot \left[ 1.1 \cdot \left( 1 - \frac{3.6}{0+3.6} \right)^4 + 1.6 / \left( 1 + \frac{5 \cdot 16.7}{3.6} \right) + 0.4 \cdot (4.40 - 0.28) \cdot \left( 1 - \frac{3.6}{0+3.6} \right)^3 / \left( 1 + \frac{0.05 \cdot 16.7}{3.6} \right) \right] \\ &= 1.17 \end{aligned}$$

Therefore,

$$F_{PASSIVE-A} = \left( 31.5 \cdot 4.40 + 2 \cdot 0 \cdot \sqrt{4.40} \right) \cdot (3.6) \cdot (16.7) \cdot (1.17) = 9,749(kN)$$

### F<sub>PILES-A</sub>

F<sub>PILES-A</sub> is calculated using the following equation

$$F_{PILES-A} = n \cdot m_p \cdot P_{ULT} \cdot L_C$$

Where,  $m_p$  is pile group modification factor.  $L_c$  is a distance from the bottom of pile cap (abutment) to the top of liquefiable layer.

$P_{ULT}$  is calculated using the following equation recommended by API (2004).

$$P_{ULT} = (C_1 \cdot \bar{H} + C_2 \cdot D) \cdot \gamma' \cdot \bar{H}$$

$C_1$  and  $C_2$  are calculated using equation (5) and (6)

$$C_1 = 3.42 - 0.295 \cdot \phi + 0.00819 \cdot \phi^2$$

$$= 3.24$$

$$C_2 = 0.99 - 0.0294 \cdot \phi + 0.00289 \cdot \phi^2$$

$$= 0.97$$

$$P_{ULT} = (3.24 \cdot 3.4 + 0.97 \cdot 0.45) \cdot 17.5 \cdot 3.6 = 721(kN / m)$$

Therefore,

$$F_{PILES-A} = 10 \cdot 0.78 \cdot 721 \cdot 1 = 5,623(kN)$$

### F<sub>SIDE-A</sub>

F<sub>SIDES-A</sub> is calculated using the following equation.

$$F_{SIDES} = 2 \cdot \left( \overline{\sigma}'_v \cdot \tan(\delta) + \alpha c' \right) \cdot W_L \cdot T$$

$$= 2 \cdot (31.5 \cdot \tan(34/3) + 0.5 \cdot 0) \cdot 1.9 \cdot 3.6 = 86(kN)$$

#### F<sub>ULT-A</sub>

The total ultimate crust load of case A becomes the following one.

$$F_{ULT-A} = 9,749 + 5,623 + 86 = 15,458(kN)$$

#### **Case B**

F<sub>ULT-B</sub> is expressed as the following equation.

$$F_{ULT-B} = F_{PASSIVE-B} + F_{SIDES-B}$$

#### F<sub>PASSIVE-B</sub>

F<sub>PASSIVE-B</sub> is calculated using the following equation.

$$F_{PASSIVE-B} = \left( \overline{\sigma}'_v \cdot K_p + 2 \cdot c' \cdot \sqrt{K_p} \right) \cdot (T) \cdot (W_T) \cdot (k_w)$$

Coefficient of passive pressure K<sub>p</sub> is calculated using Rakine theory.

$$K_p = \tan^2 \left( 45 + \frac{\phi}{2} \right)$$

$$= \tan^2 \left( 45 + \frac{34}{2} \right) = 3.53$$

k<sub>w</sub> is developed by Ovesen (1964) and is expressed as the following equation.

$$k_w = 1 + (K_p - K_a)^{\frac{2}{3}} \cdot \left[ 1.1 \cdot \left( 1 - \frac{T}{D+T} \right)^4 + 1.6 \cdot \left( 1 + \frac{5W_T}{T} \right) + 0.4 \cdot (K_p - K_a) \cdot \left( 1 - \frac{T}{D+T} \right)^3 \cdot \left( 1 + \frac{0.05W_T}{T} \right) \right]$$

$$= 1 + (4.40 - 0.228)^{\frac{2}{3}} \cdot \left[ 1.1 \cdot \left( 1 - \frac{3.6}{0+3.6} \right)^4 + 1.6 \cdot \left( 1 + \frac{5 \cdot 16.7}{3.6} \right) + 0.4 \cdot (4.40 - 0.28) \cdot \left( 1 - \frac{3.6}{0+3.6} \right)^3 \cdot \left( 1 + \frac{0.05 \cdot 16.7}{3.6} \right) \right]$$

$$= 1.14$$

Therefore,

$$F_{PASSIVE-B} = (31.5 \cdot 3.53 + 2 \cdot 0 \cdot \sqrt{3.53}) \cdot (4.6) \cdot (16.7) \cdot (1.14) = 9,737(kN)$$

### F<sub>SIDES-B</sub>

F<sub>SIDES-B</sub> is calculated using the following equation.

$$\begin{aligned} F_{SIDES-B} &= 2 \cdot (\bar{\sigma}_v' \cdot \tan(\delta) + \alpha c') \cdot W_L \cdot T \\ &= 2 \cdot (31.5 \cdot \tan(34/3) + 0.5 \cdot 0) \cdot 1.9 \cdot 4.6 = 110(kN) \end{aligned}$$

### F<sub>ULT-B</sub>

The total ultimate crust load of case B becomes following one.

$$F_{ULT-B} = 9,737 + 110 = 9,847(kN)$$

***So, Case B < Case A. Case B is selected.***

## 2.3. Determination of $\Delta_{MAX}$

The maximum displacement  $\Delta_{MAX}$  of crust layer for p-y curve at the maximum force is calculated using the following equation.

$$\Delta_{MAX} = (T) \cdot (0.05 + 0.45 \cdot f_{depth} \cdot f_{width})$$

The modification factors  $f_{depth}$  and  $f_{width}$  are calculated using the following equations

$$\begin{aligned} f_{depth} &= EXP \left[ -3 \cdot \left( \frac{Z_C - D}{T} - 1 \right) \right] \\ &= EXP \left[ -3 \cdot \left( \frac{4.6 - 0}{3.6} - 1 \right) \right] = 0.43 \end{aligned}$$

$$f_{width} = \left\{ \left[ 10 / \left( \frac{W_T}{T} + 4 \right) \right]^4 + 1 \right\}^{-1}$$

$$= \left\{ \left[ 10 / \left( \frac{16.7}{3.6} + 4 \right) \right]^4 + 1 \right\}^{-1} = 0.35$$

Then, the maximum displacement  $\Delta_{MAX}$  is as follows.

$$\Delta_{MAX} = (T) \cdot (0.05 + 0.45 \cdot f_{depth} \cdot f_{width})$$

$$= (3.6) \cdot (0.05 + 0.45 \cdot 0.43 \cdot 0.35) = 0.42(m)$$

### P-y curve for a crust layer

$F_{ULT}$  is the total lateral force of crust layer along with a pile cap (abutment) or crust layer. To obtain lateral force per pile cap (abutment) thickness for p-y curve,  $F_{ULT}$  should be divided by the pile cap (abutment) thickness  $T$ .  $p_{ult}$  is calculated below. Figure 3.24 shows the p-y curve for the abutment section.

$$p_{ULT} = F_{ULT} / T = 15,458 / 3.6 = 4,293 (kN/m) \quad (\text{Case A})$$

$$p_{ULT} = F_{ULT} / T = 9,847 / 3.6 = 2,735 (kN/m) \quad (\text{Case B})$$

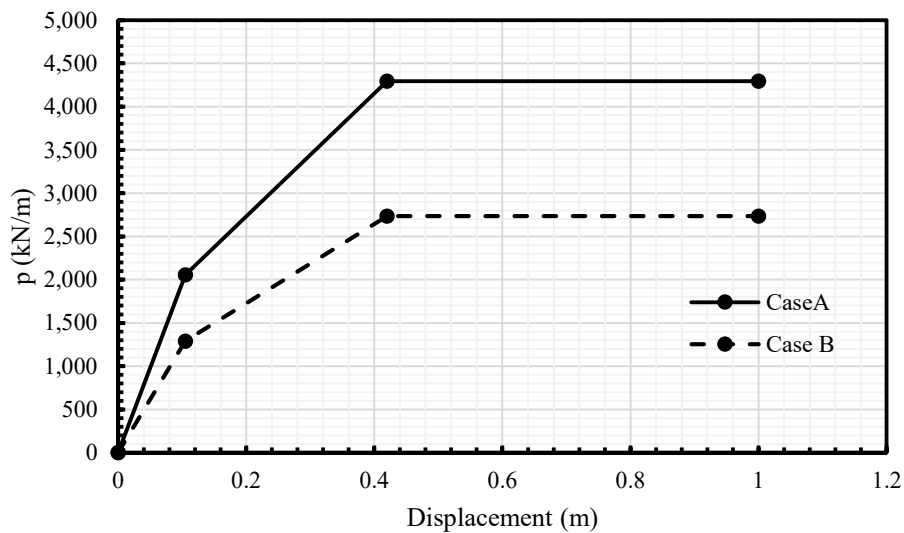


Figure 3.24 p-y curve of the abutment section, the South Brighton Bridge

### 3. Calculation of p - y Curves for Piles

An equivalent single pile reaction is described with the following equation.

$$P_{SUPER} = n \cdot m_p \cdot P_{SINGLE}$$

#### 3.1. Evaluating the reduction factor

##### Non-liquefied soil layer

The modification factor  $m_p$  for non-liquefiable soil layers for group piles can be evaluated using Mokwa et al. (2000). With this method, the reduction factor is described simply as a function of pile space. For the group pile of South Brighton Bridge, the average  $m_p$  is used.

$$m_p = \frac{First\_row + Second\_row}{2} = \frac{0.84 + 0.72}{2} = 0.78$$

##### Liquefied soil layer

Shantz (2013) recommended that the reduction factor  $m_p$  for liquefied soil is estimated using the correlated N-value. However, liquefaction potential evaluated using SPT N-value shows that factor of safety for all soil layers below ground water is over one, which is challenged by observed ground failures. Ashford et al (2011) recommended that  $m_p$  for weak soil layer ( $(N_1)_{60CS} < 8$ ) is from 0.0 to 0.1 and 0.05 to 0.2 for  $(N_1)_{60CS}$ . Therefore,  $m_p = 0.1$  and 0.15 for liquefied soil layer is utilized for the South Brighton Bridge.

#### 3.2. Modification of the group reduction factor near liquefied soil layer boundary

The effective distance vicinity of liquefied layer for p-y curve is estimated by pile diameter and modification factor  $S_b$ . The  $S_b$  and the effective distance are obtained from the following equations.

$$S_b = 2$$

$$S_b \cdot D = 2 \cdot 0.45(m) = 0.9(m)$$

The subgrade reaction of a group pile for Winkler type soils is described as a function of relative displacement of piles, stiffness factor  $k$ , and reduction factor  $m_p$ . In this analysis,  $m_p$  is also modified to consider the effect of liquefaction for  $p$ - $y$  curve in the vicinity of the liquefied layer. Table 3.17 shows reduction factor  $m_p$  in the vicinity of the liquefied layer. Table 3.18 and Figure 3.25 show reduction factors for each depth.

**Table 3.17 Reduction factor for vicinity of liquefied layer for the South Brighton Bridge**

Distance from the liquefied layer (m)	Adjustment factor	$m_p$
0.3	$\frac{1}{3} + \frac{2}{3} \cdot \frac{P_L}{P_H} = 0.4$	$0.4 \cdot 0.78 = 0.31$
0.6	$\frac{2}{3} + \frac{1}{3} \cdot \frac{P_L}{P_H} = 0.70$	$0.70 \cdot 0.78 = 0.54$
0.9	1	0.78

**Table 3.18 Reduction factor for each depth, the South Brighton Bridge**

Depth (m)	$m_p$	$n \times m_p$	
		Vertical pile	Battered pile
0-3.6	1	1	1
3.6-4.0	0.78	7.8	3.9
4.0-4.3	0.54	5.4	2.7
4.3-4.6	0.31	3.1	1.55
4.6-8.0	0.1	1.0	0.5
8.0-8.3	0.31	3.1	1.55
8.3-8.6	0.54	5.4	2.7
8.6 -	0.78	7.8	3.9

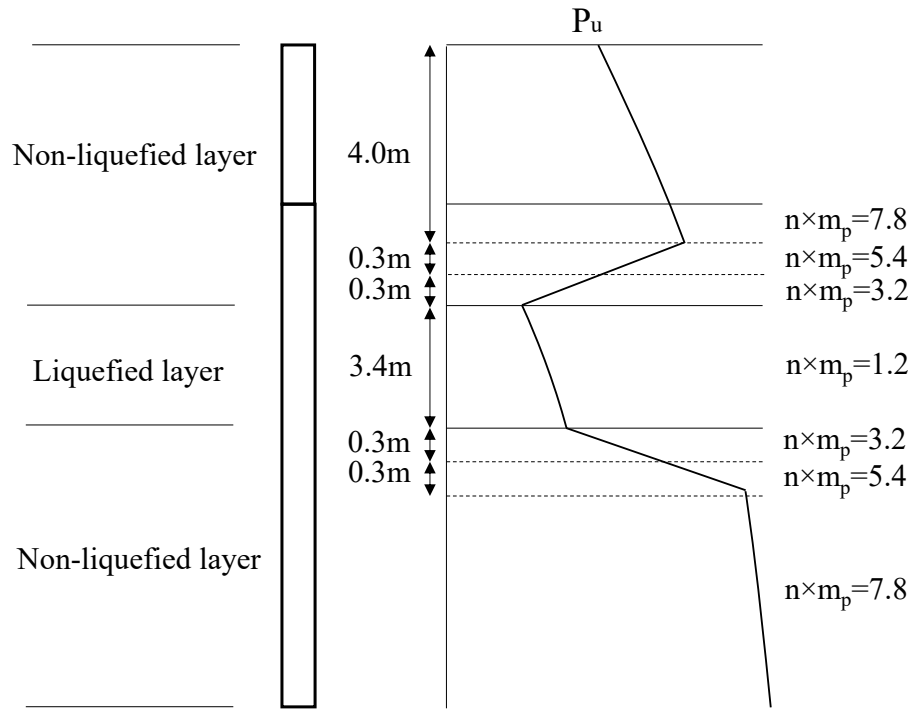


**Figure 3.25 Modification factor near liquefiable layers, the South Brighton Bridge**

#### 4. Estimation of crust displacement

##### Slope stability analysis

The restricted crust displacement is evaluated by Bray and Travasarou (2007). The horizontal acceleration is obtained using GeoStudio 2012 software. For the South Brighton Bridge, Palermo et al. (2011) reported that the South Brighton Bridge abutment was pounded by the deck. In addition, NZ-GEER (2011) reported transverse cracks on the abutment. However, judging from pictures taken by NZ-GEER (2011), the abutment did not plunge into the backfill. Therefore,  $F_{deck}$  is not considered for the South Brighton Bridge.

The residual shear strength of liquefied layer is estimated by Idriss and Boulanger (2007). For South Brighton Bridge, the residual shear strength is evaluated using CPT data because liquefaction potential estimated using CPT data provides reasonable results compared to observations. The average effective stress at the center of the liquefiable layer is given by the following equation. The average  $q_{c1N}$  in the liquefied layer is 121. The following calculation is an example of residual shear strength.

1) For the liquefiable layer under backfill soil and the abutment

$$\begin{aligned}\bar{\sigma}'_v &= 17.5(kN/m^3) \cdot 2(m) + 18(kN/m^3) \cdot 4.3(m) - 9.8(kN/m^3) \cdot 1.7(m) \\ &= 95(kPa)\end{aligned}$$

$$\begin{aligned}S_r &= \sigma'_{vo} \cdot \exp \left[ \frac{q_{c1NCS-Sr}}{24.5} - \left( \frac{q_{c1NCS-Sr}}{61.7} \right)^2 + \left( \frac{q_{c1NCS-Sr}}{106} \right)^3 - 4.42 \right] \\ &= 89(kPa) \cdot \exp \left[ \frac{121}{24.5} - \left( \frac{121}{61.7} \right)^2 + \left( \frac{121}{106} \right)^3 - 4.42 \right] = 14(kPa)\end{aligned}$$

2) For the liquefiable layer under the front of the abutment

$$\begin{aligned}\bar{\sigma}'_v &= 18(kN/m^3) \cdot 1.5(m) - 9.8(kN/m^3) \cdot 1.5(m) \\ &= 12.3(kPa)\end{aligned}$$

$$\begin{aligned}S_r &= \sigma'_{vo} \cdot \exp \left[ \frac{q_{c1NCS-Sr}}{24.5} - \left( \frac{q_{c1NCS-Sr}}{61.7} \right)^2 + \left( \frac{q_{c1NCS-Sr}}{106} \right)^3 - 4.42 \right] \\ &= 12.3(kPa) \cdot \exp \left[ \frac{121}{24.5} - \left( \frac{121}{61.7} \right)^2 + \left( \frac{121}{106} \right)^3 - 4.42 \right] = 1.9(kPa)\end{aligned}$$

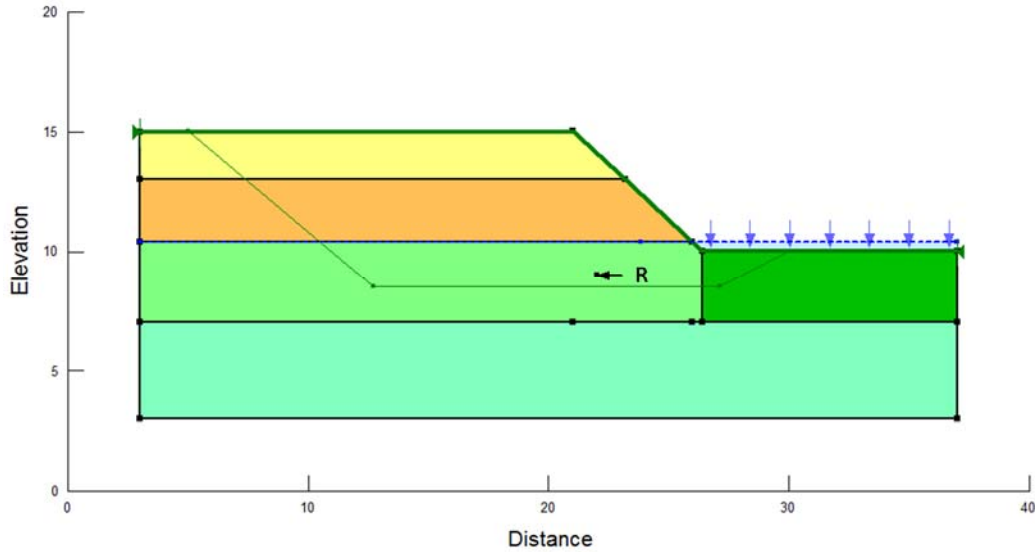


**Figure 3.26 Slope stability analysis model to determine the coefficient of horizontal acceleration, the South Brighton Bridge**

For slope stability analysis, Bishop, Janbu, and Spencer methods are utilized to calibrate possible displacements. The example of the estimated displacement by Bray and Travasarou (2007) is shown in Table 3.19. A sample calculation using Bishop method is shown below. Other calculations are shown in Appendix C. Figure 3.27 shows the displacement – shear force diagram using Bishop, Janbu, and Spencer methods.

$$\begin{aligned}
 D(cm) &= \exp \left\{ -0.22 - 2.83 \cdot \ln(0.055) - 0.333 \cdot [\ln(0.055)]^2 + 0.566 \cdot \ln(0.055) \cdot \ln(0.377) \right. \\
 &\quad \left. + 3.04 \cdot \ln(0.377) - 0.244 \cdot [\ln(0.377)]^2 + 0.278 \cdot (6.2 - 7) \right\} \\
 &= 29(cm)
 \end{aligned}$$

The effective width is calculated using the following equation.

$$\begin{aligned}
 W_{\text{effective}} &= W_T + m/2 \cdot H \\
 &= 16.7 + 2.75/2 \cdot 4.0 = 22.2(m)
 \end{aligned}$$

Where m is the inclination of the embankment slope and H is the embankment height.

**Table 3.19 Slope stability results using Bishop method, South Brighton Bridge**

Bishop			
$k_y$	R (kN/m)	$R \cdot W_{T\text{-effective}}$ (kN)	D (cm)
0.055	0	0	29
0.07	20	444	20
0.09	55	1,221	13.1
0.11	85	1,887	9
0.13	115	2,553	6.69
0.15	145	3,219	4.98
0.17	180	3,996	3.8
0.19	210	4,662	2.9
0.21	245	5,439	2.3
0.23	275	6,105	1.89

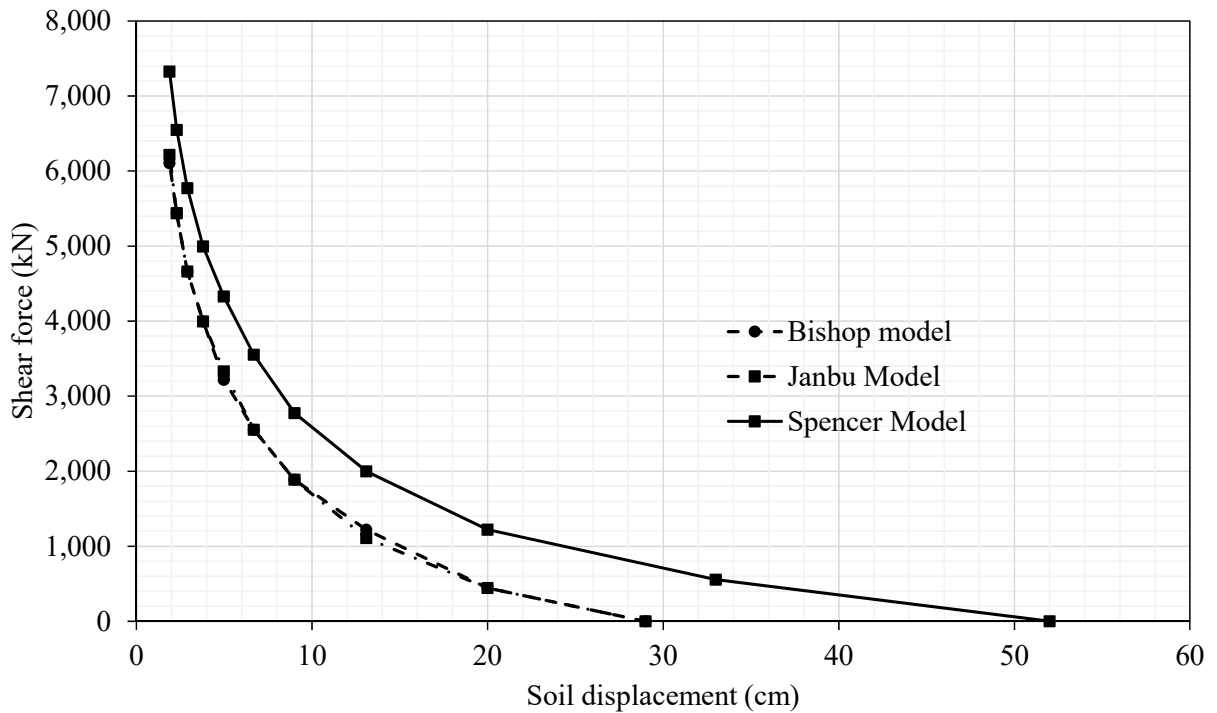


**Figure 3.27 Estimated ground displacement, the South Brighton Bridge**

## **Pushover analysis**

### *Input parameters*

The internal friction angle of both liquefied and dense sand layers is determined using empirical estimation by Hatanaka and Uchida (1996). Soil unit weight is referred from Kulhawy and Mayne (1990). The modulus of subgrade reactions are referred from Brandenberg et al. (2013).

**Table 3.20 Soil properties of the South Brighton Bridge for LPile**

p-y curve model	Elevation of top of soil layer (m)	Elevation of bottom of soil layer (m)	Effective soil unit (kN/m <sup>3</sup> )	Friction angle (degree)	Modulus of subgrade (kN/m <sup>3</sup> )
User input p-y curve	0	3.6	17.5	-	-
Sand (Reese)	3.6	4.6	17.5	37	40,000
Several soil models	4.6	8.0	-	-	-
Sand (Reese)	8.0	22.3	20.0	47	160,000

Several soil models are applied for the liquefiable layer (from 4.6m to 8.0m) to calibrate soil displacement. Shantz (2013) recommends two ways for estimating average shear force of the pile through liquefiable layer: modifying the p-y response by factor  $m_p$  and applying residual shear strength with no modification factor and Matlock soft clay model. Two sand models are used: Sand (Reese) and API sand (O'Neill). The liquefied sand (Rollins) model is also used. Table 3.21 shows the utilized soil models and input parameters for the liquefiable layer. Figure 3.28 - Figure 3.30 shows the results of the pushover analysis.

**Table 3.21 Soil models and input parameters for liquefiable layer, the South Brighton Bridge**

p-y curve model	Elevation of top of soil layer (m)	Elevation of bottom of soil layer (m)	Effective soil unit (kN/m <sup>3</sup> )	Friction angle (degree)	Undrain shear strength (KPa)	Modulus of subgrade reaction (kN/m <sup>3</sup> )	Strain Factor $\epsilon_{50}$
Sand (Reese)	4.6	8.0	18	37	-	40,000	-
API Sand (O'Neill)	4.6	8.0	18	37	-	40,000	-
Liquefied sand (Rollins)	4.6	8.0	18	-	-	-	-
Soft clay (Matlock)	4.6	8.0	18	-	14 <sup>1)</sup>	-	0.05

1) Residual strength estimated using Idriss and Boulanger (2007)

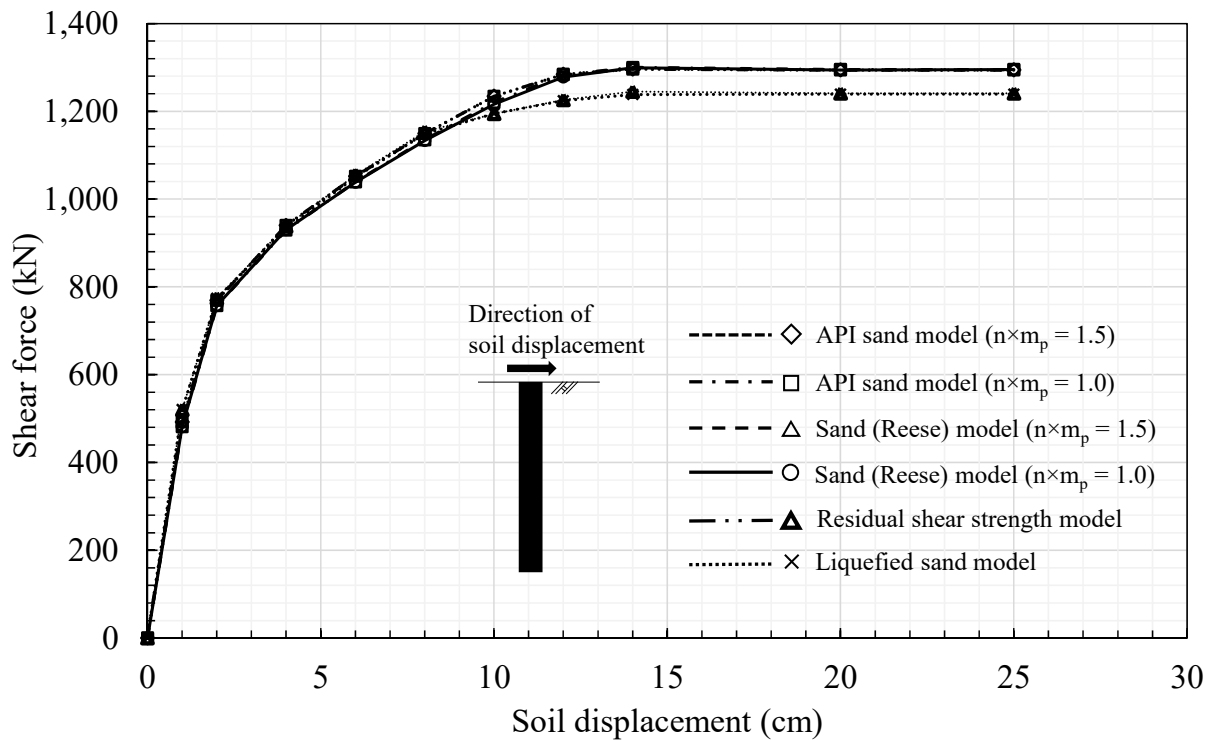


**Figure 3.28 Results of the pushover analysis with 2x5 group piles, the South Brighton Bridge**

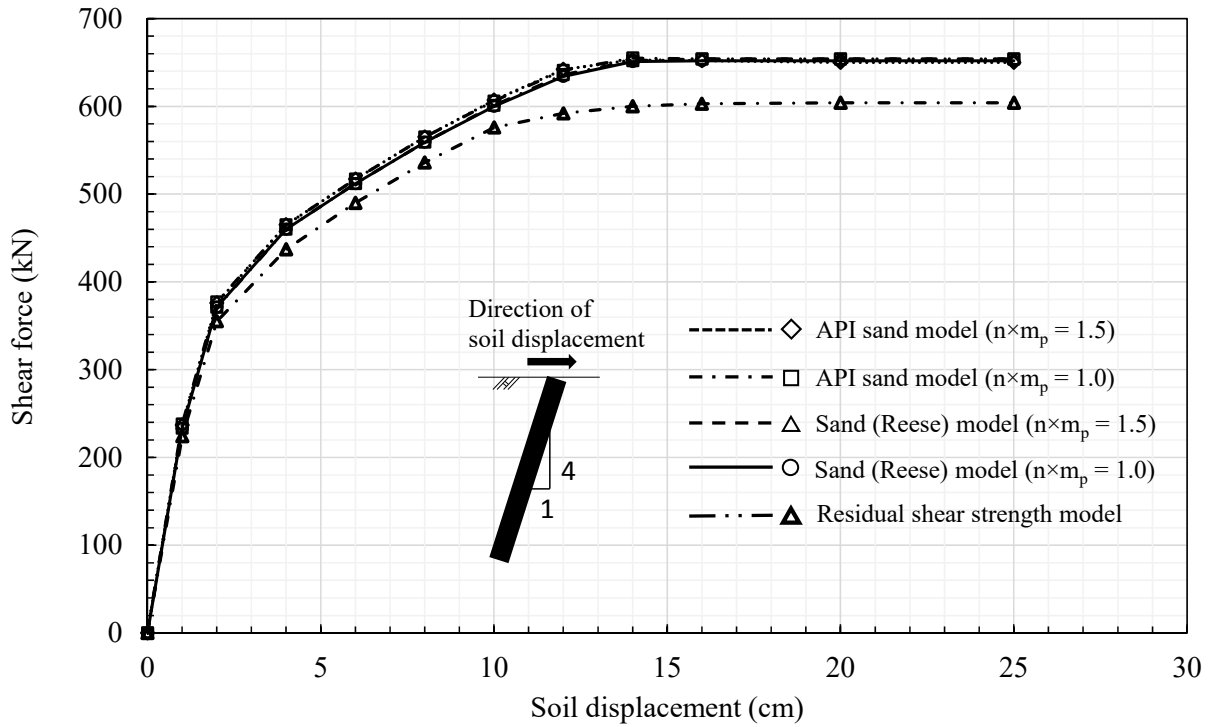


Figure 3.29 Results of the pushover analysis with battered pile (+14 degree), the South Brighton Bridge

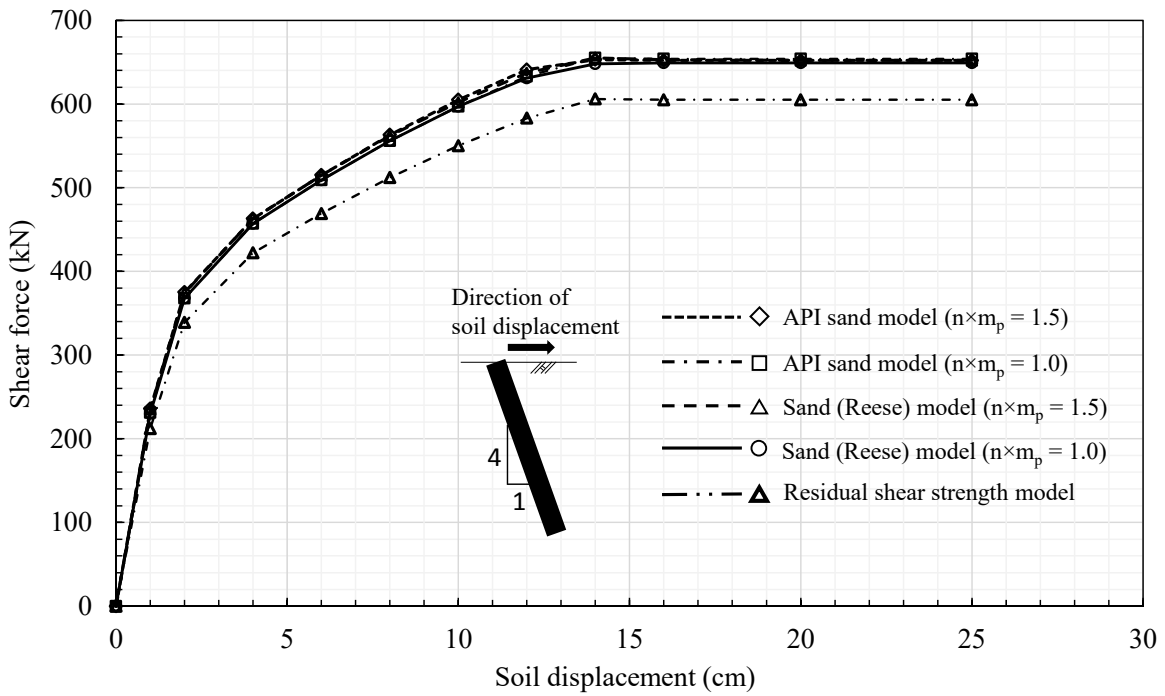
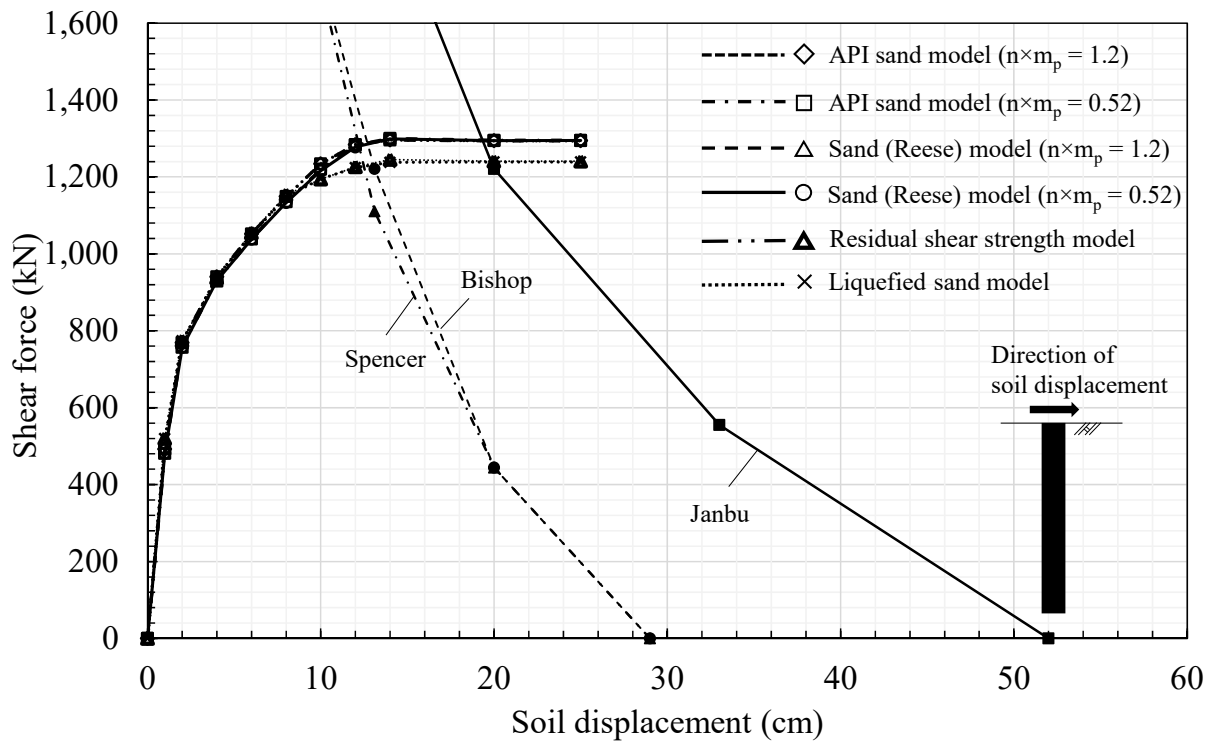


Figure 3.30 Results of the pushover analysis with battered pile (+14 degree), the South Brighton Bridge

## Ground displacement

In order to determine the displacement, the intersection points of pushover analysis and slope stability analysis are obtained. Figure 3.31 - Figure 3.33 show the intersection points for the vertical equivalent single pile and battered equivalent single pile. The both vertical and battered equivalent single pile estimate same ground displacement. The estimated ground displacements are from 11cm to 20cm.



**Figure 3.31 Pushover analysis vs slope stability analysis with 2x5 group piles, the South Brighton Bridge**

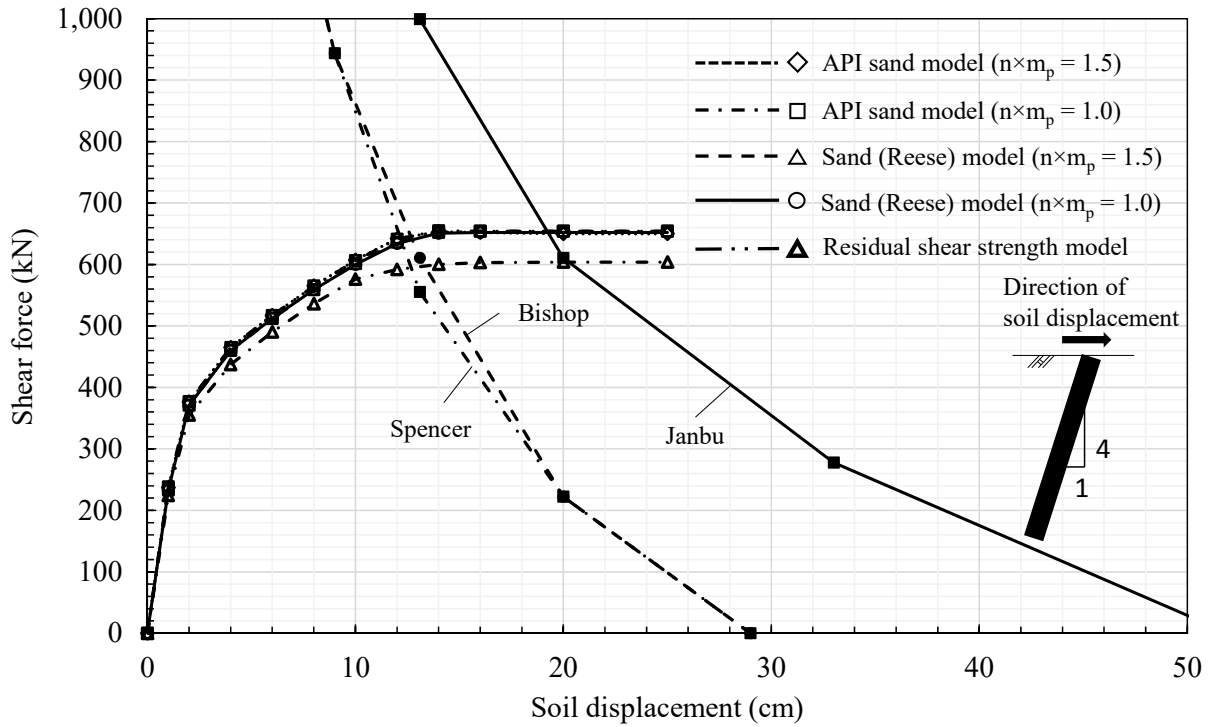


**Figure 3.32 Pushover analysis vs slope stability analysis with battered pile (+14 degree), the South Brighton Bridge**

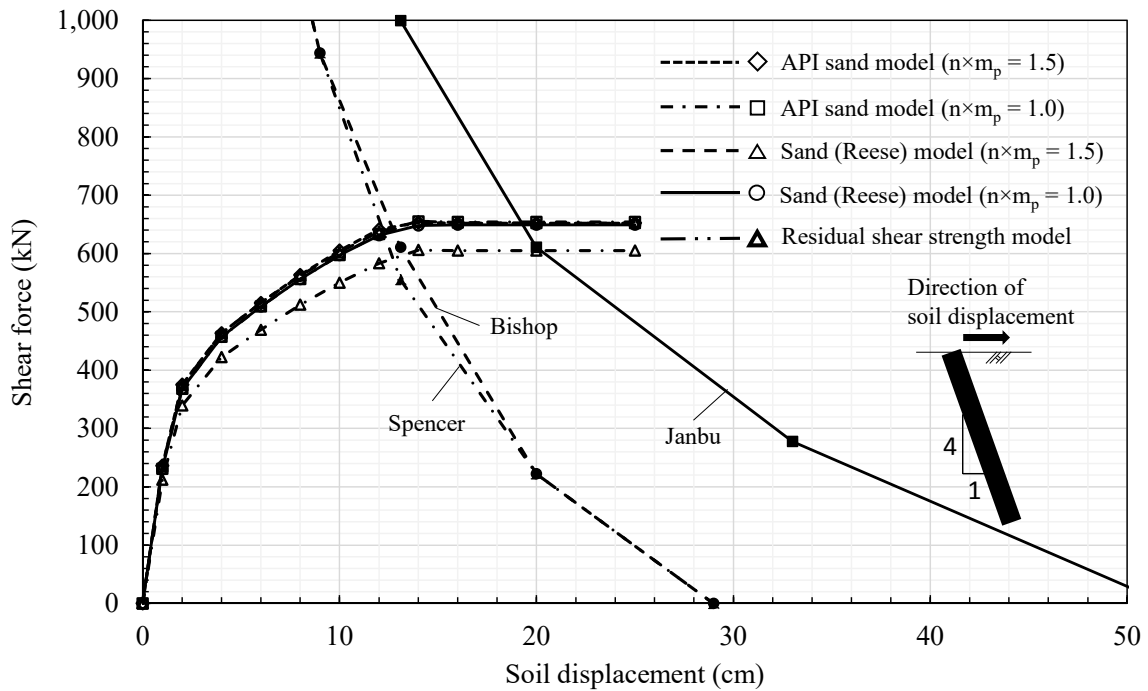


**Figure 3.33 Pushover analysis vs slope stability analysis with battered pile (-14 degree), the South Brighton Bridge**

**Table 3.22 Estimated ground displacement, the South Brighton Bridge**

	Displacement (cm)		
	Bishop	Spencer	Janbu
API sand model ( $n \times m_p = 2.8$ )	11.0	11.0	20.0
API sand model ( $n \times m_p = 0.52$ )	11.0	11.0	20.0
Sand (Reese) model ( $n \times m_p = 2.8$ )	11.0	11.0	20.0
Sand (Reese) model ( $n \times m_p = 0.52$ )	11.0	11.0	20.0
Residual shear strength model	11.5	11.0	20.0
Liquefied sand model	11.5	11.0	20.0

## 5. Results of analysis, the South Brighton Bridge

Figure 3.34 shows results of the analysis of the South Brighton Bridge. Table 3.23 shows the comparison of estimated bending moment with yield and allowable bending moment using the Sand (Reese) and the residual shear strength model.

Observations discussed in Chapter 2 reported that the abutment piles were cracked due to ground displacement and the abutment rotation. The estimated bending moment using Sand (Reese) model exceeds the yield and the allowable bending moment. However the estimated bending moment using the residual shear strength model does not exceed the allowable bending moment. The observed pile damages indicate that the piles exceeded their yield stress because of cracking, but did not reach the allowable bending moment. Sand (Reese) model with Bishop and Spencer method also provide similar results. Therefore, comparing bending moment to the observed pile damages, Sand (Reese) and API sand models with Bishop or Spencer slope stability analysis method provide reasonable results.

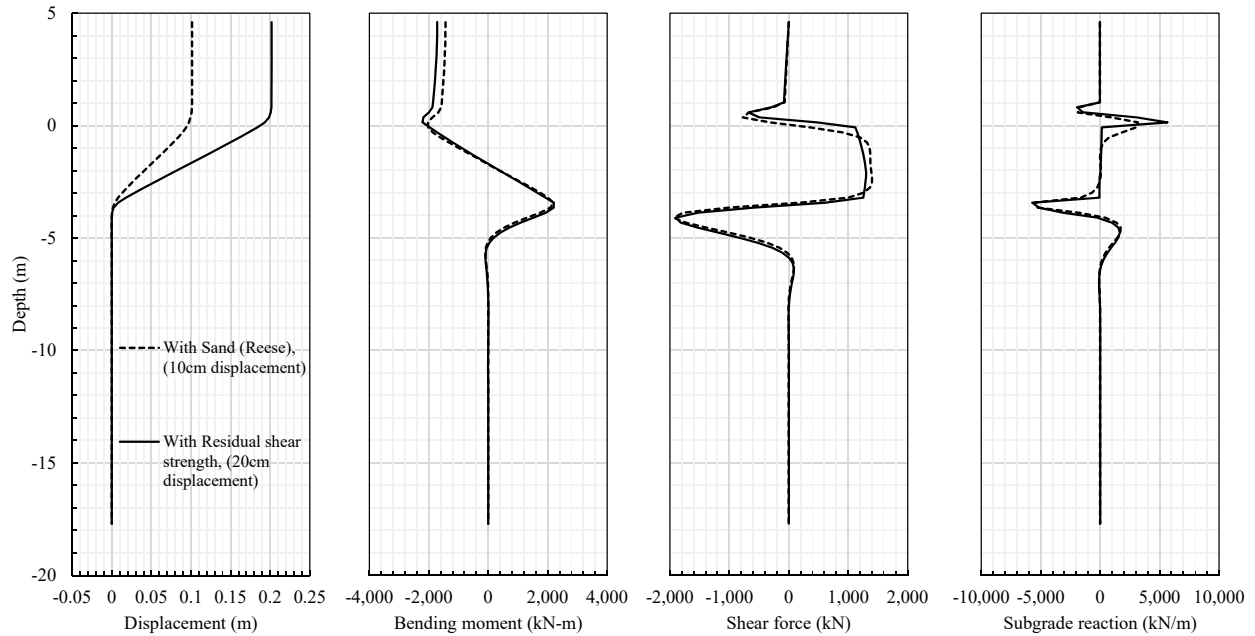


**Figure 3.34 Estimated deflection, bending moment, shear force and subgrade reaction of the abutment foundation, the South Brighton Bridge**

**Table 3.23 Comparison of the estimated bending moment to yield and allowable bending moment, the South Brighton Bridge**

Soil model	Soil displacement (cm)	Estimated maximum bending moment (kN-m)	Yield bending moment (kN-m)	Allowable bending Moment (kN-m)
Sand (Reese) model	10.0	2,204		
Residual shear strength model	20.0	2,186	1,200	2,200

Table 3.24 shows that the estimated pile head displacement and observed pile deflections (the deflections were measured at the connection just beneath the abutment bottom). The pile head displacement is corresponding to the soil displacement. The estimated soil displacement was matched with observed pile deflections.

**Table 3.24 Comparison the estimated pile head displacement to the observed abutment displacement, the South Brighton Bridge**

Soil model	Ground displacement (cm)	Pile head displacement (cm)	Observed pile deflections (cm)
Sand (Reese) model	10.0	10.0	~ 20.0cm
Residual shear strength model	20.0	20.0	

**3.4 Case study: the Mihama Bridge in Japan**

**3.4.1. Observed damages of the Mihama Bridge**

As mentioned bridge performances and ground failures of the Mihama Bridge in Chapter 2, the details are mentioned here again to compare the results of the analysis and the observed damages. Table 3.25 shows that the ground failures and bridge damages of the Mihama Bridge. The ground difference in level about 20cm against the abutment was observed at A1 abutment. The settlement about 63cm at the face of the A1 abutment was measured. The displacements 1cm and 5cm on the A1 approach road were observed. The displacements 10cm, 12.5cm, and 18cm were observed on the ground between the abutment and sea side bank. No settlement of the both abutment was observed. A1 abutment displaced approximately 7cm horizontally. No cracked on the A1 abutment due to the earthquake was observed.

Measured peak ground acceleration at Chiba city was 0.187g (Code CHB009) (K-NET).

**Table 3.25 Observed damages of the ground and bridge structure, the Mihama Bridge**

Observed damages	
Ground failures	<ul style="list-style-type: none"> <li>- The ground difference in level about 20cm against the abutment was observed at A1 abutment.</li> <li>- The settlement about 63cm at the face of the A1 abutment was measured</li> <li>- The displacements 1cm and 5cm on the A1 approach road were observed.</li> <li>- The displacements, 10cm, 12.5cm, and 18cm were observed on the ground between the abutment and sea side bank.</li> </ul>
Bridge damages	<ul style="list-style-type: none"> <li>- The bolts pinned the deck on the A1 bearings were loosened.</li> <li>- No settlement of the both abutment was observed</li> <li>- A1 abutment displaced approximately 7cm horizontally</li> <li>- No cracked on the A1 abutment due to the earthquake was observed</li> </ul>

### 3.4.2. Liquefaction potential evaluation

Liquefaction potential evaluation for the Mihama Bridge is performed using Idriss and Boulanger (2008). Details of the procedures are described in Appendix A.

The Mihama area is reclaimed land and several soil stratum are underlain below water table. According to Chiba city (2011), silty sand fill layers are embedded above -6.0m depth. Silty sand, soft clayey silt, medium dense sand, dense silty sand, and stiff sandy silt are underlain below the silty sand fill layers. Liquefaction potential is evaluated based on SPT N-value at Mihama Bridge site. SPT N-value is referred from Chiba city (2011).

Figure 3.35 shows that the factor of safety of backfill soil is less than one, so this layer is susceptible to liquefaction. Although the bottom of the medium dense silty sand layer is susceptible to liquefaction, it is close to one and the average factor of safety for this layer is over one. Therefore, the effect of excess pore water pressure for piles is negligible. Below medium dense sand layer, liquefaction is not expected because of larger confining stress and high plastic materials. From the evaluation, the backfill layer from +2.0m to -6.0m is classified as liquefiable for the earthquake.

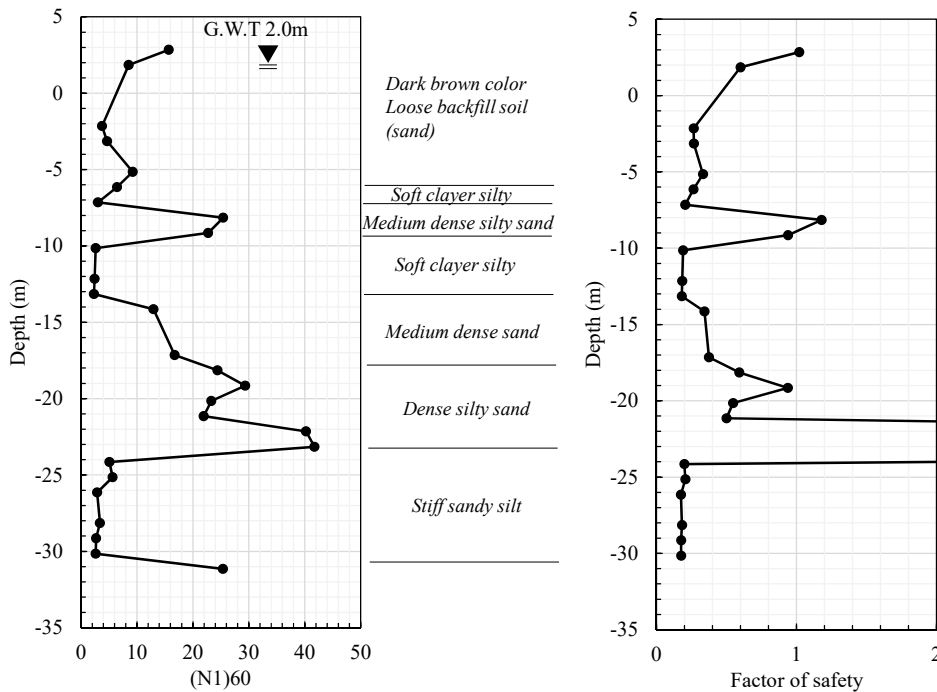


**Figure 3.35 Results of the liquefaction potential evaluation, Mihama Bridge**

### 3.4.3. Description of the Mihama Bridge

The width of the abutment of the Mihama Bridge is 39.0 m, the height is 10.0 m, and the longitudinal length is 8.0 m. 3×14 steel pile group (B = 1.016 m, Thickness = 14mm, 2.8 m spacing between piles, and 33.0 m length) supports the A1 abutment (Chiba City Register 1983). The embankment height is 8.0 m and the slope angle is approximately 30.0°. Internal friction angle of all layers is determined using empirical estimation by Hatanaka and Uchida (1996). The undrain shear strength and soil unit weight are referred from Kulhawy and Mayne (1990). Figure 3.36 and Figure 3.37 show the sketch of the soil layers and the approach embankment of Mihama Bridge.

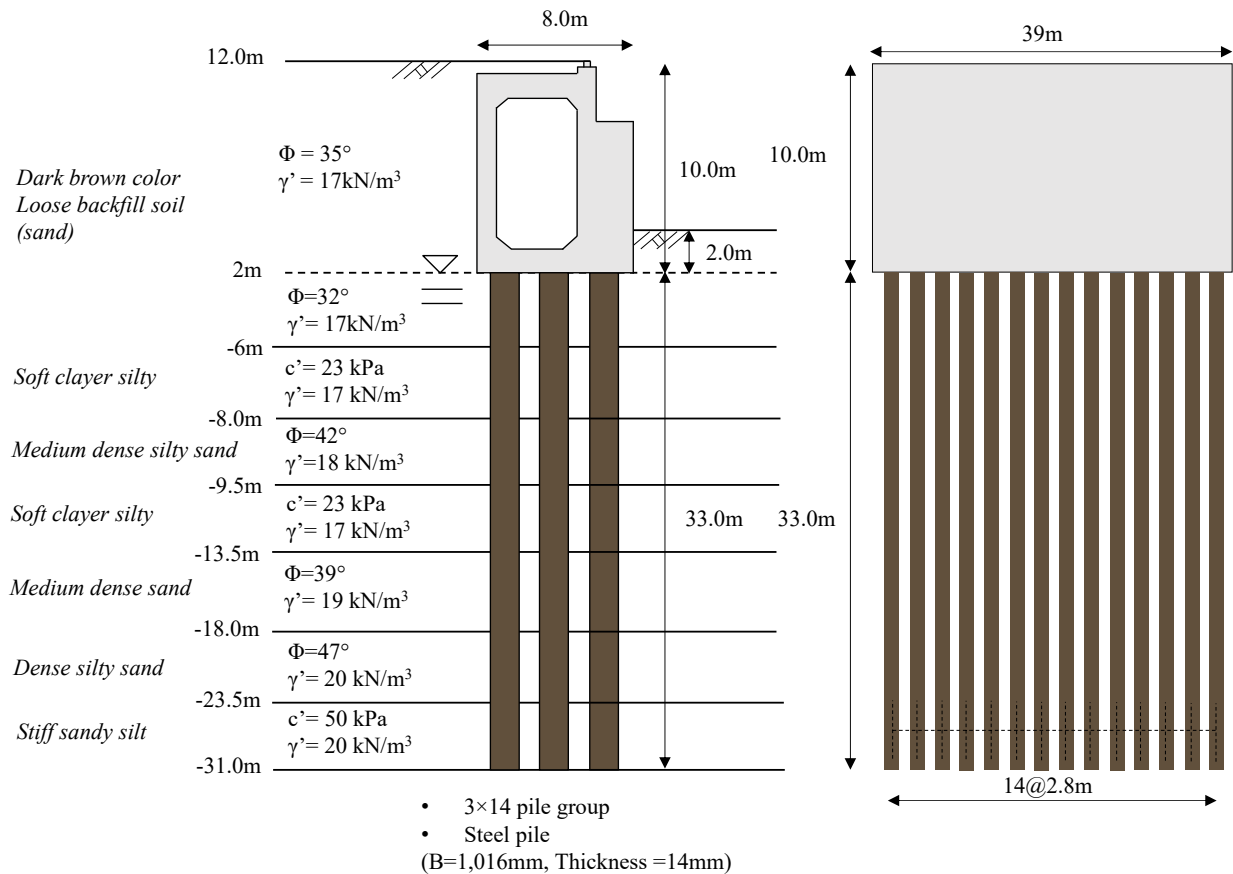
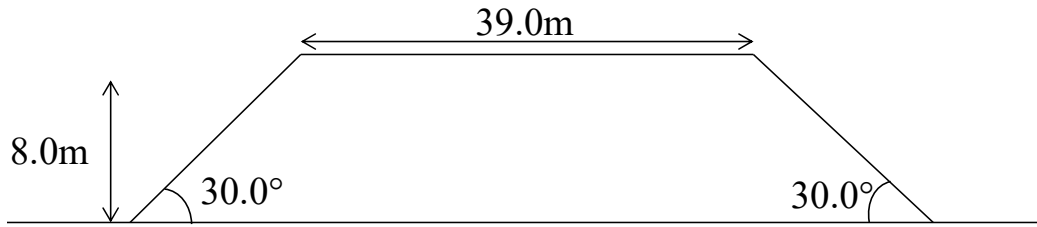


Figure 3.36 Sketch of the Mihama Bridge



**Figure 3.37 Sketch of the embankment of the Mihama Bridge**

**3.4.4. Analysis of the Mihama Bridge with equivalent single pile method**

**1. Modeling a group pile as an equivalent single pile**

The diameter of the steel pile is 1,016mm. Figure 3.38 shows the modeling of the pile group with an equivalent single pile.

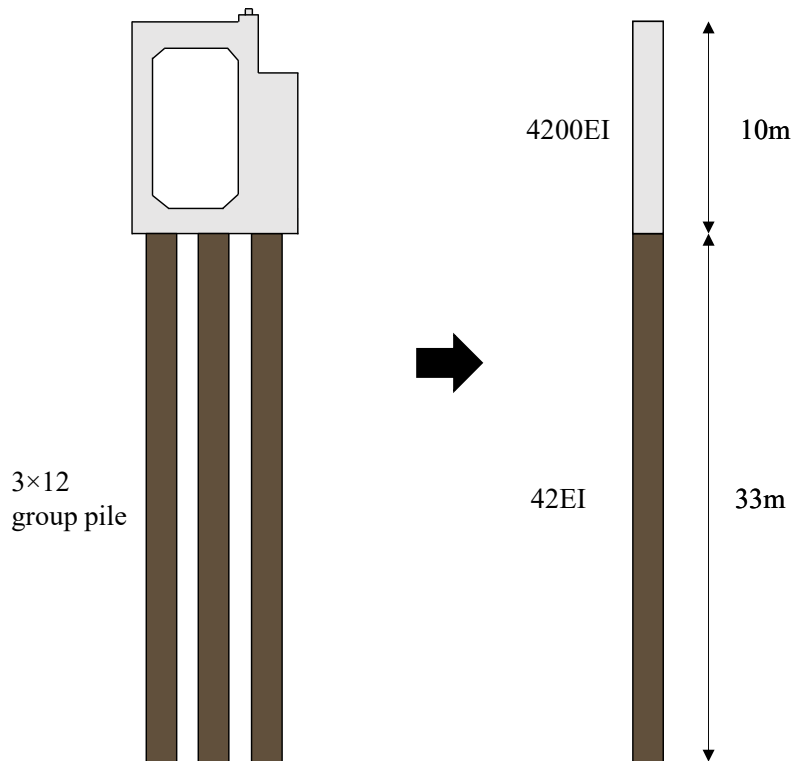


**Figure 3.38 Modeling of an equivalent single pile, the Mihama Bridge**

**Pile section parameters**

The properties shown in Table 3.26 are utilized to model the equivalent non-linear single piles. Figure 3.39 and Figure 3.40 show the bending moment and bending curvature diagram of the pile section and the abutment section. Parameters for the equivalent non-linear single pile are shown in Appendix B.

**Table 3.26 Pile section properties of the Mihama Bridge for original single pile**

Pipe outside diameter (mm)	Pipe wall thickness (mm)	Yield stress of casing (MPa)	Elastic modulus of casing (GPa)
1,016	14	250	200

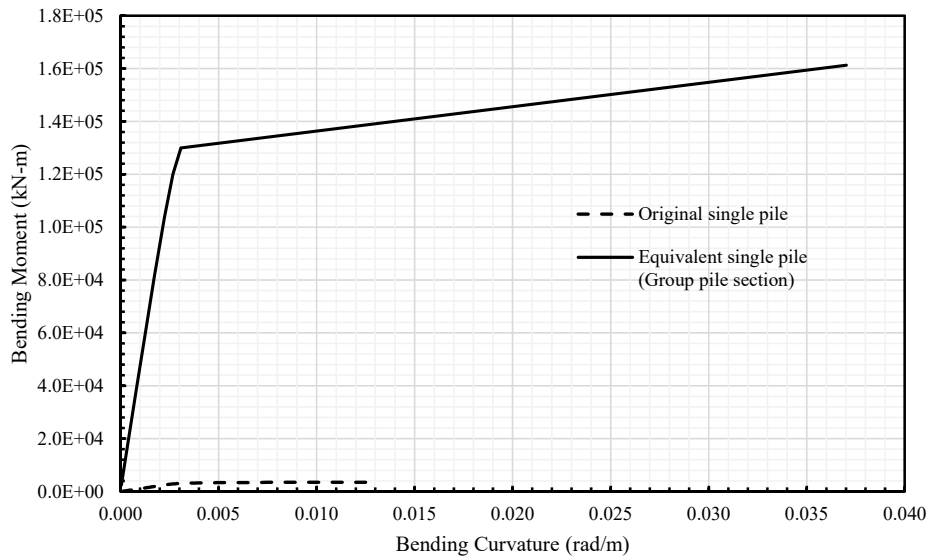


**Figure 3.39 Bending moment – bending curvature of group pile section, the Mihama Bridge**

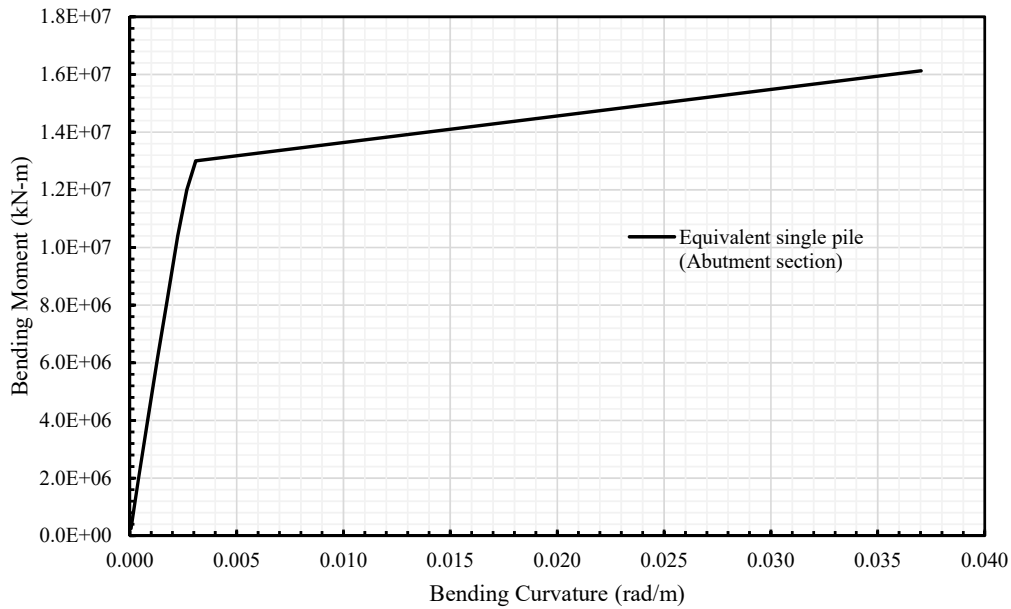


**Figure 3.40 Bending moment – bending curvature of abutment section, the Mihama Bridge**

## 2. Calculation of Foundation Loads Due to the Soil Crust movement

### 2.2. Dimension parameters of the pile cap

To estimate the lateral load of the crust layer against piles, longitudinal width dimensions  $W_T$  and  $W_L$ , pile cap thickness  $T$ , depth to top of cap  $D$ , and crust thickness  $Z_C$  are required. These parameters are shown in Table 3.27.

**Table 3.27 Dimension parameters of the Mihama Bridge**

$W_T$ (m)	$W_L$ (m)	$T$ (m)	$D$ (m)	$Z_c$ (m)
39.0	8.0	10.0	0.0	10.0

### 2.3. Determination of p-y curve for crust layer

The elevation of the abutment bottom is the same as that of the ground water table. Case A considers the case where the bottom of the abutment acts in the crust layer. This is not appropriate for the Mihama Bridge case. Thus, Case B is utilized to calculate passive loads and to develop p-y response.

$F_{ULT-B}$  is expressed as

$$F_{ULT-B} = F_{PASSIVE-B} + F_{SIDES-B}$$

#### $F_{PASSIVE-B}$

$F_{PASSIVE-B}$  is calculated using the following equation.

$$F_{PASSIVE-B} = \left( \bar{\sigma}'_v \cdot K_p + 2 \cdot c' \cdot \sqrt{K_p} \right) \cdot (T) \cdot (W_T) \cdot (k_w)$$

Coefficient of passive pressure  $K_p$  is calculated using Rankine theory.

$$\begin{aligned} K_p &= \tan^2 \left( 45 + \frac{\phi}{2} \right) \\ &= \tan^2 \left( 45 + \frac{35}{2} \right) = 3.69 \end{aligned}$$

$k_w$  is developed by Ovesen (1964) and is expressed as the following equation.

$$\begin{aligned} k_w &= 1 + (K_p - K_a)^{\frac{2}{3}} \cdot \left[ 1.1 \cdot \left( 1 - \frac{T}{D+T} \right)^4 + 1.6 / \left( 1 + \frac{5W_T}{T} \right) + 0.4 \cdot (K_p - K_a) \cdot \left( 1 - \frac{T}{D+T} \right)^3 / \left( 1 + \frac{0.05W_T}{T} \right) \right] \\ &= 1 + (3.69 - 0.27)^{\frac{2}{3}} \cdot \left[ 1.1 \cdot \left( 1 - \frac{10}{0+10} \right)^4 + 1.6 / \left( 1 + \frac{5 \cdot 39}{10} \right) + 0.4 \cdot (3.69 - 0.27) \cdot \left( 1 - \frac{10}{0+10} \right)^3 / \left( 1 + \frac{0.05 \cdot 39}{10} \right) \right] \\ &= 1.17 \end{aligned}$$

Therefore,

$$F_{PASSIVE-B} = \left( 85 \cdot 3.69 + 2 \cdot 0 \cdot \sqrt{3.69} \right) \cdot (10) \cdot (39) \cdot (1.17) = 143,118(kN)$$

#### $F_{SIDES-B}$

$F_{SIDES-B}$  is calculated using equation the following equation.

$$\begin{aligned} F_{SIDES-B} &= 2 \cdot \left( \bar{\sigma}'_v \tan(\delta) + \alpha c' \right) \cdot W_L \cdot T \\ &= 2 \cdot \left( 85 \cdot \tan(35/3) + 0.5 \cdot 0 \right) \cdot 8 \cdot 10 = 2,808(kN) \end{aligned}$$

## F<sub>ULT-B</sub>

The total ultimate crust load of case B becomes following.

$$F_{ULT-B} = 143,118 + 2,808 = 145,926(kN)$$

### 2.4. Determination of $\Delta_{MAX}$

The maximum displacement  $\Delta_{MAX}$  of crust layer for p-y curve at the maximum force is calculated using the following equation.

$$\Delta_{MAX} = (T) \cdot (0.05 + 0.45 \cdot f_{depth} \cdot f_{width})$$

The modification factor  $f_{depth}$  and  $f_{width}$  is calculated using the following equations.

$$\begin{aligned} f_{depth} &= EXP\left[-3 \cdot \left(\frac{Z_c - D}{T} - 1\right)\right] \\ &= EXP\left[-3 \cdot \left(\frac{10-0}{10} - 1\right)\right] = 1 \end{aligned}$$

$$\begin{aligned} f_{width} &= \left\{ \left[ 10 / \left( \frac{W_z}{T} + 4 \right) \right]^4 + 1 \right\}^{-1} \\ &= \left\{ \left[ 10 / \left( \frac{39}{10} + 4 \right) \right]^4 + 1 \right\}^{-1} = 0.28 \end{aligned}$$

Then, the maximum displacement  $\Delta_{MAX}$  is as follows.

$$\begin{aligned} \Delta_{MAX} &= (T) \cdot (0.05 + 0.45 \cdot f_{depth} \cdot f_{width}) \\ &= (10) \cdot (0.05 + 0.45 \cdot 1 \cdot 0.28) = 1.76(m) \end{aligned}$$

### P-y curve for a crust layer

$F_{ULT}$  is the total lateral force of crust layer and the pile cap (abutment). To obtain lateral force per pile cap (abutment) thickness for p-y curve,  $F_{ULT}$  is divided by the pile cap (abutment) thickness  $T$ .  $p_{ULT}$  is calculated by the following equation.

$$p_{ULT} = F_{ULT} / T = 145,926 / 10 = 14,592 (kN / m)$$

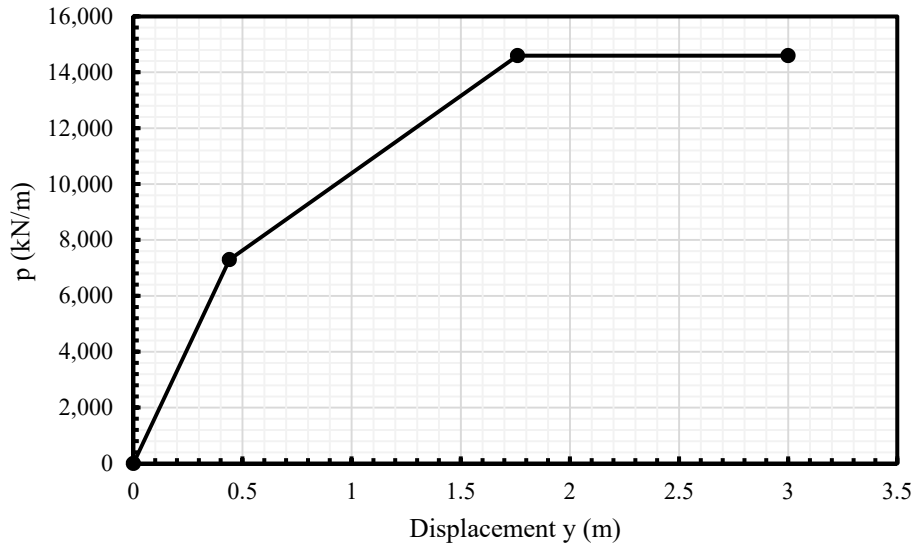


**Figure 3.41 p-y curve of crust layer of the Mihama Bridge's abutment**

### **3. Calculation of p - y Curves for Piles**

An equivalent single pile reaction is described as the following equation.

$$P_{SUPER} = n \cdot m_p \cdot P_{SINGLE}$$

#### **3.1. Evaluating the group reduction factor**

##### Non-liquefiable soil layer

The modification factor  $m_p$  for non-liquefiable soil layers for group piles can be evaluated using Mokwa et al. (2000) **Error! Reference source not found.** With this method, the

reduction factor is described simply as a function of pile space. For the group pile of the Mihama Bridge, the average  $m_p$  should be used.

$$m_p = \frac{\text{First\_row} + \text{Second\_row} + \text{Third\_row}}{3} = \frac{0.80 + 0.65 + 0.55}{3} = 0.67$$

### Liquefiable soil layer

The reduction factor for liquefiable soil layers is calculated as a function of a correlated SPT N-value.  $(N_1)_{60,CS}$  values should be averaged through the liquefiable layer. According to Chiba city's investigation (2011), the range of N-value of SPT is from 3 to 14 blow counts in the liquefiable layer and the average is 7.6. In this analysis,  $(N_1)_{60,CS}$  is assumed as equal to  $N_1$  because no information of rod properties or fines content is provided.  $(N_1)_{60,CS} = 7.6$  is used for  $m_p$ .

$$\begin{aligned} m_p &= 0.0031(N_1)_{60,CS} + 0.00034(N_1)_{60,CS}^2 \\ &= 0.0031 \cdot 7.6 + 0.00034 \cdot 7.6^2 = 0.04 \end{aligned}$$

### **3.2. Modification of the group reduction factor near liquefied soil layer boundary**

The effective distance at the vicinity of liquefied layer for p-y curve is estimated by pile diameter and modification factor  $S_b$ . The  $S_b$  and the effective distance are obtained from the following equations.

$$S_b = 2 - (D - 1) / 2 = 2 - (1.016 - 1) / 2 = 1.99$$

$$S_b \cdot D = 1.99 \cdot 1.016(m) = 2.02(m)$$

The subgrade reaction of a group pile for Winkler type soils is described as a function of relative displacement of piles, stiffness factor  $k$ , and reduction factor  $m_p$ . In this analysis,  $m_p$  is also modified to consider the effect of liquefaction for p-y curve in the vicinity of the liquefied layer. Table 3.29 shows reduction factor  $m_p$  with respect to distance from the liquefied layer and Figure 3.42 shows reduction factors for each depth.

**Table 3.28 Reduction factor for vicinity of liquefied layer for the Mihama Bridge**

Distance from the liquefied layer (m)	Adjustment factor	$m_p$
0.7	$\frac{1}{3} + \frac{2}{3} \cdot m_p = 0.36$	$0.36 \cdot 0.67 = 0.24$
1.4	$\frac{2}{3} + \frac{1}{3} \cdot m_p = 0.68$	$0.68 \cdot 0.67 = 0.45$
2.0	1	0.67

**Table 3.29 Reduction factor for each depth, the Mihama Bridge**

Depth (m)	$m_p$	$n \times m_p$
0-10.0	1	1
10.0-18.0	0.04	1.7
18.0-18.7	0.24	10.0
18.7-19.4	0.45	18.9
19.4-43.0	0.67	28.1

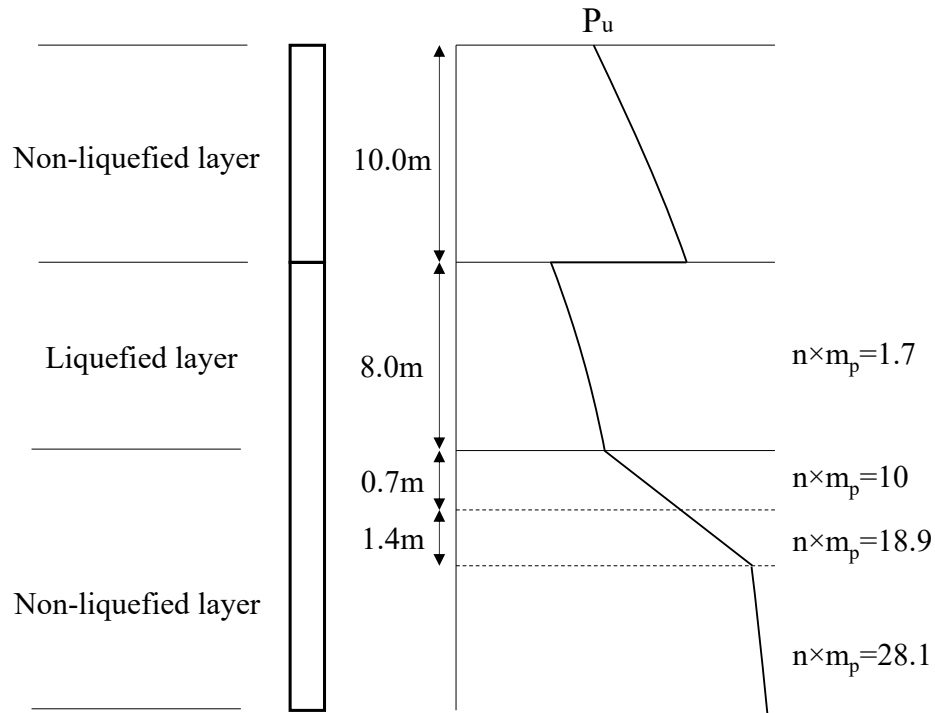


**Figure 3.42 Modification factor near liquefiable layers, the Mihama Bridge**

#### 4. Estimation of crust displacement

##### Slope stability analysis

The restricted crust displacement is evaluated by Bray and Travasarou (2007). The horizontal acceleration is obtained using GeoStudio 2012 software. For Mihama Bridge case, the abutment was not plunged into wing walls and no damages were observed on the abutment. Therefore, the lateral force from a bridge deck against the backfill soil is not expected.

The soil failure stress of liquefied layer calculated using Kramer (2008) is applied for the liquefied layer.

- 1) For the liquefiable layer under backfill soil and the abutment

$$\begin{aligned} \bar{\sigma}_v' &= 17(kN / m^3) \cdot 13.0(m) - 9.8(kN / m^3) \cdot 3.0(m) \\ &= 191(kPa) = 3,989(psf) \end{aligned}$$

$$S_r = 2116 \cdot \exp \left[ -8.444 + 0.109 \cdot \bar{N} + 5.379 \cdot \left( \frac{\bar{\sigma}_v}{2,116} \right)^{0.1} \right]$$

$$= 2,116 \cdot \exp \left[ -8.444 + 0.109 \cdot 7.2 + 5.379 \cdot \left( \frac{3,989}{2,116} \right)^{0.1} \right] = 307(\text{psf}) = 14(\text{kPa})$$

2) For the liquefiable layer under the front of the abutment

$$\bar{\sigma}_v = 17(\text{kN} / \text{m}^3) \cdot 6.0(\text{m}) - 9.8(\text{kN} / \text{m}^3) \cdot 3.0(\text{m})$$

$$= 72.6(\text{kPa}) = 1,516(\text{psf})$$

$$S_r = 2116 \cdot \exp \left[ -8.444 + 0.109 \cdot \bar{N} + 5.379 \cdot \left( \frac{\bar{\sigma}_v}{2,116} \right)^{0.1} \right]$$

$$= 2,116 \cdot \exp \left[ -8.444 + 0.109 \cdot 7.2 + 5.379 \cdot \left( \frac{1,516}{2,116} \right)^{0.1} \right] = 181(\text{psf}) = 8.6(\text{kPa})$$

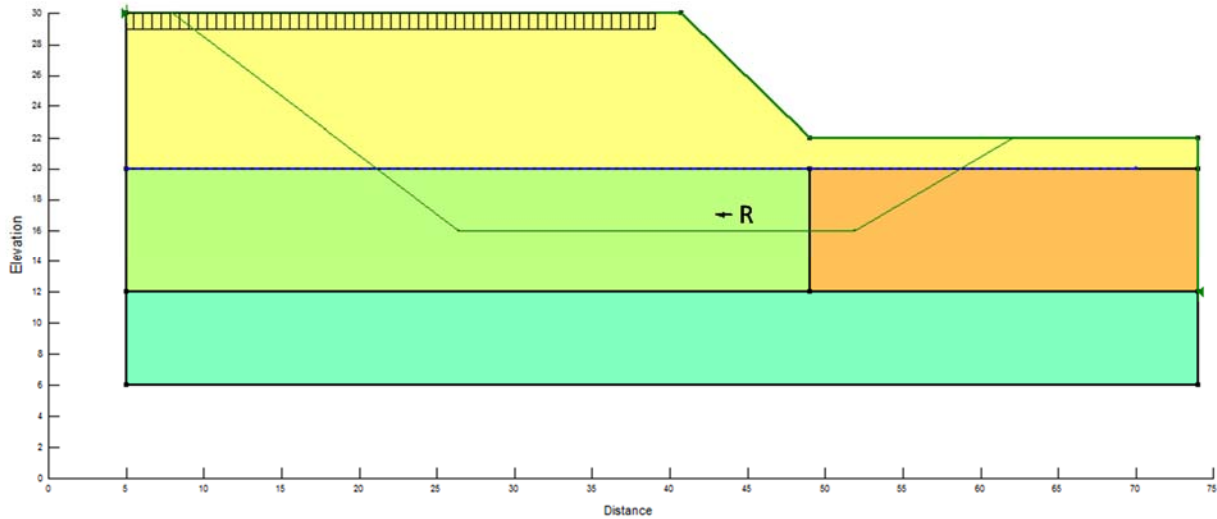


**Figure 3.43 Slope stability analysis model to determine coefficient of horizontal acceleration, the Mihama Bridge**

For slope stability analysis, Bishop, Janbu, and Spencer methods are utilized to calibrate possible displacements. The example of the estimated displacement by Bray and Travararou (2007) is shown in Table 3.30. The sample calculation using Bishop method is shown below. Other calculations are shown in Appendix C. Figure 3.44 shows the displacement – shear force diagram using Bishop, Janbu, and Spencer method.

$$D(cm) = \exp \left\{ -0.22 - 2.83 \cdot \ln(0.024) - 0.333 \cdot [\ln(0.024)]^2 + 0.566 \cdot \ln(0.024) \cdot \ln(0.189) \right. \\ \left. + 3.04 \cdot \ln(0.189) - 0.244 \cdot [\ln(0.189)]^2 + 0.278 \cdot (9.0 - 7) \right\}$$

$$= 56.4(cm)$$

The effective width is calculated using the following equation.

$$W_{\text{effective}} = W_T + m/2 \cdot H$$

$$= 39 + 1.72/2 \cdot 8.0 = 45.9(m)$$

**Table 3.30 Slope stability analysis results using Bishop method, displacements are determined using Bray and Travasarou (2007), the Mihama Bridge**

$k_y$	R (kN/m)	Bishop	
		R*W <sub>T-effective</sub> (kN)	D (cm)
0.024	0	0	56.4
0.04	70	3,213	26.8
0.05	115	5,278	18.3
0.06	160	7,344	13.1
0.07	205	9,409	9.7
0.08	250	11,475	7.3
0.09	290	13,311	5.7
0.1	330	15,147	4.5
0.11	380	17,442	3.6
0.12	420	19,278	2.9
0.13	460	21,114	2.4

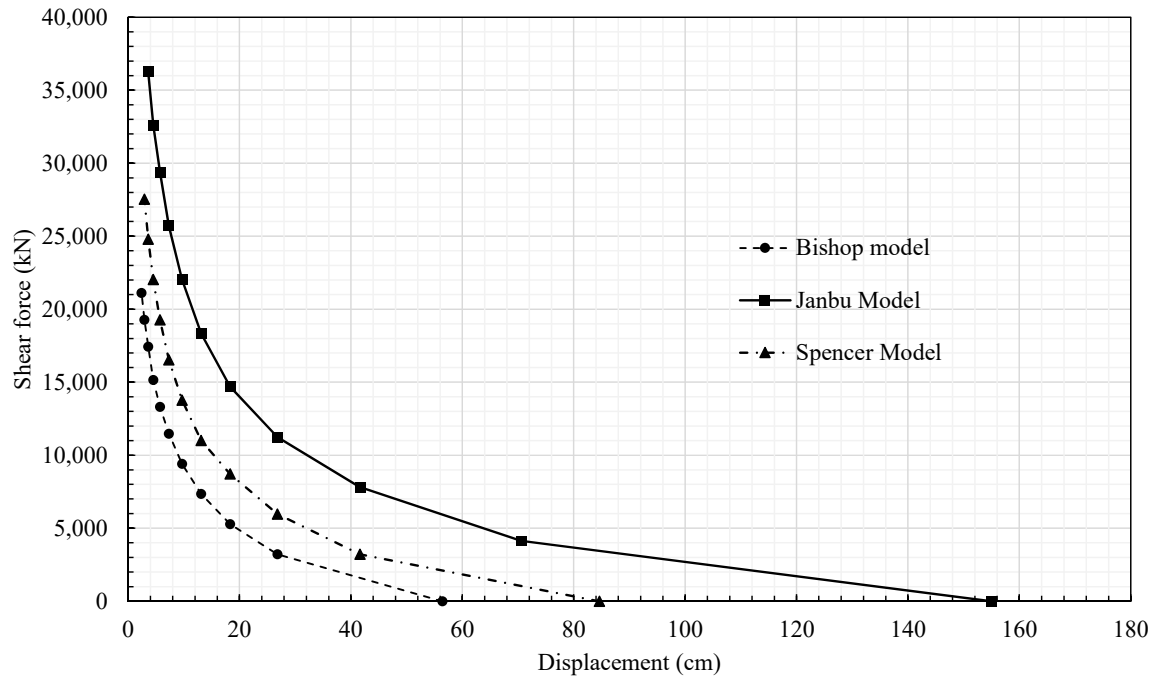


**Figure 3.44 The results of slope stability analysis, the Mihama Bridge**

## **Pushover analysis**

### *Input parameters*

Internal friction angles of all layers are determined using empirical estimation by Hatanaka and Uchida (1996). The undrain shear strength is estimated and soil unit weight are referred from Kulhawy and Mayne (1990). The modulus of subgrade reactions for non-cohesive soils are referred from Brandenberg et al. (2013). The strain factor  $\epsilon_{50}$  is referred from Reese and Van Impe (2011).

**Table 3.31 Input parameters for pushover analysis of the Mihama Bridge**

p-y curve model	Elevation of top of soil layer (m)	Elevation of bottom of soil layer (m)	Effective soil unit (kN/m <sup>3</sup> )	Friction angle (°)	Undrain shear strength (KPa)	Modulus of subgrade reaction (kN/m <sup>3</sup> )	Strain Factor $\epsilon_{50}$
User input p-y curve	0	10	17	-	-	-	-
Several soil models used	10	18.0	17	-	-	-	-
Soft clay (Matlock)	18.0	20.0	17	-	23	-	0.020
Sand (Reese)	20.0	21.5	18	42	-	80,000	-
Soft clay (Matlock)	21.5	25.5	17	-	23	-	0.020
Sand (Reese)	25.5	30	19	39	-	76,000	-
Sand (Reese)	30	35.5	20	47	-	160,000	-
Soft clay (Matlock)	35.5	43	18	-	50	-	0.010

Other soil models are also applied to calibrate the soil displacement – shear force relationships for the liquefiable soil layer. Liquefied sand model and residual shear strength models are applied with soft clay (Matlock). Table 3.32 shows p-y curve models and input parameters for liquefiable sand (10m-18.0m).

**Table 3.32 Input parameters for liquefiable layer of the Mihama Bridge**

p-y curve model	Elevation of top of soil layer (m)	Elevation of bottom of soil layer (m)	Effective soil unit (kN/m <sup>3</sup> )	Friction angle (degree)	Undrain shear strength (KPa)	Modulus of subgrade reaction (kN/m <sup>3</sup> )	Strain Factor $\epsilon_{50}$
Sand (Reese)	10	18.0	17	32	-	35,000	-
API sand (O'Neill)	10	18.0	17	32	-	35,000	-
Liquefied sand (Rollins)	10	18.0	17	-	-	-	-
Soft clay (Matlock)	10	18.0	17	-	14 <sup>1)</sup>	-	0.05

1) The residual shear strength is estimated using Kramer and Wang (2007)

Pushover analysis is performed to determine the average shear force of the equivalent single pile through liquefied layer with increasing soil displacement. The calculated shear force is corresponding to the resistance force R, which is obtained from a slope stability analysis. Figure 3.45 shows the results of the pushover analysis using several soil models.

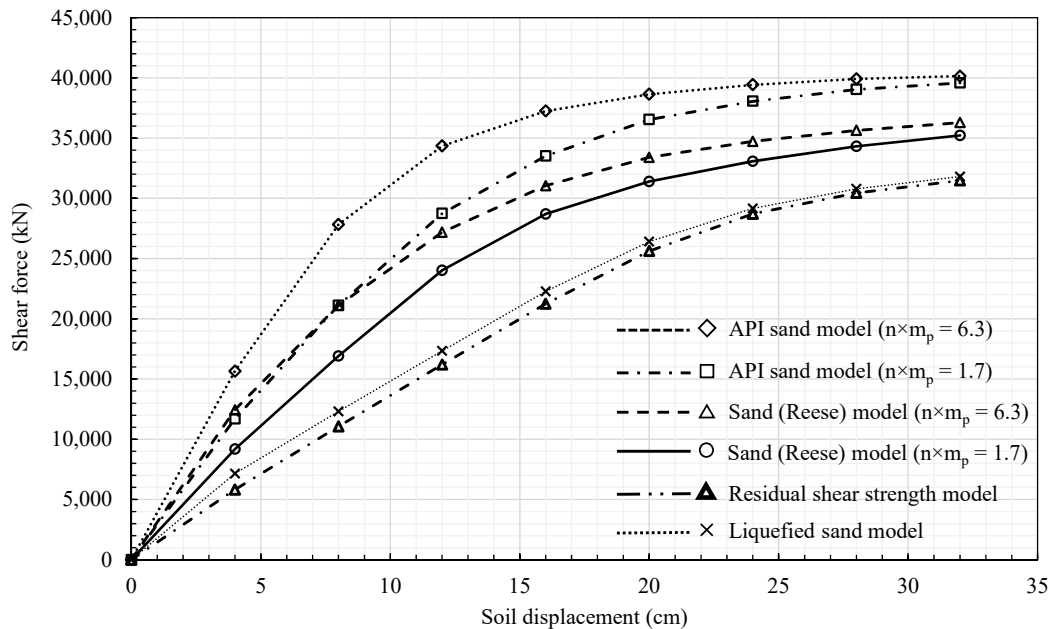


**Figure 3.45 Pushover analysis of the Mihama Bridge**

## Ground displacement

In order to determine the ground displacement, the intersection points of pushover analysis and slope stability analysis are obtained. Figure 3.46 shows the intersection points. The ground displacements are estimated from 4.0cm to 13.5cm. The observed ground displacement is from 1cm to 18cm. All estimated ground displacements are within the observed range. A comparison of the estimated ground displacements to the observed displacements is shown in Table 3.33.

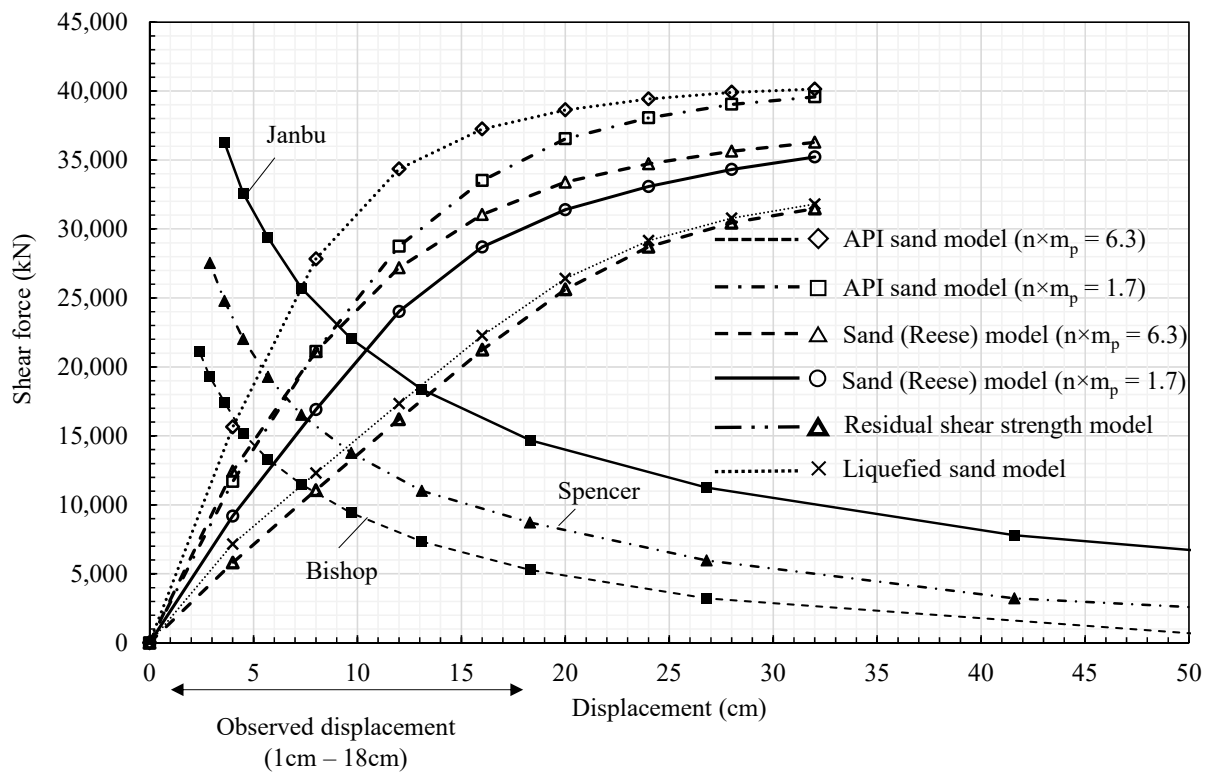


**Figure 3.46 Shear force – Displacement diagram, the Mihama Bridge**

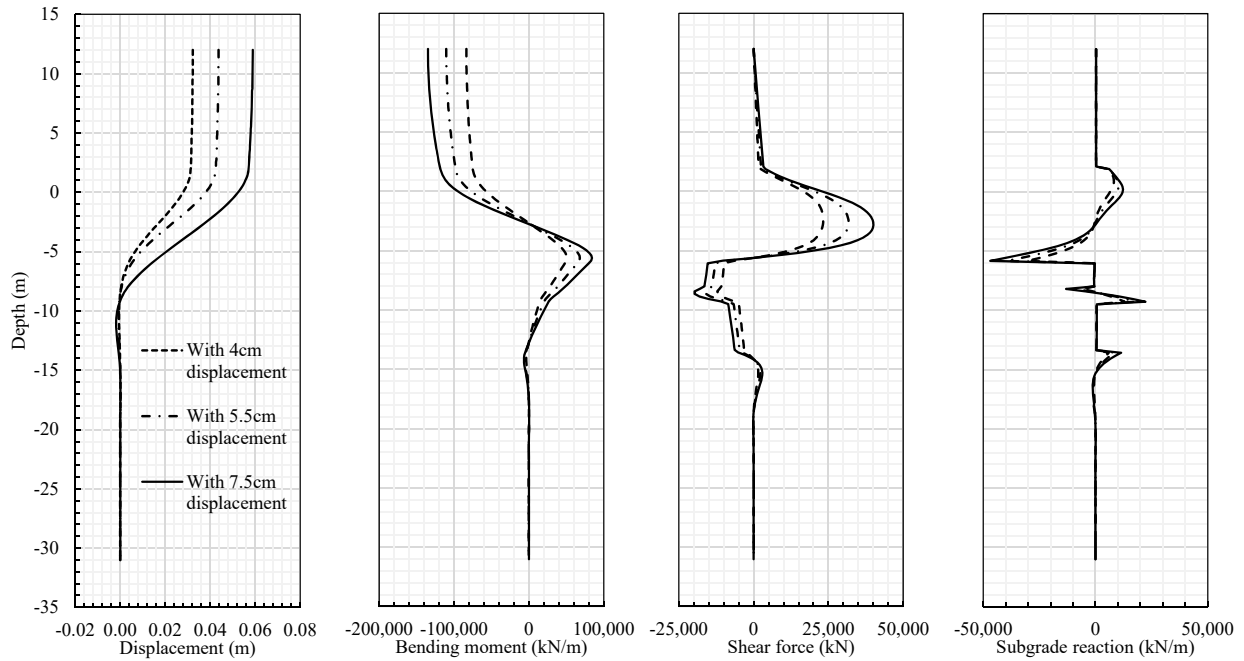
**Table 3.33 Estimated ground displacement, the Mihama Bridge**

	Displacement (cm)			Observed displacement (cm)
	Bishop	Spencer	Janbu	
API sand model ( $n \times m_p = 6.3$ )	4.0	5.5	7.0	
API sand model ( $n \times m_p = 1.7$ )	5.0	6.5	9.0	
Sand (Reese) model ( $n \times m_p = 6.3$ )	5.0	6.5	9.0	
Sand (Reese) model ( $n \times m_p = 1.7$ )	6.0	7.5	10.5	1cm – 18cm
Residual shear strength model	8.0	9.5	13.0	
Liquefied sand model	7.5	10.0	13.5	

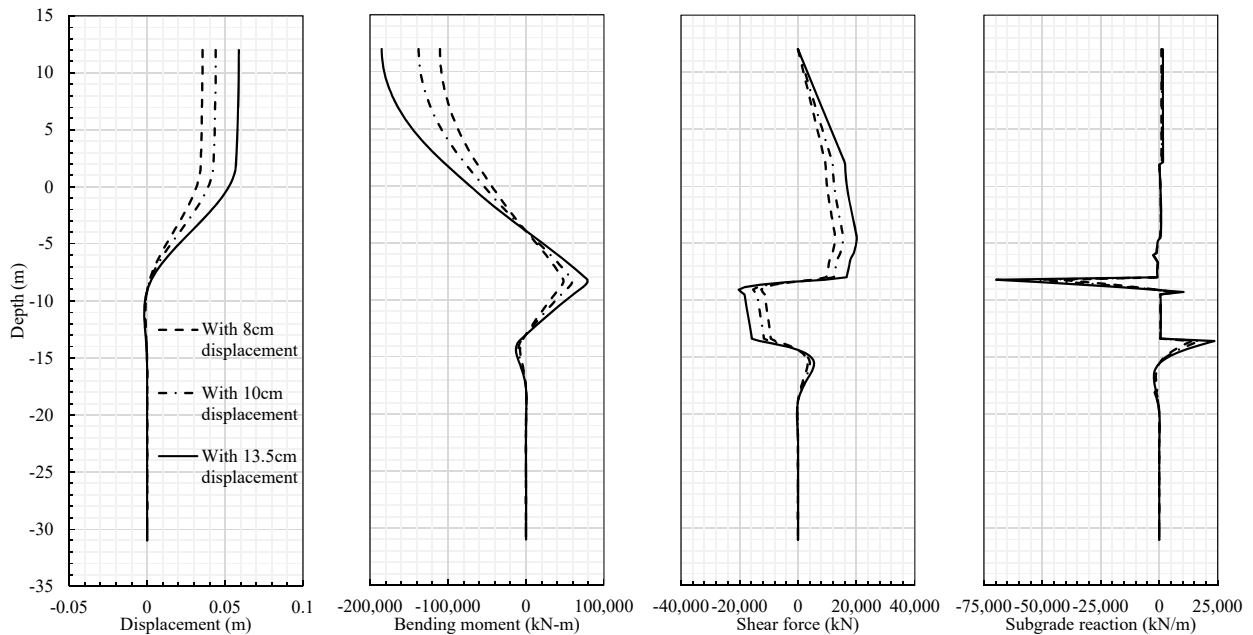
## 5. Results of analysis of Mihama Bridge

Figure 3.47 - Figure 3.49 show the analysis of the Mihama Bridge with API sand (O'Neill) model ( $n \times m_p = 6.3$ ) and the residual shear strength model. The API sand (O'Neill) and the residual shear strength model provide the maximum and minimum displacements. Table 3.34 shows the comparison of estimated bending moment with yield and allowable bending moment.

Observations showed that although the A1 abutment displaced horizontally due to liquefaction, no damaged (i.e., no cracks) or settlement were confirmed. In addition, the Mihama Bridge was still in service after the earthquake. Thus, no significant damage to the foundations and structures are expected. The results with the API sand model, the residual shear strength model, and observed ground displacement show that the estimated maximum bending moment does not exceed both yield and allowable bending moment except with 18cm ground displacement. This indicates that the estimation of the pile performances using the observed maximum soil displacement does not always correspond to the observed performances. This possibly means that the displacement cannot be determined deterministically.



**Figure 3.47 Estimated deflection, bending moment, shear force and subgrade reaction using API sand model ( $n \times m_p = 6.3$ ), Mihama Bridge**



**Figure 3.48 Estimated deflection, bending moment, shear force and subgrade reaction using the residual shear strength, Mihama Bridge**

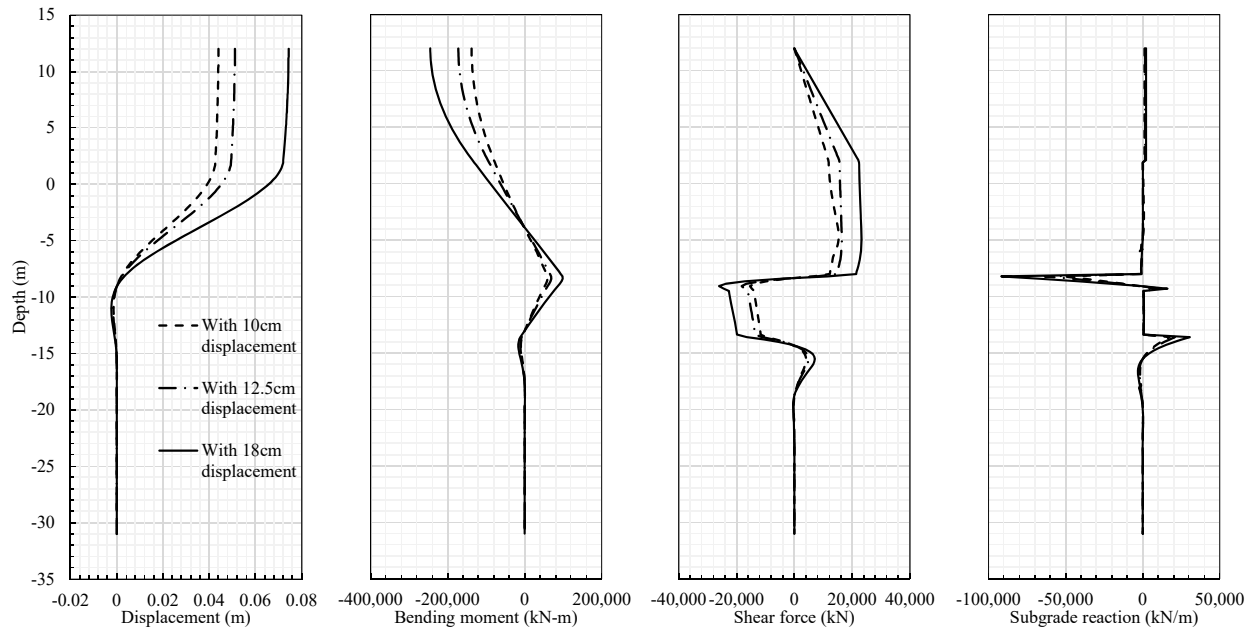


**Figure 3.49 Estimated deflection, bending moment, shear force and subgrade reaction with observed ground displacement, Mihama Bridge**

**Table 3.34 Comparison of the estimated bending moment to yield and allowable bending moment, Mihama Bridge**

Soil model	Soil displacement (cm)	Estimated maximum bending moment (kN-m)	Yield bending moment (kN-m)	Allowable bending Moment (kN-m)
API sand (O'Neill) model	4	75,083		
	5.5	98,584		
	7.5	119,154		
Residual shear strength model	8.0	62,397		
	10.0	77,245		
	13.5	102,963	130,000	161,258
Residual shear strength model (with observed displacement)	10	77,245		
	12.5	92,367		
	18.0	131,014		

Table 3.35 shows the estimated pile head displacement with API sand (O'Neill) model and the residual shear strength model. There are no measurements of the pile head or the A1 abutment displacement. However, backfill soil displacements from 1cm to 5cm were measured. This displacement may be restricted by the A1 abutment. In other words, the A1 abutment displacement may be close to the backfill soil movements. The estimated pile head displacement is from 3.2cm to 7.4cm, which is close to the observed backfill displacements.

**Table 3.35 Comparison of the estimated pile head displacements to the observed ground displacements**

Soil model	Soil displacement (cm)	Pile head displacement (cm)	Observed ground displacements (cm)
API sand (O'Neill) model	4	3.2	1 cm - 18.0cm
	5.5	4.3	
	7.5	5.5	
Residual shear strength model	8.0	3.5	
	10.0	4.4	
	13.5	5.9	
Residual shear strength model (with observed displacement)	10	4.4	
	12.5	5.1	
	18.0	7.4	

### 3.5 Summary

The Mataquito Bridge in Chile, the South Brighton Bridge in New Zealand, and the Mihama Bridge in Japan are analyzed using the guidelines and procedures recommended by Ashford et al. (2011) and Shantz (2013).

Table 3.36 shows the comparison of estimated ground displacement and pile head displacement to the observed ground displacement and the abutment displacement. The estimated ground displacement of the Mihama Bridge is within the observed ground displacement and the maximum estimated ground displacement is 75% of that observed. The results of the Mataquito Bridge slightly overestimated the pile head displacement compared to the observations. However, the Bishop method with the residual shear strength model estimates the pile head displacement less than 2cm, which matches the observation. For the South Brighton Bridge, the estimated ground displacement and pile head displacement are close to the observed pile deflections.

Table 3.37 shows the comparison of estimated maximum bending moment to the yield and allowable bending moment. The north abutment of the Mataquito Bridge moved less than 2cm due to liquefaction, yet no damages or settlements were observed, which indicate that the pile foundation did not exceed the yield bending moment. Judging from the results, Sand (Reese) and API sand (O'Neill) model overestimate the maximum bending moment. On the other hand, the estimated values using the residual shear strength model do not exceed the yield bending moment and provide acceptable results. For the South Brighton Bridge, cracks on the piles were observed. The results show that the estimated bending moment exceeds the yield bending moment. Moreover, the bending moment using Sand (Reese) and API sand (O'Neill) is beyond the allowable bending moment. However, the residual shear strength model estimated the bending moment under the allowable bending moment, which provides pile performance similar to the observations. For the Mihama Bridge, no damages and no settlement of the A1 abutment were observed. The results using all soil models and the observed ground displacement match with the observed performances, except with 18 cm of displacement.

In summary, the Bishop slope stability analysis method with the residual shear strength model provides reasonable results for each bridges compared to the observed ground failures, bridge damages, and pile foundation damages.

**Table 3.36 Comparison of estimated displacement with observed displacement of each bridge**

Bridge	Estimated ground displacement (cm)	Estimated pile head displacement (cm)	Observed ground displacement (cm)	Observed abutment displacement or deflection (cm)
Mataquito Bridge (Chile)	4-10 (PGA = 0.461) 3.5-8 (PGA=0.390)	1.5-6.1	-	Less than 2cm
South Brighton Bridge (New Zealand)	11-20	10-20	-	~20cm
Mihama Bridge (Japan)	4-13.5	3.2-7.4	1 -18	-

**Table 3.37 Comparison of estimated the yield and allowable bending moment of each bridge**

Bridge	Estimated maximum bending moment (kN-m)	Yield bending Moment (kN-m)	Allowable bending moment (kN-m)
Mataquito Bridge (Chile)	38,099 - 55,815	45,000	62,920
South Brighton Bridge (New Zealand)	2,186-2,204	1,200	2,200
Mihama Bridge (Japan)	75,083-119,154 (using estimated ground displacement) 77,245-131,014 (using observed ground displacement)	130,000	161,258

## Chapter 4. DISCUSSION

### 4.1. Introduction

In Chapter 3, the pile performances experienced in liquefaction-induced lateral spreading are analyzed using the guideline and procedures recommended by Ashford et al. (2011) and Shantz (2013) for three case histories. The Caltrans recommended procedure, in simple terms, is completed by modeling a pile group as an equivalent single pile, developing a p-y curve for a pile cap (abutment), estimating a reduction factor  $m_p$ , estimating the kinematic and inertial loads against foundation-superstructure interaction, estimating crust layer displacement, and considering the pile pinning effect.

In this chapter, some interesting initial results and discussions regarding important analysis parameters are given. In future work, more sensitive analyses should be performed to investigate the Caltrans procedure more fully.

### 4.2. Pile modeling

An equivalent non-linear single pile is simply modeled by  $nEI$ , where  $n$  is number of piles, and  $EI$  is the original pile's bending stiffness. For the abutment section, the bending stiffness is modeled by the  $100nEI$  to achieve rigidity.

For the three cases, the bending moment and the shear force of the abutment section do not exceed the yield bending moment. This matches the observed abutment damages. In addition, the deflections of the abutment section are very small. The pile deflections of an equivalent non-linear single pile are only caused by the group pile section. These are sufficient for modeling abutments and group piles as a single pile.

However, the earthquake case history data show that the abutment was damaged by the excessive moment force. For the Fitzgerald Bridge in Christchurch, New Zealand, the cracks on the abutment was developed due to liquefaction induced lateral spreading and the interaction with the deck, which indicate that the lack of bending stiffness of the abutment is a possible difficulty for an equivalent non-linear single pile model. However, it is a rare case. If the thickness of the abutment is similar to the pile diameter, and the high bending stiffness is not expected, more accurate modeling for the abutment section is required.

### 4.3. P-y curve

Observed and estimated abutment displacements are less than a quarter of the estimated maximum displacement for the developed p-y curve of the abutment section. From these results, the important parameter for p-y curve for an abutment is the degree of initial slope of the p-y curve.

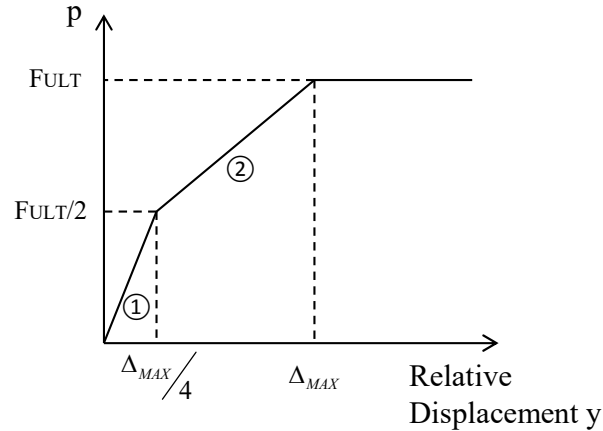
Brandenberg et al. (2007) concluded that the subgrade reaction against the pile cap is reduced by cyclic loading because crust layers underlain by liquefiable layer are softened by the influence of degradation and developing cracks. Then, passive pressure acting on pile caps is smaller than the static loading in lateral spreading. This effect should work on the abutment.

Table 4.1 shows the estimated slopes of p-y curves,  $k_{py}$ , for the three bridge cases. According to Reese and Van Impe (2011), the slope of p-y curve of medium dense sand above the water table for a single pile and static loading is  $24,400 \text{ (kN/m}^3) \times \text{depth}$ . For each bridge case, the slope  $E_{py}$  of p-y curve becomes  $122,000 \text{ kN/m}^2$  (Mataquito Bridge),  $43,920 \text{ kN/m}^2$  (South Brighton Bridge),  $122,000$  (Mihama Bridge) respectively. The estimated initial slope  $k_{py}$  for each bridge case is approximately  $1/4 - 1/5$  of the above values. These values provide same results to Brandenberg et al. (2007).

Note that the estimated pile head displacements for the Mataquito Bridge and the South Brighton Bridge cases match with the observed abutment displacements using the residual shear strength model with Bishop slope stability method. Although only two cases are compared, the subgrade reaction can estimate reasonable lateral loads. Therefore, the estimated p-y curve for the abutment section is sufficient with observations.

**Table 4.1 Comparison of initial slope of p-y curve for each abutment**

	First slope ① ( $\text{kN/m}^2$ )	Second slope ② ( $\text{kN/m}^2$ )	$k_{py}$ recommended by Reese and Van Impe (2011) ( $\text{kN/m}^2$ )
Mataquito Bridge	24,023	12,011	122,000
South Brighton Bridge	12,280	4,093	43,920
Mihama Bridge	16,581	5,527	122,000



**Figure 4.1 Recommended model of p-y curve for pile cap or abutment**

#### 4.4. Pushover analysis

Sand (Reese), API sand (O'Neill), Liquefied sand (Rollins), and the residual shear strength model with Matlock soft clay model are applied for each analysis. For the South Brighton Bridge case, all soil models resulted in no significant differences of shear force – displacement diagram. However, for The Mataquito Bridge and the Mihama Bridge cases, the shear forces are affected by several soil models. The effects of the soil models are larger for the Mihama Bridge case than the Mataquito Bridge. There are two reasons for this. First is the liquefiable layer thickness. For the South Brighton and the Mataquito Bridge cases, the liquefiable layer thickness is 3.4m and 4.5m, respectively. On the other hand, for the Mihama Bridge case, it is 8.0m. If liquefiable layer thickness increases through the pile, the lateral load acting on the pile increases. As a result, the differences of the shear force through liquefiable layer become much larger. Second is the pile flexibility. The South Brighton Bridge abutment is supported by prestressed concrete piles. The bending stiffness of prestressed concrete piles is much smaller than that of steel piles or reinforced concrete piles. The estimated pile head displacement is almost the same as the applied ground displacement considering several soil models. This shows that pile deflection is corresponding to a crust displacement. Therefore, for flexible piles, the crust layer displacement dominates the pile performances, while for the non-flexible piles, soil models and liquefiable layer thickness impact pile performances.

#### **4.5. Other consideration**

##### **Battered pile**

In three earthquakes cases, bridge foundations supported by battered piles were damaged by liquefaction-induced lateral spreading. These foundations were similarly displaced by ground movement, which is the same as the non-battered piles.

In this paper, the South Brighton Bridge abutment supported by battered piles is analyzed using same procedures as the Mataquito and Mihama Bridges. In the analysis, the  $\pm 14^\circ$  inclination is applied to model battered piles using LPile 2012. However, the results are similar to the equivalent vertical single pile. The pile head displacement is corresponding to the ground displacement because of the flexibility of the pile. The effect of inclination is small for the South Brighton Bridge case. The effectiveness of the guidelines and procedures by Ashford et al (2011) and Shantz (2013) for battered piles needs to be confirmed for non-flexible battered pile foundations.

## Chapter 5. CONCLUSIONS

Three significant earthquakes (or earthquake sequences) occurred in 2010 and 2011 (Chile, New Zealand and Japan). The earthquakes caused widespread liquefaction and liquefaction-induced lateral spreading around bridge sites in all three earthquakes. Case history data including bridge details, soils properties, earthquake information, and bridge damage details, were collected from three earthquakes. The case history data make it possible to benchmark current procedures used to estimate bridge performance during liquefaction-induced lateral spreading. In this report, the current Caltrans method (Ashford et al. 2011; Shantz 2013) is benchmarked.

Three bridge case histories are selected to benchmark the Caltrans method – the Mataquito Bridge in Chile, the South Brighton Bridge in New Zealand, and the Mihama Bridge in Japan because they had the most complete data sets. Since the work was started, more complete case history data have become available – especially in New Zealand. The Caltrans method was used, assuming no prior knowledge of the earthquake event, to estimate the potential damage to these three bridges. The estimates of potential damage were then compared to the actual recorded damage.

The p-y response for the abutment section is acceptable, which can show the backfill soil softening discussed by Brandenberg et al. (2007). Pushover analysis shows that the ground displacement corresponds to the pile deflection for the flexible piles. For non-flexible piles the liquefiable layer thickness, soil models, and ground displacements are critical. Each of the three case history analyses show that the Bishop slope stability analysis method and the residual shear strength model estimate reasonable results compared to the observed pile foundations, abutment damages, and ground failures. In addition, the Mihama Bridge case indicates that the estimation of the ground displacement cannot be determined deterministically. Therefore, several soil displacements should be considered for pile performances analysis.

This analysis of three bridge abutment deep foundations show that the recommended guidelines and procedures by Ashford et al. (2011) and Shantz (2013) are effective to evaluate deep foundation performances in liquefaction and laterally spreading ground.

## REFERENCES

- American Association of State Highway and Transportation Officials. (2006). *AASHTO/PCI standard prestressed concrete pile sections*. Vol. V-PART 2, FILE NO. 12.06.
- American Petroleum Institute (API). (1993). “Recommended practice for planning, designing and constructing fixed offshore platforms – working stress design.” RP 2A-WSD, 20th Edition, July 1, 1993, American Petroleum Institute, Washington, DC
- Ashford, S., Boulanger, R., and Brandenburg, S. (2011). “Recommended design practice for pile foundations in laterally spreading ground.” Report PEER 2011/04, Pacific Earthquake Engineering Research Center (PEER), Berkeley, CA.
- Brandenberg, S.J., Boulanger, R.W., Kutter, B.L., and Chang, D. (2007). “Liquefaction-induced softening of load transfer between pile groups and laterally spreading crusts.” *J. Geotech. Geoenviron. Eng.*, ASCE, 133(1), 91-103.
- Brandenberg, S., Zhao, M., and Kashighandi, P. (2013). ”Analysis of Three Bridges That Exhibited Various Performance Levels in Liquefied and Laterally Spreading Ground.” *J. Geotech. Geoenviron. Eng.*, 139(7), 1035–1048.
- Bray, J. and Travasarou, T. (2007). ”Simplified Procedure for Estimating Earthquake-Induced Deviatoric Slope Displacements.” *J. Geotech. Geoenviron. Eng.*, 133(4), 381–392.
- Boroschek, R., Soto, P., Leon, R., and Comte, D. (2010). *Terremoto Centro Sur Chile, 27 de Febrero de 2010, Informe Preliminar No. 4*, University of Chile, Department of Civil Engineering and Department of Geophysics, Santiago, Chile.
- Chiba city. (1983). “Chiba City's bridge register.” Personal communication
- Chiba city. (2011). Damage of Mihama Bridge, Personal communication.
- Chiba prefecture. (2013). “Investigation of liquefaction in Chiba prefecture due to 2011 Tohoku earthquake.” Available in online  
<https://www.pref.chiba.lg.jp/bousaik/ekijoka/ekityosa.html> \*in Japanese

- Cubrinovski, M., Winkley, A., Haskell, J., Palermo, A., Wotherspoon, L., Robinson, K., Bradley, B., Brabhaharan, P., and Hughes, M. (2013). "Spreading-induced damage to short-span bridge in Christchurch (New Zealand)." *ASCE Journal of Performance of Constructed Facilities*. (draft only)
- Cubrinovski, M., Bradley, B., Wotherspoon, L., Green, R., Bray, J., Wood, C., Pender, M., Allen, J., Bradshaw, A., Rix, G., Taylor, M., Robinson, K., Henderson, D., Giorgini, S., Ma, K., Winkley, A., Zupan, J., O'Rourke, T., DePascale, G. and Wells, D. (2011). "Geotechnical aspects of the 22 February 2011 Christchurch earthquake." *Bulletin of NZ Society for Earthquake Engineering*, Vol.44, No. 4, 205-226.
- Federal Highway Administration. (2011). "Post earthquake reconnaissance report on transportation infrastructure impact of the February 27, 2010, Offshore Maule Earthquake in Chile." Publication No. FHWA-HRT-11-030.
- Geo-engineering Extreme Events Reconnaissance association. (2011). *Geo-engineering Reconnaissance of the 2010 Maule, Chile Earthquake*. Report No. GEER-022.
- Haskell, J. I. M., Madabhushi, S.P.G., Cubrinovski, M., and Winkley, A. (2013). "Lateral spreading-induced abutment rotation in the 2011 Christchurch earthquake: observations and analysis." *Géotechnique*, Volume 63, Issue 15, 1310 –1327.
- Hatanaka, M., and Uchida, A. (1996). "Empirical correlation between penetration resistance and internal friction angle of sandy soils." *Soils and foundations*, Vol. 36, No. 4, 1-9.
- Idriss, I.M. and Boulanger, R.W. (2007). "SPT and CPT-based relationships for the residual shear strength of liquefied soils." *4<sup>th</sup> International Conference on Earthquake Geotechnical Engineering*, K.D. Pitilakis, ed., Springer, Dordrecht, The Netherlands, 1-22.
- Idriss, I.M. and Boulanger, R.W. (2008). *Soil liquefaction during earthquakes*, EERI Monograph 12, Earthquake Engineering Research Institute, Oakland, California, 262.

- Japanese Geotechnical Society, and Ministry of Land, Infrastructure, Transport and Tourism. Kanto Regional Development Bureau. (2011). "Analysis of liquefaction in Kanto area due to Tohoku earthquake." \*In Japanese.
- Kramer, S.L. (2008). "Evaluation of liquefaction hazards in Washington State." *Washington State of Department of Transportation Research report*, WA-RD 668.1.
- Kawashima, K., Unjoh, S., Hoshikuma, J. and Kosa, K. (2010). "Damage of bridges due to 2010 Chile Earthquake." Proc. 3rd Asia Conference on Earthquake Engineering, ACEE-A-036, 1-8.
- Kawashima, K., Kosa, K., Takahashi, Y., Akiyama, M., Nishioka, T., Watanabe, G., Koga, H., and Matsuzaki H. (2011). "Damage of bridges during 2011 Great East Japan Earthquake." Proc. 43rd Joint Meeting, US-Japan Panel on Wind and Seismic Effects, UJNR.
- Kulhawy, F. H., and Mayne, P. W. (1990). "Manual on estimating soil properties for foundation design." Report No. EL-6800, Electric Power Research Institute, Palo Alto, CA
- Ledezma, C., Hutchinson, T., Ashford, S. A., Moss, R., Arduino, P., Bray, J. D., Olson, S., Hashash, Y. M. A., Verdugo, R., Frost, D., Kayen, R., and Rollins, K. (2012). "Effects of ground failure on bridges, roads, and railroads." *Earthquake Spectra*, Vol. 28, No. 1, 119–143.
- Matlock, H. (1970). "Correlations of design of laterally loaded piles in soft clay." *Proc. Offshore Technology Conference*, Houston, TX, Vol. 1, No. 1204, 577-594.
- McGann, C., Arduino, P., and Mackenzie-Helnwein, P. (2012). "Simplified procedure to account for a weaker soil layer in lateral load analysis of single piles." *J. Geotech. Geoenviron. Eng.*, 138(9), 1129–1137.
- Miyagi Prefecture. (2011). "Miyagi Prefecture's bridge register." Personal communication
- Mokwa, R.L., and Duncan, J.M. (2000). "Experimental evaluation of lateral-load resistance of pile caps." *J. Geotech. Geoenviron. Eng.*, ASCE. 127(2). 185-192.

- National Institute for land and Infrastructure Management. (2011). "Report of field survey for highway bridges damaged by Great East Japan Earthquake." \*in Japanese
- New Zealand Geo-engineering extreme events reconnaissance association. (2011). "Geotechnical reconnaissance of the 2011 Christchurch, New Zealand earthquake." Version 1
- Oka, F., Nakanishi, N., Kimoto, S., Kato, R. (2011). "Investigation report on the damage off river embankments due to the 2011 off the Pacific coast of Tohoku Earthquake (Central and north areas of Miyagi prefecture)." The report of the investigation of Tohoku earthquake, JGS. \*in Japanese
- Ovesen, N. K. (1964). "Anchor slabs, calculation methods and model tests". *Bulletin No. 16, The Danish Geotechnical Institute, Copenhagen.*
- Palermo, A., Wotherspoon, L., Wood, J., Chapman, H., Scott, A., Hogan, L., Kivell, A., Camnasi, E., Yashinsky, M., Bruneau, M., and Chouw, N. (2011). "Lessons learnt from 2011 Christchurch earthquake: analysis and assessment of bridges." *Bulletin of the New Zealand society for earthquake engineering*, Vol. 44, No. 4, 319-333.
- Petrus Consultores Geotecnicos (2006). *Informe Complementario de Mec'anica de Suelos, Puente Mataquito (Ruta Costera), Camino Quivolgo-Iloca (Cruce J-60)*. Informe No. 2619-ING-SGC-150/2006 (Rev 1).
- Priestley, M, J, N., and Stockwell, M, J. (1978). "Seismic design of south brighton bridge a decision against mechanical energy dissipators." *Bulletin of the New Zealand society for earthquake engineering*, Vol. 11, No. 2, 110-120.
- Public works research institute. (2011). "Quick report on damage to infrastructures by the 2011 off the Pacific coast of Tohoku Earthquake." Technical Note of Public Works Research Institute, No.4202 \*in Japanese
- Reese, C, L., and Van Impe, W, F. (2011). *Single pile and pile groups under lateral loading 2nd edition*. Taylor & Francis Group, London, UK.
- Shantz, T. (2013). "Guidelines on foundation loading and deformation due to liquefaction induced lateral spreading." *Caltrans Technical Reference*. Available online.

Strong-motion-Seismograph Networks (K-NET , KiK-net). <http://www.kyoshin.bosai.go.jp/>

Tohoku Regional Development Bureau. (2011). “Damages of highway related facilities by Great East Japan Earthquake.” \*in Japanese

Tohoku Regional Bureau Ministry of Land, Infrastructure and Transport. (2011). [http://www.thr.mlit.go.jp/bumon/kisya/saigai/33437\\_kisya\\_preview.html](http://www.thr.mlit.go.jp/bumon/kisya/saigai/33437_kisya_preview.html). \*\*in Japanese.

Verdugo, R., and Peters, G. (2010). *Informe Geotécnico Fase Anteproyecto Infraestructura Puente Mecano Eje Chacabuco*, Rev7, August 2010.

## APPENDIX A

### Liquefaction potential evaluation

Liquefaction potential evaluation is followed using the procedures developed by Idriss and Boulanger (2008).

#### Step 1) Cyclic resistance ratio (CRR) evaluations

Liquefaction resistance is evaluated using following equation.

$$CRR_{M=7.5, \sigma'_{vc}=1} = \exp \left[ \frac{(N_1)_{60CS}}{14.1} + \left( \frac{(N_1)_{60CS}}{126} \right)^2 - \left( \frac{(N_1)_{60CS}}{23.6} \right)^3 + \left( \frac{(N_1)_{60CS}}{25.4} \right)^4 - 2.8 \right]$$

Where  $(N_1)_{60CS}$  is correlated N-value by percentage of fine content.

1.  $N_{60}$  is evaluated using following equation.

$$N_{60} = C_E C_B C_R C_S N_m$$

Where  $C_E$  is the energy ration correction factor,  $C_B$  is a correction factor for borehole diameter,  $C_R$  is a correction factor for rod length,  $C_S$  is a correction factor for a sampler, and  $N_m$  is the measured blow count.

2.  $(N_1)_{60}$  is evaluated using following equation.

$$(N_1)_{60} = C_N N_{60}$$

Where  $C_N$  is an overburden correction factor.  $C_N$  is calculated using following equations.

$$C_N = \left( \frac{P_a}{\sigma'_{vc}} \right)^m$$

$$m = 0.784 - 0.521 \cdot \left( \frac{N_1}{46} \right)^{0.5}$$

3. Finally, the correlated N-value  $(N_1)_{60CS}$  is obtained from the following equation.

$$(N_1)_{60CS} = (N_1)_{60} + \Delta(N_1)_{60}$$

Where  $\Delta(N_1)_{60}$  is the increment of N-value due to fine content.  $\Delta(N_1)_{60}$  is estimated using following equation.

$$\Delta(N_1)_{60} = \exp \left[ 1.63 + \frac{9.7}{FC + 0.01} - \left( \frac{15.7}{FC + 0.01} \right)^2 \right]$$

*Step 2) Earthquake induced cyclic shear stress ratio (CSR) evaluation*

Earthquake induced cyclic shear stress ratio is evaluated using following equation.

$$CSR_{M=7.5, \sigma'_{vc}=1} = 0.65 \cdot \frac{a_{\max}}{\sigma'_{vc}} \cdot r_d \cdot \frac{1}{MSF} \cdot \frac{1}{K_\sigma}$$

Where  $a_{\max}$  is the maximum ground surface acceleration,  $\sigma'_{vc}$  is the vertical effective stress,  $r_d$  is a stress reduction coefficient, MSF is a magnitude scaling factor, and  $K_\sigma$  is an overburden correction factor.

1. Stress reduction coefficient  $r_d$  is calculated using following equation.

$$r_d = \exp(\alpha(z) + \beta(z) \cdot M)$$

$$\alpha(z) = -1.012 - 1.126 \sin \left( \frac{z}{11.73} + 5.133 \right)$$

$$\beta(z) = 0.106 + 0.118 \sin \left( \frac{z}{11.28} + 5.142 \right)$$

Where  $z$  is depth, and  $M$  is moment magnitude.

2. Magnitude scaling factor is calculated using following equation.

$$MSF = 6.9 \cdot \exp \left( -\frac{M}{4} \right) - 0.058$$

3. Overburden correction factor is calculated using following equation.

$$K_{\sigma} = 1 - C_{\sigma} \ln \left( \frac{\sigma'_{vc}}{P_a} \right)$$

$$C_{\sigma} = \frac{1}{18.9 - 2.55 \sqrt{(N_1)_{60}}}$$

Where  $P_a$  is atmospheric pressure.

### Step 3) Estimating factor of safety against liquefaction

Factor of safety against liquefaction is estimated using following equation.

$$FS = \frac{CRR_{M=7.5, \sigma'_{vc}=1}}{CSR_{M=7.5, \sigma'_{vc}=1}}$$

### Liquefaction potential evaluation for the Mataquito Bridge

For SPT N-value at the Mataquito Bridge, the correction factor  $C_E$  is assumed 1.0.  $C_B$  and  $C_s$  are negligible (Idriss and Boulanger 2008). Also, fine content is assumed to equal zero. The soil layers for which N-value is over 30 is classified as non-liquefied layer because such soils are dense. SPT N-value is referred by Ledezma et al. (2011)

**Table A-1 Liquefaction potential evaluation for the Mataquito Bridge**

Depth (m)	N	(N1) <sub>60</sub>	r <sub>d</sub>	MSF	K <sub>σ</sub>	CSR <sub>M=7,σ'vc=1</sub>	CRR <sub>M=7,σ'vc=1</sub>	FS
2	5	-	1.00	0.71	1.30	0.28	0.18	0.64
1	4	7.2	1.00	0.71	1.11	0.33	0.10	0.30
0	9	11.0	1.00	0.71	1.08	0.34	0.13	0.37
-1	27	27.0	1.00	0.71	1.12	0.39	0.35	0.89
-2	26	25.9	1.00	0.71	1.09	0.45	0.31	0.70
-3	12	12.5	1.00	0.71	1.04	0.51	0.14	0.27
-4	21	20.2	1.00	0.71	1.04	0.54	0.21	0.39
-5	41	40.9	1.00	0.71	1.06	0.54	5.61	10.31
-6	40	38.5	0.99	0.71	1.01	0.58	2.64	4.53
-7	35	32.6	0.99	0.71	0.99	0.61	0.71	1.16

Depth (m)	N	(N1) <sub>60</sub>	r <sub>d</sub>	MSF	K <sub>σ</sub>	CSR <sub>M=7,σ'vc=1</sub>	CRR <sub>M=7,σ'vc=1</sub>	FS
-8	-	-	-	-	-	-	-	-
-9	-	-	-	-	-	-	-	-
-10	31	28.7	0.98	0.71	0.94	0.66	0.37	0.56
-11	32	27.9	0.98	0.71	0.93	0.67	0.38	0.56
-12	50	44.8	0.98	0.71	0.75	0.84	28.09	33.57
-13	50	44.1	0.97	0.71	0.73	0.86	20.39	23.79
-14	50	43.5	0.97	0.71	0.72	0.87	15.38	17.60
-15	50	42.9	0.96	0.71	0.71	0.89	11.99	13.50
-16	50	42.3	0.96	0.71	0.70	0.90	9.59	10.67
-17	50	41.8	0.95	0.71	0.69	0.91	7.86	8.65
-18	50	41.3	0.94	0.71	0.68	0.92	6.56	7.17
-19	50	40.9	0.94	0.71	0.68	0.92	5.57	6.05
-20	50	40.5	0.93	0.71	0.67	0.92	4.80	5.19
-21	16	10.3	0.92	0.71	0.91	0.68	0.12	0.18
-22	22	14.6	0.91	0.71	0.89	0.69	0.15	0.22
-23	50	39.3	0.90	0.71	0.66	0.93	3.29	3.55

### Liquefaction potential evaluation for the South Brighton Bridge

For SPT N-value at South Brighton Bridge, the correction factor  $C_E$  is assumed 1.0.  $C_B$  and  $C_s$  are negligible (Idriss and Boulanger 2008). Also, fine content is assumed to equal zero. The soil layers for which  $(N_1)_{60}$ -value is over 30 is classified as non-liquefied layer because such soils are dense. SPT N-value and CPT data is referred by Cubrinovski et al. (2013).

**Table A-2 SPT based liquefaction potential evaluation for the South Brighton Bridge**

Depth (m)	N	(N1) <sub>60</sub>	r <sub>d</sub>	MSF	K <sub>σ</sub>	CSR <sub>M=7,σ'vc=1</sub>	CRR <sub>M=7,σ'vc=1</sub>	FS
0.8	2	4.0	1.00	1.41	1.14	0.15	0.08	0.52
1.1	6	10.5	0.99	1.41	1.16	0.15	0.12	0.80

Depth (m)	N	(N1) <sub>60</sub>	r <sub>d</sub>	MSF	K <sub>σ</sub>	CSR <sub>M=7,σ'vc=1</sub>	CRR <sub>M=7,σ'vc=1</sub>	FS
1.3	12	19.2	0.99	1.41	1.20	0.15	0.20	1.34
1.6	15	21.7	0.99	1.41	1.19	0.15	0.23	1.55
2	15	19.4	0.98	1.41	1.14	0.15	0.20	1.30
2.2	19	23.4	0.98	1.41	1.15	0.15	0.26	1.70
2.5	12	13.8	0.97	1.41	1.09	0.16	0.15	0.93
2.9	12	12.8	0.96	1.41	1.07	0.16	0.14	0.87
3.2	11	12.7	0.96	1.41	1.06	0.16	0.14	0.86
3.5	17	17.6	0.95	1.41	1.06	0.16	0.18	1.13
3.9	18	17.6	0.95	1.41	1.05	0.16	0.18	1.13
4.1	17	17.3	0.94	1.41	1.04	0.16	0.18	1.10
4.4	20	19.6	0.94	1.41	1.04	0.16	0.20	1.25
4.8	31	29.4	0.93	1.41	1.04	0.16	0.45	2.78
5	42	39.5	0.92	1.41	1.07	0.16	3.52	21.87
6.5	26	25.7	0.89	1.41	1.01	0.19	0.31	1.62
7.1	21	20.2	0.88	1.41	1.00	0.20	0.21	1.07
8.3	33	30.3	0.85	1.41	0.99	0.21	0.51	2.45
9.7	59	53.5	0.82	1.41	0.19	1.08	1000 >	1000 >
10.5	66	57.9	0.80	1.41	1.51	0.14	1000 >	1000 >
11.9	51	42.5	0.77	1.41	0.84	0.24	10.07	41.22
13	47	37.7	0.74	1.41	0.86	0.23	2.08	8.85
14.8	48	36.3	0.70	1.41	0.84	0.23	1.49	6.37
15.7	69	50.9	0.68	1.41	0.14	1.39	1000 >	1000 >

**Table A-3 CPT based liquefaction potential evaluation for the South Brighton Bridge**

Depth (m)	q <sub>c</sub> (Mpa)	q <sub>c1N</sub>	r <sub>d</sub>	MSF	K <sub>σ</sub>	CSR <sub>M=7,σ'vc=1</sub>	CRR <sub>M=7,σ'vc=1</sub>	FS
0	0	-	-	-	-	-	-	-
0.2	8	445	1.01	1.41	0.17	1.08	1>	1>
0.4	10	393	1.00	1.41	0.02	11.85	1>	1>

Depth (m)	$q_c$ (Mpa)	$q_{c1N}$	$r_d$	MSF	$K_\sigma$	$CSR_{M=7, \sigma'_{vc}=1}$	$CRR_{M=7, \sigma'_{vc}=1}$	FS
0.6	5	161	1.00	1.41	1.40	0.13	0.33	2.60
0.8	2.5	70	1.00	1.41	1.17	0.15	0.10	0.65
1	5	124	0.99	1.41	1.23	0.14	0.19	1.32
1.2	8	182	0.99	1.41	1.34	0.13	0.56	4.30
1.4	4	84	0.99	1.41	1.14	0.15	0.12	0.76
1.6	1	20	0.99	1.41	1.07	0.16	0.06	0.34
1.8	1	19	0.98	1.41	1.06	0.16	0.05	0.33
2	2	35	0.98	1.41	1.07	0.16	0.06	0.40
2.2	3	50	0.98	1.41	1.07	0.16	0.08	0.48
2.4	3.5	56	0.97	1.41	1.07	0.16	0.08	0.52
2.6	4	61	0.97	1.41	1.06	0.16	0.09	0.55
2.8	5	74	0.97	1.41	1.06	0.16	0.10	0.65
3	7	100	0.96	1.41	1.07	0.16	0.14	0.89
3.2	7	97	0.96	1.41	1.06	0.16	0.14	0.86
3.4	8	107	0.96	1.41	1.06	0.16	0.15	0.97
3.6	7	91	0.95	1.41	1.05	0.16	0.13	0.80
3.8	8.5	108	0.95	1.41	1.05	0.16	0.16	0.97
4	7.5	93	0.94	1.41	1.04	0.16	0.13	0.81
4.2	8	96	0.94	1.41	1.03	0.16	0.14	0.85
4.4	10	118	0.94	1.41	1.03	0.16	0.17	1.09
4.6	12	138	0.93	1.41	1.03	0.16	0.23	1.41
4.8	13	148	0.93	1.41	1.03	0.16	0.26	1.61
5	13	147	0.92	1.41	1.03	0.17	0.26	1.54
5.2	13.5	151	0.92	1.41	1.03	0.17	0.28	1.62
5.4	12	133	0.92	1.41	1.02	0.17	0.21	1.21
5.6	11.5	126	0.91	1.41	1.02	0.18	0.19	1.10
5.8	11	120	0.91	1.41	1.02	0.18	0.18	1.00
6	11	119	0.90	1.41	1.01	0.18	0.18	0.97
6.2	12.5	134	0.90	1.41	1.01	0.19	0.21	1.16

Depth (m)	$q_c$ (Mpa)	$q_{c1N}$	$r_d$	MSF	$K_\sigma$	$CSR_{M=7, \sigma'_{vc}=1}$	$CRR_{M=7, \sigma'_{vc}=1}$	FS
6.4	12	128	0.89	1.41	1.01	0.19	0.20	1.05
6.6	11.5	121	0.89	1.41	1.01	0.19	0.18	0.96
6.8	10	105	0.89	1.41	1.01	0.19	0.15	0.78
7	6	62	0.88	1.41	1.00	0.19	0.09	0.46
7.2	11	113	0.88	1.41	1.00	0.20	0.17	0.85
7.4	8.5	87	0.87	1.41	1.00	0.20	0.12	0.62
7.6	13	132	0.87	1.41	1.00	0.20	0.21	1.04
7.8	9.5	96	0.86	1.41	1.00	0.20	0.14	0.67
8	13	130	0.86	1.41	1.00	0.20	0.20	1.00
8.2	16.5	164	0.85	1.41	0.99	0.21	0.35	1.71
8.4	16	157	0.85	1.41	0.99	0.21	0.31	1.49
8.6	14	136	0.84	1.41	0.99	0.21	0.22	1.06
8.8	11.5	111	0.84	1.41	0.99	0.21	0.16	0.78
9	13	124	0.83	1.41	0.98	0.21	0.19	0.90
9.2	14	132	0.83	1.41	0.98	0.21	0.21	1.00
9.4	15	141	0.83	1.41	0.98	0.21	0.23	1.11
9.6	14	130	0.82	1.41	0.97	0.21	0.20	0.96
9.8	14.5	134	0.82	1.41	0.97	0.21	0.21	1.00
10	14	128	0.81	1.41	0.97	0.21	0.20	0.93
10.2	13	118	0.81	1.41	0.97	0.21	0.18	0.82
10.4	12.5	112	0.80	1.41	0.97	0.21	0.16	0.77
10.6	14	125	0.80	1.41	0.97	0.21	0.19	0.89
10.8	14.5	128	0.79	1.41	0.96	0.21	0.20	0.93
11	15	132	0.79	1.41	0.96	0.22	0.21	0.97
11.2	15.5	135	0.78	1.41	0.96	0.22	0.22	1.01
11.4	14.5	125	0.78	1.41	0.96	0.22	0.19	0.89
11.6	14	120	0.77	1.41	0.96	0.21	0.18	0.84
11.8	13.5	115	0.77	1.41	0.96	0.21	0.17	0.79

Depth (m)	$q_c$ (Mpa)	$q_{c1N}$	$r_d$	MSF	$K_\sigma$	$CSR_{M=7, \sigma'_{vc}=1}$	$CRR_{M=7, \sigma'_{vc}=1}$	FS
12	14	118	0.76	1.41	0.95	0.21	0.18	0.82
12.2	13.5	113	0.76	1.41	0.95	0.21	0.17	0.78
12.4	14	117	0.76	1.41	0.95	0.21	0.17	0.81
12.6	14	116	0.75	1.41	0.95	0.21	0.17	0.80
12.8	14.5	119	0.75	1.41	0.95	0.21	0.18	0.83
13	13.5	110	0.74	1.41	0.95	0.21	0.16	0.75
13.2	15	122	0.74	1.41	0.94	0.21	0.18	0.86
13.4	15.5	125	0.73	1.41	0.94	0.21	0.19	0.89
13.6	14	112	0.73	1.41	0.94	0.21	0.16	0.77
13.8	13.5	108	0.72	1.41	0.94	0.21	0.16	0.73
14	13	103	0.72	1.41	0.94	0.21	0.15	0.70
14.2	15	118	0.71	1.41	0.94	0.21	0.18	0.82
14.4	14	109	0.71	1.41	0.94	0.21	0.16	0.75
14.6	17.5	136	0.71	1.41	0.92	0.21	0.22	1.02
14.8	17.5	135	0.70	1.41	0.92	0.21	0.22	1.02
15	16	123	0.70	1.41	0.93	0.21	0.19	0.88
15.2	18	137	0.69	1.41	0.92	0.21	0.22	1.05
15.4	17	129	0.69	1.41	0.92	0.21	0.20	0.95
15.6	17	128	0.68	1.41	0.92	0.21	0.20	0.94
15.8	16	120	0.68	1.41	0.92	0.21	0.18	0.86
16	15.5	116	0.67	1.41	0.92	0.21	0.17	0.82
16.2	15	111	0.67	1.41	0.93	0.21	0.16	0.78
16.4	16	118	0.67	1.41	0.92	0.21	0.18	0.84
16.6	13	95	0.66	1.41	0.93	0.20	0.14	0.66
16.8	8	58	0.66	1.41	0.95	0.20	0.09	0.43
17	12	87	0.65	1.41	0.93	0.20	0.12	0.61
17.2	8	58	0.65	1.41	0.95	0.20	0.09	0.43
17.4	10	72	0.65	1.41	0.94	0.20	0.10	0.51
17.6	11	79	0.64	1.41	0.94	0.20	0.11	0.56

Depth (m)	$q_c$ (Mpa)	$q_{c1N}$	$r_d$	MSF	$K_\sigma$	$CSR_{M=7, \sigma'_{vc}=1}$	$CRR_{M=7, \sigma'_{vc}=1}$	FS
17.8	13.5	96	0.64	1.41	0.93	0.20	0.14	0.68
18	13.5	96	0.63	1.41	0.92	0.20	0.14	0.68
18.2	14.5	102	0.63	1.41	0.92	0.20	0.15	0.73
18.4	14.5	102	0.63	1.41	0.92	0.20	0.15	0.73
18.6	14	98	0.62	1.41	0.92	0.20	0.14	0.70
18.8	13	90	0.62	1.41	0.92	0.20	0.13	0.65
19	14	97	0.61	1.41	0.92	0.20	0.14	0.70
19.2	15	103	0.61	1.41	0.91	0.20	0.15	0.75
19.4	13	89	0.61	1.41	0.92	0.19	0.13	0.64
19.6	16	109	0.60	1.41	0.91	0.20	0.16	0.80
19.8	15	102	0.60	1.41	0.91	0.20	0.15	0.74
20	14.5	98	0.60	1.41	0.91	0.19	0.14	0.72
20.2	17.5	118	0.59	1.41	0.90	0.20	0.17	0.89
20.4	17.5	117	0.59	1.41	0.90	0.20	0.17	0.88
20.6	16	107	0.59	1.41	0.90	0.19	0.15	0.79
20.8	19	126	0.58	1.41	0.89	0.20	0.19	0.98
21	18.5	122	0.58	1.41	0.89	0.20	0.18	0.94
21.2	19	125	0.58	1.41	0.89	0.20	0.19	0.98
21.4	19.5	128	0.57	1.41	0.88	0.20	0.20	1.01
21.6	20	130	0.57	1.41	0.88	0.20	0.20	1.04
21.8	19.5	127	0.57	1.41	0.88	0.19	0.19	1.00
22	18	116	0.56	1.41	0.89	0.19	0.17	0.90

## Liquefaction potential evaluation for the Mihama Bridge

For SPT N-value at Mihama Bridge, the correction factor  $C_E$  is assumed 1.0.  $C_B$  and  $C_s$  are negligible (Idriss and Boulanger 2008). According to Chiba prefecture (2013), fines content in Mihama area is from 6% to 32 %. The soil layer, for which N-value is over 30, is classified as non-liquefied layer because soils are so dense. SPT N-value is referred by Chiba city (2011)

**Table A-4 SPT based liquefaction potential evaluation for the Mihama Bridge**

Depth (m)	N	(N1) <sub>60</sub>	r <sub>d</sub>	MSF	K <sub>σ</sub>	CSR <sub>M=7,σ'vc=1</sub>	CRR <sub>M=7,σ'vc=1</sub>	FS
2.85	8	15.7	1.00	0.71	1.30	0.28	0.18	0.64
1.85	6	8.5	1.00	0.71	1.11	0.33	0.10	0.30
-2.15	3	3.8	1.01	0.71	1.08	0.34	0.13	0.37
-3.15	4	4.7	1.01	0.71	1.12	0.39	0.35	0.89
-5.15	9	9.2	1.01	0.71	1.09	0.45	0.31	0.70
-6.15	6	6.4	1.00	0.71	1.04	0.51	0.14	0.27
-7.15	3	3.1	1.00	0.71	1.04	0.54	0.21	0.39
-8.15	26	25.4	1.00	0.71	1.06	0.54	5.61	10.31
-9.15	24	22.7	1.00	0.71	1.01	0.58	2.64	4.53
-10.15	3	2.6	1.00	0.71	0.99	0.61	0.71	1.16
-12.15	3	2.4	0.99	-	-	-	-	-
-13.15	3	2.3	0.99	-	-	-	-	-
-14.15	16	12.9	0.99	0.71	0.94	0.66	0.37	0.56
-17.15	20	16.8	0.97	0.71	0.93	0.67	0.38	0.56
-18.15	29	24.4	0.96	0.71	0.75	0.84	28.09	33.57
-19.15	35	29.4	0.96	0.71	0.73	0.86	20.39	23.79
-20.15	29	23.3	0.95	0.71	0.72	0.87	15.38	17.60
-21.15	28	21.9	0.94	0.71	0.71	0.89	11.99	13.50
-22.15	48	40.2	0.93	0.71	0.70	0.90	9.59	10.67
-23.15	50	41.7	0.92	0.71	0.69	0.91	7.86	8.65
-24.15	8	5.1	0.91	0.71	0.68	0.92	6.56	7.17
-25.15	9	5.6	0.91	0.71	0.68	0.92	5.57	6.05

Depth (m)	N	(N1) <sub>60</sub>	r <sub>d</sub>	MSF	K <sub>σ</sub>	CSR <sub>M=7,σ'vc=1</sub>	CRR <sub>M=7,σ'vc=1</sub>	FS
-26.15	5	2.9	0.90	0.71	0.67	0.92	4.80	5.19
-28.15	6	3.4	0.88	0.71	0.91	0.68	0.12	0.18
-29.15	5	2.7	0.87	0.71	0.89	0.69	0.15	0.22
-30.15	5	2.6	0.86	0.71	0.66	0.93	3.29	3.55
-31.15	36	25.4	0.85	0.67	0.82	0.41	0.30	0.73

## APPENDIX B

### Pile section properties of the Mataquito Bridge

**Table B-1 the pile section properties for the original single pile**

Concrete compressive strength (MPa)	Yield stress of reinforcing bar (MPa)	Elastic modulus of reinforcing bar (GPa)	Bar size (mm)	Number of bars	Concrete Cover to Edge of Bar (mm)
25	412	200	36	30	70

**Table B-2 Pile Stiffness Properties of the group pile section for equivalent single pile**

Bending Curvature (rad/m)	Bending Moment (kN-m)	Bending Stiffness, EI (GN-m <sup>2</sup> )
7.38E-05	4,700	63.7
1.23E-04	7,800	63.4
1.48E-04	9,300	63.0
4.92E-04	9,600	19.5
7.87E-04	15,000	19.1
1.06E-03	20,000	18.9
1.30E-03	25,000	19.2
1.60E-03	30,000	18.8
1.85E-03	35,000	19.0
2.14E-03	40,000	18.7
2.58E-03	45,000	17.4
1.03E-02	50,000	4.8
2.20E-02	57,000	2.6
3.10E-02	62,920	2.0

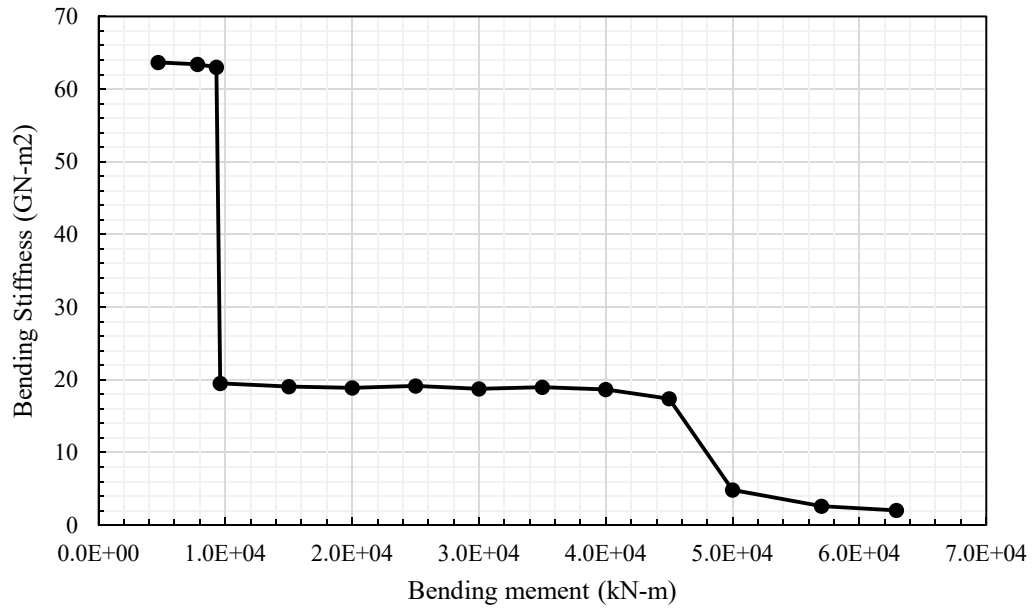


**Figure B-1 Mataquito Bridge, equivalent single pile: Bending stiffness and bending moment diagram of the group pile section**

**Table B-3 Pile Stiffness Properties of the abutment section for equivalent non-linear single pile**

Bending Curvature (rad/m)	Bending Moment (MN-m)	Bending Stiffness, EI (GN-m <sup>2</sup> )
7.38E-05	4,700	6,369
1.23E-04	7,800	6,341
1.48E-04	9,300	6,301
4.92E-04	9,600	1,951
7.87E-04	15,000	1,905
1.06E-03	20,000	1,890
1.30E-03	25,000	1,917
1.60E-03	30,000	1,876

1.85E-03	35,000	1,897
2.14E-03	40,000	1,869
2.58E-03	45,000	1,742
1.03E-02	50,000	484
2.20E-02	57,000	260
3.10E-02	62,920	203

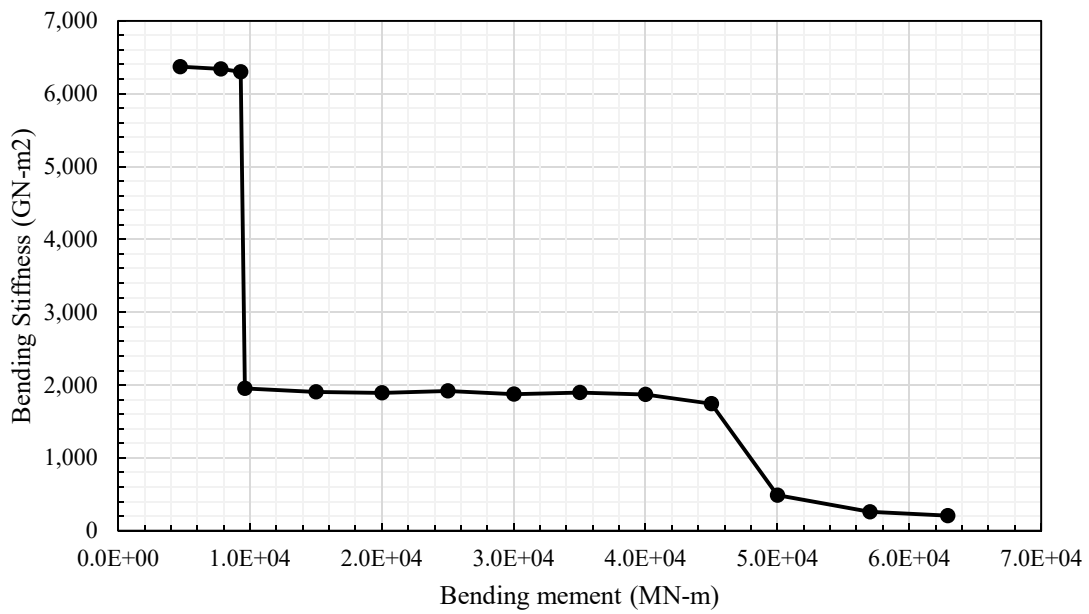


**Figure B-2 Mataquito Bridge, equivalent single pile: Bending stiffness and bending moment diagram of the group pile section**

### **Pile section properties of the South Brighton Bridge**

The following concrete properties and prestressing properties are applied for original single pile to obtain bending stiffness and bending moment diagram.

**Table B-4 Concrete Properties for the original single pile**

Compressive Strength (MPa)	24
Max. Coarse Aggregate Size (mm)	19.05

**Table B-5 Prestressing Properties for the original single pile**

Prestressing Strand Type	Grade 270 ksi Lo-Lax
Strand/Bar Size	1 / 2'' 7-wire A=0.153sq. in.
Number of Strands / PS Bars	10
Prestress Force Before Losses (kN)	1370
Fraction of Loss of Prestress	0.1
Cover Over Strands (mm)	25

**Table B- 6 Pile stiffness properties of group pile section for equivalent non-linear single pile**

Bending Curvature (Rad/m)	Bending Moment (kN-m)	Bending Stiffness, EI (MN-m <sup>2</sup> )
0.000394	200	5,080
0.000738	400	5,420
0.001476	800	5,420
0.002018	1,000	4,960
0.002805	1,200	4,280
0.005610	1,400	2,500
0.011220	1,600	1,430
0.016831	1,800	1,070
0.023843	2,000	840
0.033661	2,200	654

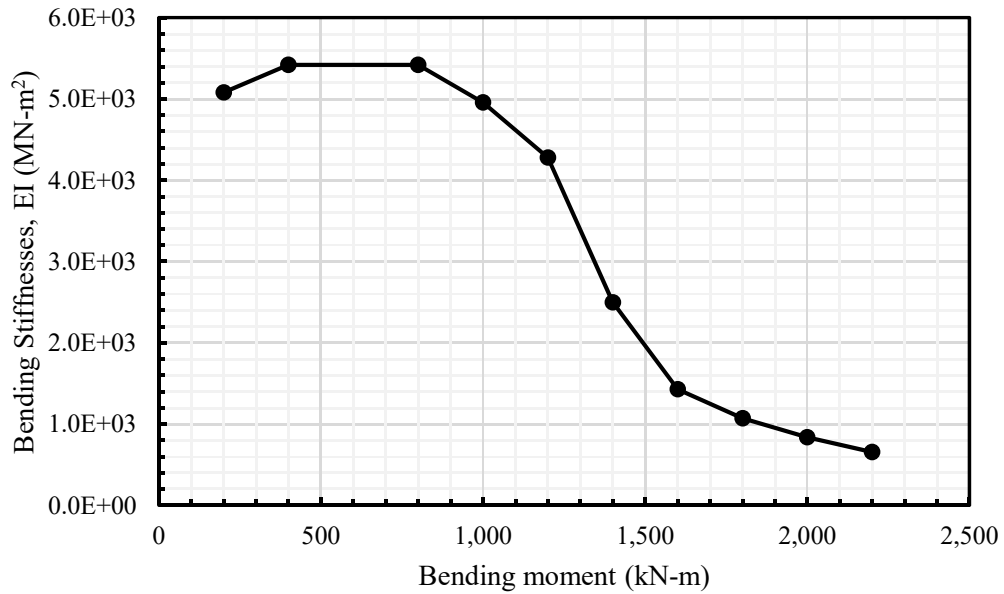


**Figure B-3 South Brighton Bridge, equivalent single pile: Bending stiffness and bending moment diagram of the group pile section**

**Table B- 7 Pile stiffness properties of the abutment section for equivalent non-linear single pile**

Bending Curvature (Rad/m)	Bending Moment (kN-m)	Bending Stiffness, EI (MN-m <sup>2</sup> )
0.000394	20,000	508,000
0.000738	40,000	542,000
0.001476	80,000	542,000
0.002018	100,000	496,000
0.002805	120,000	428,000
0.005610	140,000	250,000
0.011220	160,000	143,000
0.016831	180,000	107,000
0.023843	200,000	8,4000
0.033661	220,000	65,400

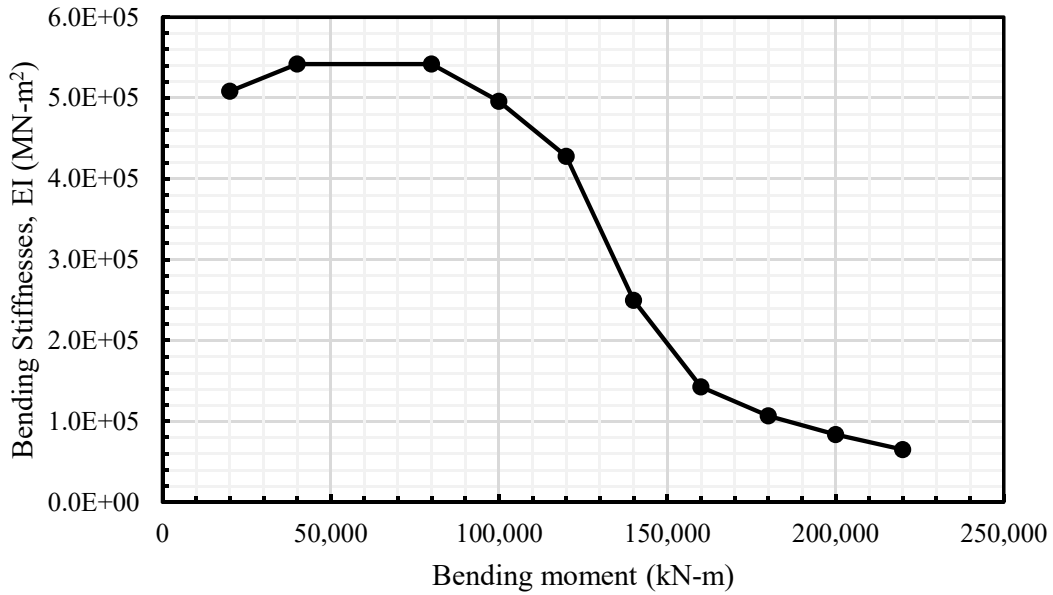


**Figure B-4 South Brighton Bridge, equivalent single pile: Bending stiffness and bending moment diagram of the group pile section**

The following values are applied for the battered piles

**Table B-8 Pile stiffness properties of the group pile section for the battered pile, South Brighton Bridge**

Bending Curvature (Rad/m)	Bending Moment (kN-m)	Bending Stiffness, EI (MN-m <sup>2</sup> )
0.000394	100	2,540
0.000738	200	2,700
0.001476	400	2,700
0.002018	500	2,480
0.002805	600	2,140
0.005610	700	1,250
0.011220	800	713
0.016831	900	534
0.023843	1,000	420
0.033661	1,100	326

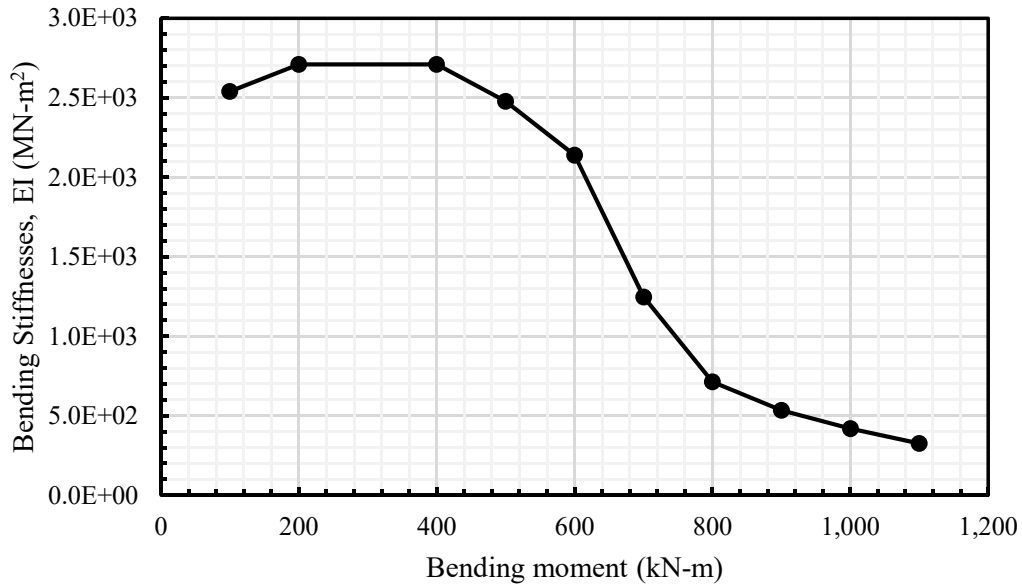


**Figure B-5 South Brighton Bridge, equivalent single pile: Bending stiffness and bending moment diagram of group pile section for the battered pile**

**Table B-9 Pile stiffness properties of the abutment section for battered pile, South Brighton Bridge**

Bending Curvature (Rad/m)	Bending Moment (kN-m)	Bending Stiffness, EI (MN-m <sup>2</sup> )
0.000394	10,000	254,000
0.000738	20,000	270,000
0.001476	40,000	270,000
0.002018	50,000	248,000
0.002805	60,000	214,000
0.005610	70,000	125,000
0.011220	80,000	71,300
0.016831	90,000	53,400
0.023843	100,000	42,000
0.033661	110,000	32,600

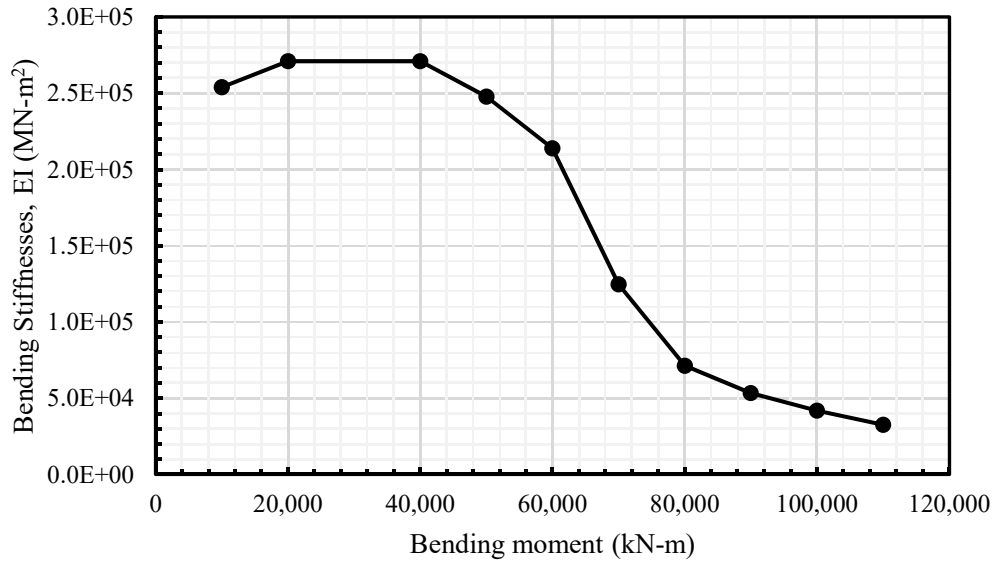


**Figure B-6 South Brighton Bridge, equivalent single pile: Bending stiffness and bending moment diagram of abutment section for the battered pile**

## Pile section properties of the Mihama Bridge

**Table B-8 Steel pipe pile section dimensions**

Pipe outside diameter (mm)	1,016
Pipe wall thickness (mm)	14

**Table B-9 Steel pipe, casing, and core material properties**

	Original single pile
Yield stress of casing (MPa)	28.8
Elastic modulus of casing (GPa)	23.2

**Table B-10 Pile stiffness properties of the group pile section for equivalent single pile**

Bending Curvature (Radians/m)	Bending Moment (kN-m)	Bending Stiffness, EI (kN-m <sup>2</sup> )
0.0000523	2,500	4.78E+07
0.0004183	20,000	4.78E+07
0.0008366	40,000	4.78E+07
0.0013072	62,000	4.74E+07
0.0017255	81,000	4.69E+07
0.0022484	104,000	4.63E+07
0.0026667	120,000	4.50E+07
0.003085	130,000	4.21E+07
0.03702	161,258	4.36E+06

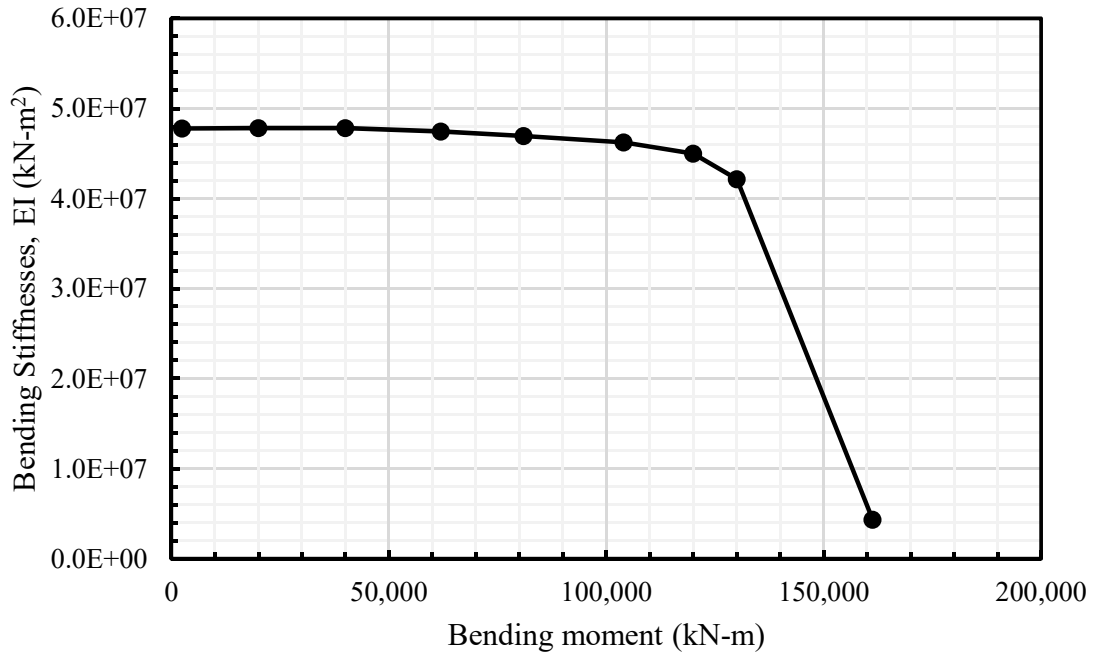


**Figure B- 7 Mihama Bridge, equivalent single pile: Bending stiffness and bending moment diagram of group pile section**

**Table B-11 Pile stiffness properties of the abutment section for equivalent single pile**

Bending Curvature (Radians/m)	Bending Moment (kN-m)	Bending Stiffness, EI (kN-m <sup>2</sup> )
0.0000523	250,000	4.78E+09
0.0004183	2,000,000	4.78E+09
0.0008366	4,000,000	4.78E+09
0.0013072	6,000,000	4.74E+09
0.0017255	8,000,000	4.69E+09
0.0022484	10,500,000	4.63E+09
0.0026667	12,000,000	4.50E+09
0.003085	13,000,000	4.21E+09
0.03702	16,125,800	4.36E+08

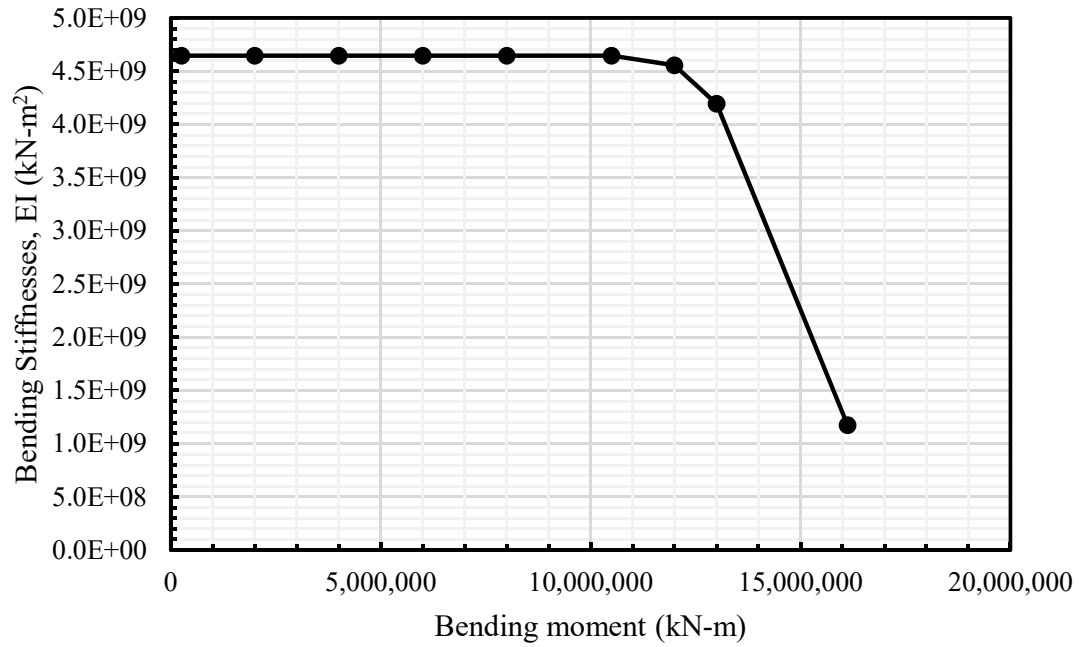


**Figure B-8 Mihama Bridge, equivalent single pile: Bending stiffness and bending moment diagram of abutment section**

## APPENDIX C

### Estimation of the ground displacement

#### Mataquito Bridge

With PGA = 0.461g

**Table C-2 the estimated ground displacement with Spencer method**

Spencer			
$k_y$	R (kN/m)	$R * W_{T-effective}$ (kN)	D (cm)
0.06	0	0	76.6
0.09	140	3,122	41.2
0.12	290	6,467	24.8
0.15	440	9,812	16.1
0.18	590	13,157	11
0.21	740	16,502	7.9
0.24	900	20,070	5.8
0.27	1060	23,638	4.4

**Table C-1 the estimated ground displacement with Janbu method**

Janbu			
$k_y$	R (kN/m)	$R * W_{T-effective}$ (kN)	D (cm)
0.04	0	0	166
0.07	180	4,014	76.6
0.1	360	8,028	41.2
0.13	530	11,819	24.8
0.16	710	15,833	16.1
0.19	880	19,624	11
0.22	1060	23,638	7.9
0.25	1230	27,429	5.8

With PGA = 0.390g

**Table C-3 the estimated ground displacement with Spencer method**

Spencer			
$k_y$	R (kN/m)	$R * W_{T-effective}$ (kN)	D (cm)
0.06	0	0	56.1
0.09	140	3,122	29
0.12	290	6,467	17
0.15	440	9,812	10
0.18	590	13,157	7.3
0.21	740	16,502	5.1
0.24	900	20,070	3.7
0.27	1,060	23,638	2.8

**Table C-4 the estimated ground displacement with Janbu method**

Janbu			
$k_y$	R (kN/m)	$R * W_{T-effective}$ (kN)	D (cm)
0.04	0	0	97.1
0.07	180	4,014	44.2
0.1	360	8,028	24
0.13	530	11,819	14.5
0.16	710	15,833	9.4
0.19	880	19,624	6.4
0.22	1,060	23,638	4.6
0.25	1,230	27,429	3.4

## South Brighton Bridge

**Table C-5 the estimated ground displacement with Spencer method**

Spencer			
$k_y$	R (kN/m)	$R * W_{T-effective}$ (kN)	D (cm)
0.055	0	0	0
0.07	20	444	222
0.09	50	1,110	555
0.11	85	1,887	943
0.13	115	2,553	1276
0.15	150	3,330	1,665
0.17	180	3,996	1,998
0.19	210	4,662	2,331
0.21	245	5,439	2,719
0.23	280	6,216	3,108

**Table C-6 the estimated ground displacement with Janbu method**

Janbu			
$k_y$	R (kN/m)	$R * W_{T-effective}$ (kN)	D (cm)
0.035	0	0	52
0.05	25	555	33
0.07	55	1,221	20
0.09	90	1,998	13.1
0.11	125	2,775	9
0.13	160	3,552	6.69
0.15	195	4,329	4.98
0.17	225	4,995	3.8
0.19	260	5,772	2.9
0.21	295	6,549	2.3
0.23	330	7,326	1.89

## Mihama Bridge

**Table C-8 the estimated ground displacement with Spencer method**

Spencer			
$k_y$	R (kN/m)	$R * W_{T-effective}$ (kN)	D (cm)
0.017	0	0	84.6
0.03	70	3,213	41.6
0.04	130	5,967	26.8
0.05	190	8,721	18.3
0.06	240	11,016	13.1
0.07	300	13,770	9.7
0.08	360	16,524	7.3
0.09	420	19,278	5.7
0.1	480	22,032	4.5
0.11	540	24,786	3.6
0.12	600	27,540	2.9

**Table C-7 the estimated ground displacement with Janbu method**

Janbu			
$k_y$	R (kN/m)	$R * W_{T-effective}$ (kN)	D (cm)
0.008	0	0	155
0.02	90	4,131	70.6
0.03	170	7,803	41.6
0.04	245	11,245	26.8
0.05	320	14,688	18.3
0.06	400	18,360	13.1
0.07	480	22,032	9.7
0.08	560	25,704	7.3
0.09	640	29,376	5.7
0.1	710	32,589	4.5
0.11	790	36,261	3.6

## APPENDIX D

The following show the modification factor with  $m_p=0.15$  near liquefiable layers for each bridge.

### Mataquito Bridge

**Table D-1 Reduction factor for vicinity of liquefied layer with  $m_p=0.15$ , the Mataquito Bridge**

Distance from the liquefied layer (m)	Adjustment factor	$m_p$
0.9	$\frac{1}{3} + \frac{2}{3} \cdot \frac{P_L}{P_H} = 0.43$	$0.37 \cdot 0.82 = 0.35$
1.7	$\frac{2}{3} + \frac{1}{3} \cdot \frac{P_L}{P_H} = 0.71$	$0.69 \cdot 0.82 = 0.58$
2.62	1	0.82

**Table D-2 Reduction factor for each depth with  $m_p=0.15$ , the Mataquito Bridge**

Depth (m)	$m_p$	$n \times m_p$
0-10	1	1
10-14.5	0.15	1.2
14.5-15.4	0.35	2.8
15.4-16.2	0.58	4.6
16.2-27	0.82	6.5

## South Brighton Bridge

**Table D-3 Reduction factor for vicinity of liquefied layer with  $m_p=0.15$ , the South Brighton Bridge**

Distance from the liquefied layer (m)	Adjustment factor	$m_p$
0.3	$\frac{1}{3} + \frac{2}{3} \cdot \frac{P_L}{P_H} = 0.43$	$0.43 \cdot 0.78 = 0.33$
0.6	$\frac{2}{3} + \frac{1}{3} \cdot \frac{P_L}{P_H} = 0.71$	$0.71 \cdot 0.78 = 0.55$
0.9	1	0.78

**Table D-4 Reduction factor for each depth with  $m_p=0.15$ , the South Brighton Bridge**

Depth (m)	$m_p$	$n \times m_p$	
		Vertical pile	Battered pile
0-3.6	1	1	1
3.6-4.0	0.78	7.8	3.9
4.0-4.3	0.55	5.5	2.75
4.3-4.6	0.33	3.3	1.65
4.6-8.0	0.15	1.5	0.75
8.0-8.3	0.33	3.3	1.65
8.3-8.6	0.55	5.5	2.75
8.6 -	0.78	7.8	3.9

## Mihama Bridge

**Table D-5 Reduction factor for vicinity of liquefied layer with  $m_p=0.15$ , the Mihama Bridge**

Distance from the liquefied layer (m)	Adjustment factor	$m_p$
0.7	$\frac{1}{3} + \frac{2}{3} \cdot \frac{P_L}{P_H} = 0.43$	$0.43 \cdot 0.67 = 0.28$
1.4	$\frac{2}{3} + \frac{1}{3} \cdot \frac{P_L}{P_H} = 0.71$	$0.71 \cdot 0.67 = 0.47$
2.0	1	0.67

**Table D-6 Reduction factor for each depth with  $m_p=0.15$ , the Mihama Bridge**

Depth (m)	$m_p$	$n \times m_p$
0-10.0	1	1
10.0-18.0	0.15	6.3
18.0-18.7	0.28	11.7
18.7-19.4	0.47	19.7
19.4-43.0	0.67	28.1